International
Progress Report

IPR-00-12

Äspö Hard Rock Laboratory

Measurements with the he-gas methods of the disturbed zone caused by boring

Mika Laajalahti, Tapani Aaltonen, Kalle Kuoppamäki,
Jani Maaranen, Jussi Timonen
University of Juväskulä, Department of Physics

Jorma Autio
Saanio & Riekkola Consulting Engineers

April 1999

Svensk Kärnbränslehantering AB
Swedish Nuclear Fuel
and Waste Management Co
Box 5864
SE-102 40 Stockholm Sweden
Tel 08-459 84 00
+46 8 459 84 00
Fax 08-661 57 19
+46 8 661 57 19

Äspö Hard Rock
Laboratory

Report no.	No.
IPR-00-12	F19K
Author	Date
M Laajalahti, T Aaltonen, K Kuoppamäki, J Maaranen, J Timonen	1999-04-30
Checked by	Date
Christer Svemar	2000-04-12
Approved	Date
Olle Olsson	2000-04-13

Äspö Hard Rock Laboratory

Measurements with the he-gas methods of the disturbed zone caused by boring

Mika Laajalahti, Tapani Aaltonen, Kalle Kuoppamäki,
Jani Maaranen, Jussi Timonen

University of Juväskulä, Department of Physics

Jorma Autio

Saanio & Riekkola Consulting Engineers

April 1999

Keywords: He-gas methods, pycnometer, porosity, diffusivity, permeability, disturbed zone

FOREWORD

This work is part of the characterisation of the experimental full-scale deposition holes bored in the Research Tunnel at Olkiluoto, a project commissioned by Posiva Oy and SKB (Svensk Kärnbränslehantering AB) in co-operation. The work was managed and supervised by Jorma Autio at Saanio & Riekkola Oy on behalf of Posiva Oy and SKB. The contact person at Posiva Oy was Jukka-Pekka Salo and at SKB Christer Svemar.

ABSTRACT

Three experimental holes the size of deposition holes in a KBS-3 type repository (depth 7.5 m and diameter 1.5 m) were bored in hard granitic rock in the Research Tunnel at Olkiluoto and the porosities, effective diffusivities and permeabilities of rock in the excavation-disturbed zone were determined in a direction parallel to the disturbed surface using permeability, through-diffusion and pycnometer techniques based on the He-gas. Those properties had previously been determined in direction perpendicular to the disturbed surface.

Permeability and diffusivity parallel to the rock orientation were found to be clearly larger than in a direction perpendicular to the rock orientation. The porosity of disturbed rock samples obtained by using He-pycnometry (0.45%) was clearly higher than that of the undisturbed ones (0.24%). The permeabilities and diffusion coefficients obtained for the disturbed rock samples were also clearly higher than those obtained for the undisturbed ones. The ratio between the average permeabilities of the disturbed and undisturbed rock samples was 3.2, and the ratio between the diffusion coefficients was 3.1.

The permeabilities and diffusion coefficients were also clearly oriented, being larger in the direction of the schistosity of the rock than at an angle of approximately 45° to the schistocity. The ratio between the average diffusion coefficients in these two directions (2.8) was the same in both the disturbed and the undisturbed rock samples, whereas the ratio between the average permeabilities was larger in the undisturbed (7.4) than in the disturbed rock samples (1.8).

SAMMANFATTNING

Tre provhål med samma storlek som deponeringshål (djup 7,5 m och 1,5 m diameter) har borrats i hård granit i forskningstunneln i Olkiluoto. Den störda zonens porositet, effektiva diffustivitet och permeabilitet har nu också bestämts parallellt med bergväggen med hjälp av en metod som bygger på diffusion av heliumgas samt permeabilitets- och pyknometerteknik för diffunderande heliumgas. En tidigare studie bestämde motsvarande värden vinkelrätt mot bergväggen.

Permeabilitet och diffusivitet parallellt med bergstrukturen visade sig vara signifikant större än vinkelrätt mot denna. Porositet hos borrpåverkade bergprover uppmätt med heliumgaspyknometer (0,45%) är signifikant större än uppmätt porositet hos opåverkade bergprover (0,24%). De permeabilitets- och diffusionskoefficienter som erhållits för borrpåverkade bergprover är signifikant större än de som erhållits för opåverkade bergprover. Kvoten mellan de genomsnittliga permeabiliteterna hos de borrstörda resp. ostörda bergproverna erhålls till 3,2 och kvoten mellan diffusionskoefficienterna till 3,1.

Permeabilitets- och diffusionskoefficienterna är också tydligt orienterade och är större parallellt med bergets skiffrighet än i en 45-gradig riktning däremot. Kvoten på 2,8 mellan de genomsnittliga diffusionskoefficienterna i dessa två riktningar är densamma i både borrpåverkade och opåverkade bergprover, medan kvoten mellan de genomsnittliga permeabiliteterna är större i de opåverkade proverna (7,4) än i de borrpåverkade (1,8)

TABLE OF CONTENTS:

APPENDICES:

1 INTRODUCTION

In a nuclear waste repository, rock in the excavation-disturbed zone adjacent to the walls of deposition holes for waste canisters is a potential pathway of transport of corrosive agents and radionuclides. Rock in this zone may also act as a mixing tank, or, in the case of low axial conductivity and dead-end type radial fissures, efficiently sorb and retard the radionuclides that diffuse through the bentonite buffer. Rock characteristics in the excavation-disturbed zone may also play a role in saturation of the bentonite buffer and in gas release. To assess the characteristics of rock in the disturbed zone, investigations have taken place in three experimental holes of the size of deposition holes (depth 7.5 m and diameter 1.5 m) in a KBS-3 type repository in hard granitic rock in the Research Tunnel at Olkiluoto. Details of the boring technique (Autio&Kirkkomäki 1996), previous characterisation of the excavation disturbance caused by boring (Autio 1996, Autio&Siitari-Kauppi 1997), and the He-gas method (Väätäinen et al. 1993, Hartikainen et al. 1994, Hartikainen et al. 1995a, b, Hartikainen et al. 1996a, b) have been reported earlier. He-gas methods were used in this study to establish the degree of rock disturbance in terms of porosity, effective diffusion coefficient and permeability. Measurements were based on either the diffusion or flow of helium through a rock sample saturated with nitrogen gas, and included porosity determinations using He-gas pycnometry.

Two types of sample geometry were used in the He-gas measurements. Disc samples with a central hole (i.e. rings) were used to establish the undirectional averaged permeability and diffusion coefficient. Cubic samples were used to measure the same properties in two different perpendicular directions.

2 SAMPLES

2.1 RING SAMPLES

The shape and dimensions of the two ring samples from the Research Tunnel at Olkiluoto, measured by the through-diffusion method, are shown in Figure 2.1-1. The upper side of the sample comprised the disturbed zone sealed by fluorescent epoxy.

The intention by using this measuring geometry was to obtain results averaged over all possible lateral directions, and thus independent of any possible orientational effects caused by the structure of the samples. The accurate dimensions of the samples are given in Table 2.1-1.

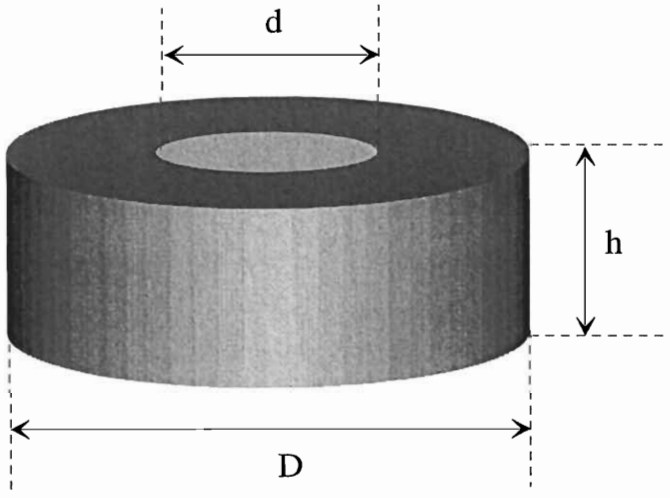

Figure 2.1-1. Ring sample.

Table 2.1-1. Dimensions of the perforated disc samples D12 and D13.

Sample	h [mm]	D [mm]	d [mm]
D12	31.8±0.5	89.3±0.5	38.1±0.5
D13	31.2±0.5	89.5±0.5	38.3±0.5

2.2 CUBIC SAMPLES

Parallelepiped samples were sawn from cylindrical core samples as shown in Figure 2.2-1. After measuring the porosity with the helium pycnometer, these samples were cut into two approximately cubic parts as shown in Figure 2.2-2 so that one part included the disturbed zone (Samples A) and the other part was intact rock (Samples B). Codings of the samples are shown in Figures 2.2-3.

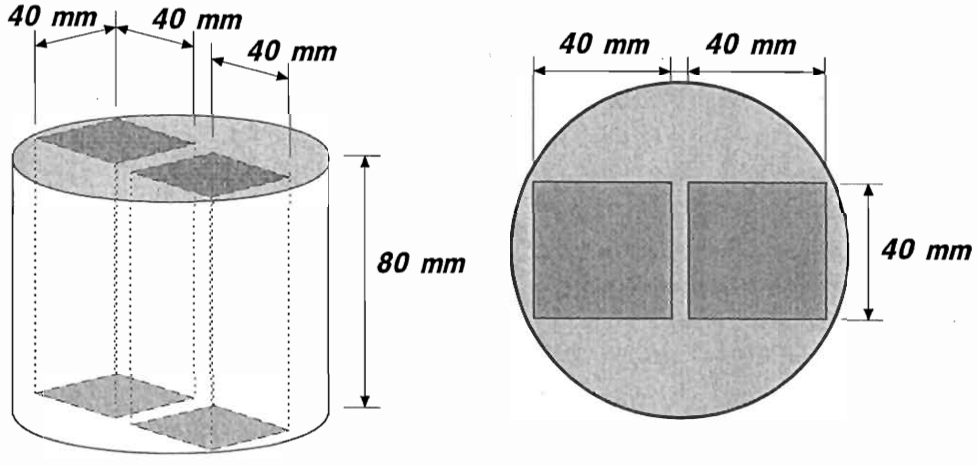

Figure 2.2-1. *Sawing of cylindrical samples into parallelepiped samples.*

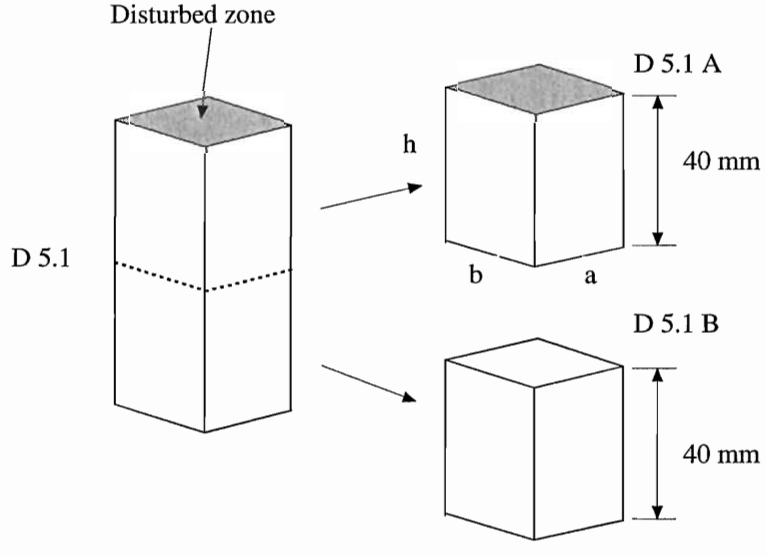

Figure 2.2-2. *Further cutting into cubic samples.*

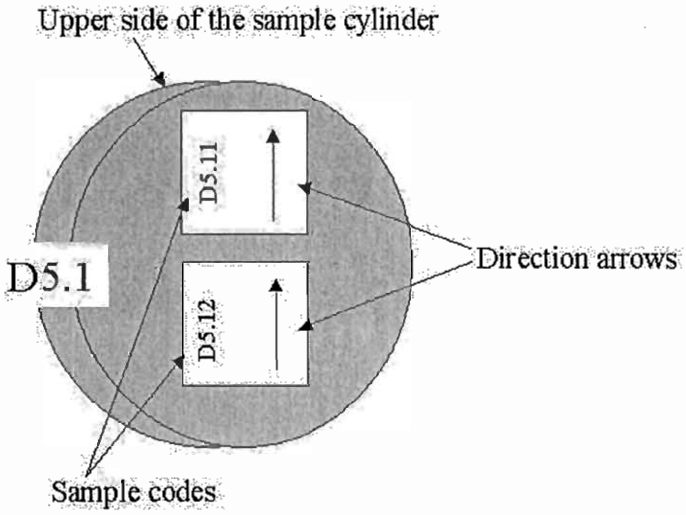

Figure 2.2-3. *Coding of the parallelepiped and cubic samples.*

The detailed dimensions of the cubic samples are given in Table 2.2-1. The upper part of the table shows the dimensions of the samples measured perpendicular to the structural orientation, and the lower part those measured parallel to the structural orientation. The dimensions are slightly different in the two cases because removal of excessive epoxy was made in two phases, the second of which took place in between the two measurements.

Table 2.2-1. Dimensions of the cubic samples.

In measurements perpendicular to the structural orientation

Sample	h [mm]	a [mm]	b [mm]
D 5.1 A	39.5±0.5	29.3±0.5	40.0±0.5
D 5.1 B	38.9±0.5	40.6±0.5	38.9±0.5
D 14.2 A	39.5±0.5	32.5±0.5	40.0±0.5
D 14.2 B	40.5±0.5	40.6±0.5	39.8±0.5
D 15.1 A	39.4±0.5	33.9±0.5	39.9±0.5
D 15.1 B	37.9±0.5	40.5±0.5	39.4±0.5

In measurements parallel to the structural orientation

Sample	H [mm]	a [mm]	b [mm]
D 5.1 A	39.2±0.5	29.0±0.5	37.8±0.5
D 5.1 B	38.7±0.5	40.6±0.5	36.8±0.5
D 14.2 A	39.2±0.5	32.0±0.5	37.5±0.5
D 14.2 B	40.5±0.5	40.6±0.5	37.6±0.5
D 15.1 A	39.4±0.5	33.4±0.5	37.7±0.5
D 15.1 B	37.8±0.5	40.5±0.5	37.3±0.5

2.3 SEALING OF THE DISTURBED SURFACE

The material used for sealing the disturbed surface was a fast-curing epoxy resin, brand name Caldofix HQ by Struers A/S, which is composed of two fluid components. Caldofix has to be heated to at least 70°C to cure and it is characterised by minimal shrinkage. The resin/hardener mixing ratio is 20/6. The pot life of the mixed resin at 20°C is 4 hours. The curing time at 70°C is 90 minutes. The gelation time when the material begins to polymerise is approximately 50 minutes. Fluorescent dye, brand name EpoDye by Struers, was mixed with the epoxy.

The resin and hardener were mixed at room temperature. Before carrying out the actual sealing of the samples, the polymerisation time (assumed here to be 50 minutes) of the specific batch was checked. The sealing procedure after drying of the samples was the following:

1) The sample is heated to 70°C.

2) The dye (1.2 g) is mixed with the hardener (69.5 g).

3) The two components of the epoxy (233 g resin and 69.5 g hardener) are mixed together.

4) The sample and the epoxy are kept in an oven at 70°C for 46 minutes.

5) When 46 minutes have elapsed from the mixing of the epoxy, the polymerising mixture is poured onto the disturbed surface of the rock sample so that a layer of epoxy of less than 1 mm thick is formed.

6) The coated sample is kept in an oven at 70°C until the resin is completely cured.

The procedure described here was used for all rock samples taken from the Research Tunnel at Olkiluoto. However, at the time of writing of this report, the exact penetration depth of the epoxy sealant into the samples used was not measured. It will be quantitatively investigated by fluorescent microscopy before the end of 1998. If needed, the penetration depth of the epoxy can be adjusted by lengthening the settling time or by using a different type of polymer.

3 POROSITY MEASUREMENTS

3.1 GENERAL

Porosity measurements were carried out using the He-gas pycnometer method which is based on the equation of state of ideal gas. Helium gas is used because it is non-reactive and penetrates easily small pores, and because it very accurately fulfils the ideal gas law. Also, a porosity value obtained by helium gas will obviously be closer to that measured in a He-gas diffusion experiment, than a value obtained by using some other media such as water. The values obtained by He-gas pycnometry are complementary to those of the diffusion measurements. The latter are quite insensitive to porosity because it only appears in Equation 4.4-3 through parameters D_a and h.

Before any measurements were made, samples were cleaned by pressurized air and dried in a vacuum oven. After drying, grain (i.e. solid) volumes of the samples were measured using a helium gas pycnometer developed in the Department of Physics at the University of Jyväskylä ($V_{grain} = V_{bulk} - V_{pore}$). Bulk volume determinations were based on the water-immersion method. The procedure of porosity measurements is shown in Figure 3.1-1.

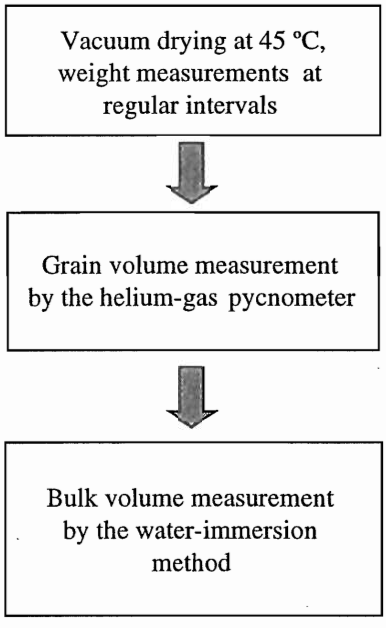

Figure 3.1-1. *The procedure of porosity measurements.*

After the first porosity measurements for the rectangular through-diffusion samples, samples were cut into two halves. One half, which represented undisturbed rock, was used as a reference sample for the second half which included the disturbed zone.

3.2 DRYING OF THE SAMPLES

All samples were dried in a vacuum oven at a temperature of 45°C. This slightly elevated temperature is not expected to cause any damage to the rock structure. Before drying, samples were carefully cleaned by pressurized air and weighed with a balance in ambient conditions. In order to follow the drying process, samples were weighed after suitable intervals. For weighing the temperature of the oven was switched back to room temperature, the oven was filled with nitrogen, and the sample was left in the nitrogen atmosphere for four hours. The purpose of nitrogen saturation of the samples was to decrease the absorbtion of water vapour from the air. After weighing, vacuum drying was immediately continued. The level and rate of drying were estimated from the weight measurements by using a fit of two exponentials to the drying curve. An example of the drying curves is shown in figure 3.2-1. All the drying curves measured are given in Appendix A.

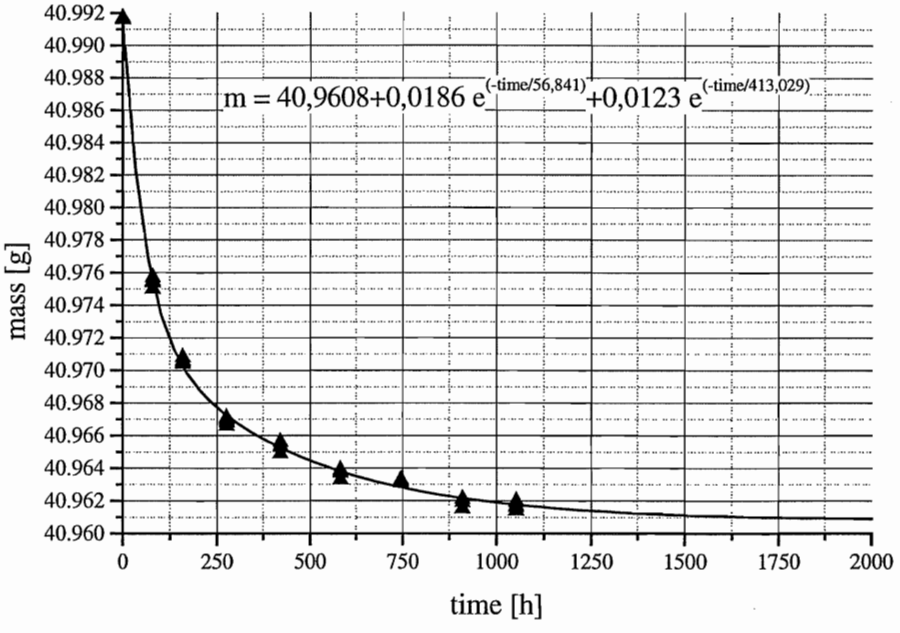

Figure 3.2-1. *The drying curve of sample C9.1.*

Drying of rock samples takes a long time. The samples from the Research Tunnel at Olkiluoto of size 4x4x8 cm^3 e.g. were dried for about 2500 hours. Drying time can be significantly reduced by increasing the temperature, and it is suggested that the drying temperature should be increased in the future to 105°C or, if alteration are expected to occur, to 80°C.

3.3 MEASURING TECHNIQUES

3.3.1 Pycnometer

The experimental arrangement of the pycnometer used in the porosity measurements is shown in Figure 3.3-1. The volumes of the cells, V_R and V_S, are first determined by using calibration samples. A polished aluminium calibration sample of volume V_N is inserted into the sample cell V_S, the whole system is evacuated, and the pressure P_V and temperature T_V are measured after stabilisation. The reference cell is then pressurised with helium. The pressure P_R and the temperature T_R are measured after stabilisation, whereafter the helium is allowed to expand into the measuring chamber. After stabilisation, the resulting pressure P_S and temperature T_S of the whole volume are measured. The unknown volumes in the system can be determined when the volume V_N, pressures P_V, P_R and P_S, and temperatures T_V, T_R and T_S are known for at least two calibration samples. The same procedure is then repeated on the sample to be measured.

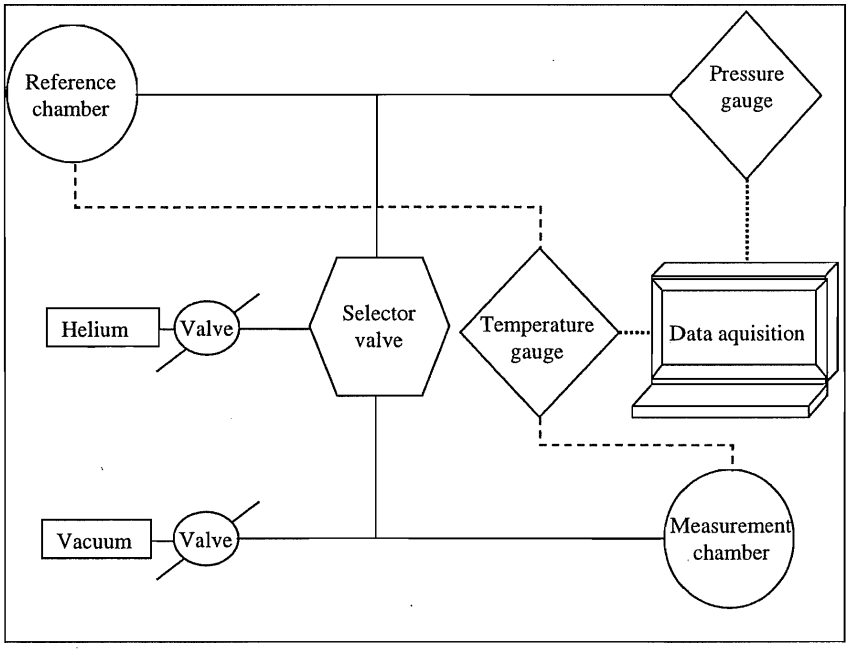

Figure 3.3-1. Experimental set-up of the He-pycnometer.

3.3.2 Grain volume

According to the ideal-gas law, the porosity of the sample can be determined when the pressures P_V, P_R and P_S, the temperatures T_V, T_R and T_S, the volumes of the cells V_R and V_S, and the bulk volume of the sample V_b are all known. The porosity ε_p [%] can then be expressed in the form

$$\varepsilon_p = \frac{V_b - V_g}{V_b} \cdot 100, \tag{3.3-1}$$

where the grain volume V_g is given by

$$V_g = V_S - V_R \frac{(P_R T_S T_V - P_S T_V T_R)}{(P_S T_V T_R - P_V T_S T_R)}. \tag{3.3-2}$$

3.3.3 Bulk volume

Bulk volume was measured using the water-immersion method. The sample was weighed in ambient conditions and then in water. The temperature of the water was also measured to determine its density. The density of water ρ_w [kg/m^3] as a function of temperature T [°C] is given by [Kell G. S. 1967]

$$\rho_w = 0{,}99995 + 0{,}00005 \cdot T - 7{,}545 \cdot 10^{-6} \cdot T^2 + 3{,}6131 \cdot 10^{-8} \cdot T^3 \tag{3.3-3}$$

Using the difference in the two masses and the density of water, the bulk volume of the sample can be determined from

$$V_b = \frac{m_d - m_f}{\rho_w}, \tag{3.3-4}$$

where m_d is the mass of the sample in ambient conditions [kg], and m_f is the mass of the sample in water [kg].

The masses of the samples were determined with a Metler Toledo AT400 balance. The balance resolution was 0.1 mg and measuring accuracy was 0.2 mg. The mass of the sample at the moment of immersion was determined by using a polynomial fit to the measured points. The mass of the sample grows rapidly during the measurement as water penetrates the open pores. The time of stabilization of the balance is about one minute which sets the first value measured (Figure 3.3-2a).

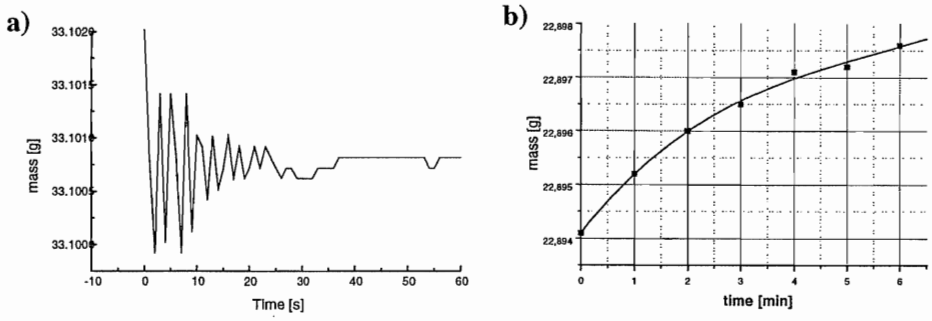

Figure 3.3-2. *The short time behaviour of a typical wet-weighing curve (a test sample) (a), and the wet-weighing curve of sample L 10.1. (b).*

Deionized water was used in the immersion measurements to reduce bubble formation. An example of the wet-weighing curves is shown in Figure 3.3-2b, where the first point (t=0) has been extrapolated from the curve fitted from measured points. All the wet-weighing curves measured are shown in Appendix B.

3.4 ERROR ANALYSIS OF THE HE-PYCNOMETER MEASUREMENTS

3.4.1 Error propagation

The general formula for error propagation in the dependent quantity $q(x,\ldots,z)$, with independent uncertainties $dx,\ldots,dz$ in the measured quantities $x,\ldots,z$, is given by

$$dq = \sqrt{\left(\left(\frac{\partial q}{\partial x}dx\right)^2 + \cdots + \left(\frac{\partial q}{\partial z}dz\right)^2\right)}. \qquad (3.4\text{-}1)$$

The effective porosities of the samples were determined from Equation (3.3-1) where the grain volumes V_g were determined from Equation (3.3-2).

The uncertainties of the grain volumes were determined from Equation (3.4-1). The relevant quantities and their uncertainties are explained in Table 3.4-1.

Table 3.4-1. Uncertainties of the quantities involved.

Uncertainty of the volume of the measuring cell	dV_S	0.002 [cm^3]
Uncertainty of the volume of the reference cell	dV_R	0.002 [cm^3]
Uncertainty of the pressure in the reference cell	dP_R	10 [Pa]
Uncertainty of the temperature in the reference cell	dP_R	0.02 [K]
Uncertainty of the temperature in the measuring cell	dT_R	0.02 [K]
Uncertainty of the pressure in the measuring ce	dT_S	10 [Pa]
Uncertainty of the pressure in the whole system	dP_V	10 [Pa]
Uncertainty of the temperature in the whole system	dT_V	0.02 [K]

The uncertainties in volumes V_s and V_R were estimated from the standard deviations in the calibration measurements. All pressures were measured by the same Beamex PC 106 pressure calibrator. Its accuracy was 10 Pa. Temperature measurements were made by J-type (Iron-Constantan) thermocouples, and the accuracy of the measurements was 0.02 K in the measuring range 292-298 K.

The partial differentials involved are given by

$$\frac{\partial V_g}{\partial Vs} \cdot dV_S = dV_S , \tag{3.4-2}$$

$$\frac{\partial V_g}{\partial V_R} \cdot dV_R = \frac{-T_V}{T_R}\left(\frac{P_R T_S - P_S T_R}{P_S T_V - P_V T_S}\right) \cdot dV_R , \tag{3.4-3}$$

$$\frac{\partial V_g}{\partial P_R} \cdot dP_R = \frac{-V_R T_V T_S}{T_R P_S T_V - P_V T_S T_R} \cdot dP_R , \tag{3.4-4}$$

$$\frac{\partial V_g}{\partial T_R} \cdot dT_R = \frac{V_R T_V}{T_R^2}\left(\frac{P_R T_S - P_S T_R}{P_S T_V - P_V T_S} + \frac{V_R T_V P_S}{T_R P_S T_V - T_R P_V T_S}\right) \cdot dT_R , \tag{3.4-5}$$

$$\frac{\partial V_g}{\partial T_S} \cdot dT_S = \frac{-V_R T_V}{T_R}\left(\frac{P_R}{P_S T_V - P_V T_S} + \frac{P_V P_R T_S - P_V P_S T_R}{(P_S T_V - P_V T_S)^2}\right) \cdot dT_S , \tag{3.4-6}$$

$$\frac{\partial V_g}{\partial P_S} \cdot dP_S = \frac{-V_R T_V}{T_R}\left(\frac{-T_R}{P_S T_V - P_V T_S} + \frac{T_V P_R T_S - P_S T_R T_V}{(P_S T_V - P_V T_S)^2}\right) \cdot dP_S , \tag{3.4-7}$$

$$\frac{\partial V_g}{\partial P_V} \cdot dP_V = \frac{-V_R T_V}{T_R}\left(\frac{T_S P_R T_S - P_S T_R T_S}{(P_S T_V - P_V T_S)^2}\right) \cdot dP_V \quad \text{and} \tag{3.4-8}$$

$$\frac{\partial V_g}{\partial T_V} \cdot dT_V = \frac{-V_R}{T_R}\left(\frac{P_R T_S - P_S T_R}{P_S T_V - P_V T_S}\right) + \frac{V_R T_V}{T_R}\left(\frac{P_R T_S P_S - P_S{}^2 T_R}{(P_S T_V - P_V T_S)^2}\right) \cdot dT_V . \tag{3.4-9}$$

3.4.2 Standard deviation

Uncertainties in the porosities of the samples were also estimated statistically by standard deviation of the independent measurements. The formula of the standard deviation $\delta_{\bar{x}}$ used here is given by

$$\delta_{\bar{x}} = \sqrt{\frac{\sum_{i=1}^{N}(x_i - \bar{x})^2}{N(N-1)}}, \qquad (3.4\text{-}10)$$

where x_i is the result of an independent measurement,
N is the number of the measurements done,
$\bar{x}$ is the average of the measured values x_i.

The term N-1 in the denominator is used because N^2 has a tendency to underestimate the uncertainty for small N.

A summary of the uncertainties for the cubic samples is given in Table 3.4-2. Samples A have a disturbed zone. Samples without a label A or B are the original uncut samples.

Table 3.4-2. Summary of uncertainties for the cubic samples.

Sample	Porosity [%]	Uncertaintity by error propagation	Uncertaintity by standard deviation
D5.1	0.32	± 0.020	± 0.011
D14.2	0.25	± 0.012	± 0.004
D15.1	0.30	± 0.018	± 0.004
D5.1A	0.44	± 0.024	± 0.036
D5.1B	0.22	± 0.025	± 0.023
D14.2A	0.42	± 0.012	± 0.007
D14.2B	0.29	± 0.008	± 0.004
D15.1A	0.49	± 0.028	± 0.015
D15.1B	0.22	± 0.006	± 0.004

3.4.3 Calibration samples

Measuring uncertainties in the volumes of the cylindrical aluminium calibration samples were also determined by Equation (3.4-1). Their total difference dV_b is

$$dV_b = \frac{dm_d}{\rho} - \frac{dm_f}{\rho} - \frac{(m - m_v)d\rho}{\rho^2}, \qquad (3.4\text{-}11)$$

where dm_d and dm_f both were 0.2 mg.

With an uncertainty in the water density $d\rho = \pm 0.1\%$ in the used temperature range, the maximum uncertainty in V_b was within $\pm 0.2\%$.

3.5 RESULTS OF POROSITY MEASUREMENTS

3.5.1 Cubic samples

Porosity was measured for the three orginal parallelepiped and six cubic samples, described in Section 2.2, and the results are shown in Table 3.5-1. The original samples and cubic samples with label A include a disturbed zone.

It is evident from these results that the behaviour of samples D5.1 and D14.2 is consistent under cutting in two, because the porosities of the original samples are very close to the averages of the corresponding A and B samples. It is also evident that the disturbed zone has a markedly increased porosity. If one assumes that the depth of the disturbed zone is approximately 6 mm [Autio 1996], it is easy to estimate from the measured porosities that the average porosity of the disturbed zone in sample D5.1 is about 1.5%, and that in sample D14.2 about 2.5%.

In the case of sample D15.1, the porosity of the original sample is not consistent with those of its halves. Either there has been a technical complication in the measurements which was left unnoticed, or the porosity of especially the intact sample B has increased in the cutting.

The uncertainty in the measurements done with the He-pycnometer were estimated by the general formula for error propagation [Taylor 1997] and by statistical analysis. The accuracy of porosity by this formula was within $\pm 12\%$, whereas the standard deviations of repeated measurements were within $\pm 10\%$.

The main source of possible systematic errors is in the calibration of the pycnometer. As explained before, calibration was done with two calibration samples whose volumes were known very accurately. The volumes of the calibration samples were determined by the water immersion method in the same way as the bulk volumes of the rock samples. This may have caused a systematic error in the porosity measurements depending on the measuring accuracy of the water-immersion method. Measuring uncertainties in the volumes of the calibration samples were estimated to be within $\pm 0.2\%$ of the volume.

Table 3.5-1. Bulk volumes, grain volumes and porosities of the rectangular and cubic samples.

Sample	Bulk volume V_b 10^{-6} [m^3]	Grain volume V_g 10^{-6} [m^3]	Porosity ε_p [%]
D 5.1	125.409	125.008	0.32±0.02
D 14.2	130.080	129.687	0.30±0.01
D 15.1	126.146	125.829	0.25±0.02
D 5.1 A	60.143	59.880	0.44±0.04
D 5.1 B	59.235	59.103	0.22±0.03
D 14.2 A	61.035	60.780	0.42±0.01
D 14.2 B	58.956	58.783	0.29±0.01
D 15.1 A	60.425	60.130	0.49±0.03
D 15.1 B	63.362	63.224	0.22±0.01

The He-pycnometer method is sensitive to errors in the measurement of both pressure and temperature. The temperature measurement is based on thermocouples and computer-based data acquisition. The measuring system provides a resolution of 0.01 K which means that the uncertainty in temperature is ± 0.02 K. This uncertainty and the possible systematic error in calibration affect most the total error.

3.5.2 Test samples

In addition to the cubic through-diffusion samples, the porosities of eight drill-core samples were measured by the He-pycnometer method. The samples used were about 25 mm thick slices of drill cores with a diameter of about 27 mm. These samples were also taken from the full-scale experimetal deposition holes in the Research Tunnel at Olkiluoto. Four of the samples included a disturbed zone from the surfaces of the hole, and these samples are denoted by an affix 1 in the Table 3.5-2 below.

Before the porosity measurements, the samples were dried as described in Section 3.2. The drying curves are shown in Appendix A.

The bulk and grain volume measurements and the error analysis were done as described in the previous sections, and the results together with the related porosities are given in Table 3.5-2. The error values shown were found by the error propagation formula Equation 3.4-1.

Table 3.5-2. Bulk volumes, grain volumes and porosities of the test samples by the He-pycnometer method.

Sample	W_d [g]	W_a [g]	V_{bulk} [cm^3]	V_{grain} [cm^3]	ε_p [%]
C 9.1	40.962	26.285	14.716	14.591	0.85 ± 0.07
C 9.2	39.312	25.160	14.183	14.105	0.55 ± 0.07
D 16.1	38.956	25.244	13.747	13.649	0.71 ± 0.07
D 16.2	40.584	26.383	14.232	14.155	0.54 ± 0.07
L 10.1	37.292	22.963	14.421	14.331	0.62 ± 0.07
L 10.2	37.508	23.196	14.346	14.275	0.49 ± 0.07
L 11.1	40.054	26.110	13.978	13.901	0.55 ± 0.07
L 11.2	30.900	26.020	13.910	13.861	0.35 ± 0.07

4 TROUGH-DIFFUSION MEASUREMENTS

4.1 MEASURING TECHNIQUES

In the through-diffusion measurements the injection chamber is first flushed with nitrogen and then evacuated by using a vacuum pump. This is continued until the He-concentration from the air in the sample is stabilized at a very low level. After evacuation the pressure of the injection chamber will be less than 0.08 bar.

During the evacuation, helium flows through the injection loop. After the evacuation, the loop containing helium is connected to the injection chamber by using a 6-way valve and an injector valve. At the same time the other end of the loop is connected to nitrogen flow that goes through a pressure equalizer. Because of this, only the helium in the loop (5 ml) will be injected. Helium is sucked from the loop to the injection chamber by the vacuum. After connecting the loop to the injection chamber, the system is let to stabilize for two minutes. In that time all helium is transferred to the injection chamber, and the valve is turned off. Helium now diffuses through the sample to the sniffer chamber, which is continuously flushed with nitrogen. The helium concentration of this nitrogen is then measured with a Leybold helium-leak tester. During the through-diffusion, the injection chamber is sealed. The whole through-diffusion measurement takes about 1200 minutes. The purity of the helium used is 99.995% and that of the nitrogen is 99.9%. It is important in the through-diffusion method that there is no pressure difference between the injection and sniffer chambers, and that helium migrates through the sample only by diffusion.

The sealing material used in the through-diffusion and permeability measurements is He-tight Terostat by Würth GmbH. Terostat is widely used in vacuum technology, and in these measurements it is used between the boundary surfaces of the sample and the measuring chamber (Figures 4.2-1 and 4.3-2). The sealing tests of Terostat are reported in Section 4.5.1.

4.2 RING SAMPLES

In the case of ring samples the helium pulse is injected into the hole at the centre of the sample. The outer cylindrical surface is flushed with nitrogen to remove the helium molecules that have diffused through the sample, and

the helium concentration of the nitrogen is then measured. The geometry of the measuring chamber is shown in Figure 4.2-1, and the experimental set-up is shown in Figure 4.2-2. The approximate dimensions of the samples are: hole diameter 38 mm, core diameter 90 mm, length of core 32 mm. The exact dimensions of the samples are given in Section 2.

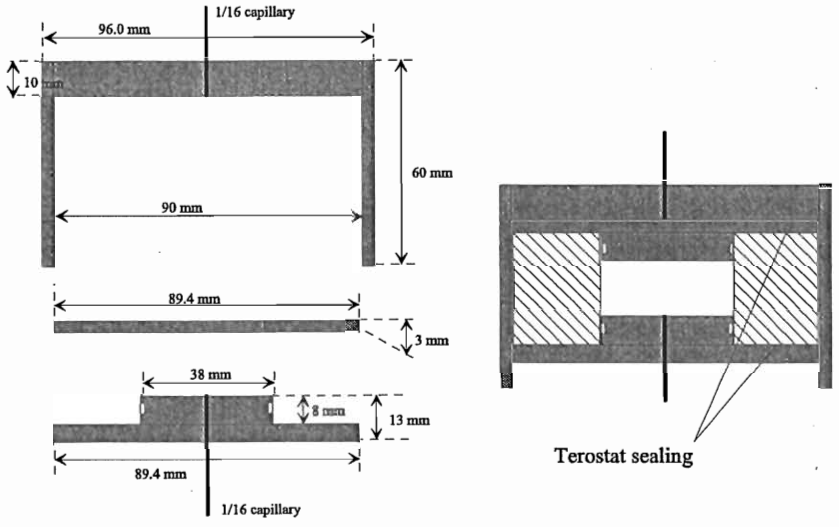

Figure 4.2-1. *The measuring chamber for ring samples.*

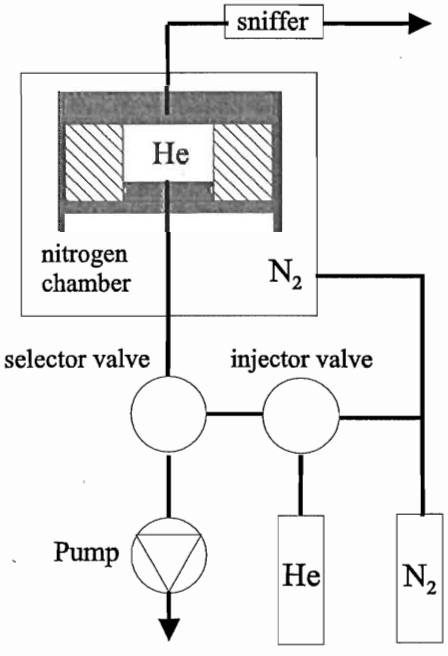

Figure 4.2-2. *The experimental set-up for ring samples.*

4.3 CUBIC SAMPLES

In principle, measurements on the cubic samples are similar to those on the ring samples. In the case of cubic samples, the helium pulse is injected into the injection chamber so that one rectangular face of the sample is exposed to a concentration of helium. The opposite face of the sample is continuously flushed with nitrogen in order to collect the helium molecules that have diffused through the sample. The helium concentration of the nitrogen is then measured. Samples are kept at ambient temperature and pressure. The experimental set-up for cubic samples is shown in Figure 4.3-1, and some details of the measuring chamber are shown in Figure 4.3-2.

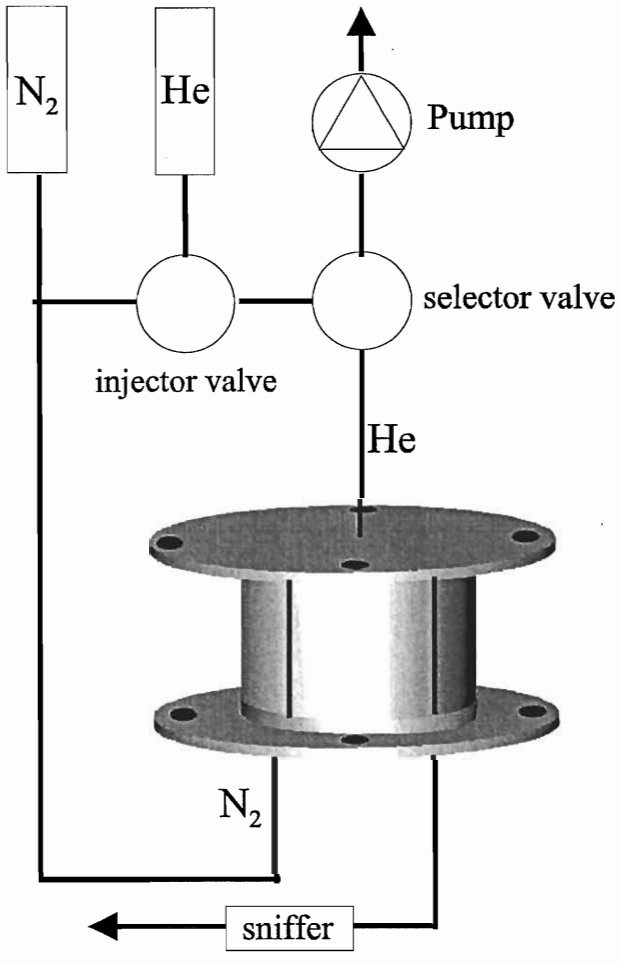

Figure 4.3-1. *The experimental set-up for cubic samples*

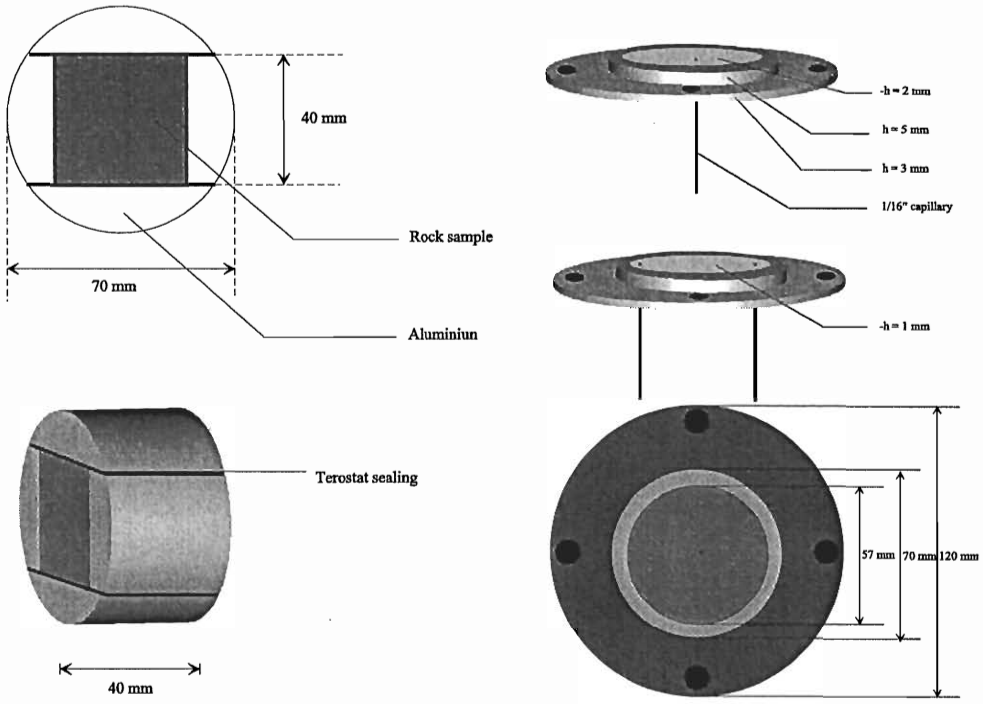

Figure 4.3-2. *The aluminium parts that transform the cube to a cylindrical form, and the end plates of the measuring chamber.*

4.4 MODELLING

Modelling of the through-diffusion measurements is based on the solution of an appropriate diffusion equation. Because of the planar geometry of the samples and reflective boundary conditions in the transverse directions, one can use a one-dimensional approximation, and the diffusion equation to be applied for the concentration of helium C(x,t) [kg/m^3] is simply

$$\frac{\partial C}{\partial t} = \frac{D_e}{\varepsilon_p}\frac{\partial^2 C}{\partial x^2}, \qquad (4.4\text{-}1)$$

where t [s] is time, D_e [m^2/s] is the effective diffusion coefficient, ε_p is the porosity and x is the position inside the sample.

The boundary conditions in the direction of helium transport are such that the concentration of helium in the injection chamber is assumed to decrease according to the diffused amount. It is also assumed that there is no sorption and that the helium concentration at the outer surface of the sample is zero due to continuous flushing with nitrogen.

Porosity ε_p and the effective diffusion coefficient D_e [m^2/s] can both be determined from the breakthrough curves of helium by fitting the curves with the relevant solution of Equation (4.4-1). In this one-dimensional approximation it is in fact possible to derive (Väätäinen et al. 1993, Carslaw

1959) an analytical expression for the mass flow of helium through the sample,

$$\dot{m} = -D_e A \left.\frac{\partial C}{\partial x}\right|_{x=1} \quad [kg/s], \tag{4.4-2}$$

in the form

$$\frac{\dot{m}}{m_0} = D_a h \sum_{n=1}^{\infty} \frac{2h\alpha_n e^{-D_a \alpha_n^2 t}}{\sin(\alpha_n l)\left[l\left(\alpha_n^2 + h^2\right) + h\right]} \quad , \tag{4.4-3}$$

where A [m^2] is the cross-sectional area of the sample, m_o [kg] is the mass of the injected helium, $D_a = D_e/\varepsilon_p$ [m^2/s] is the apparent diffusion coefficient, $h = \varepsilon_p/s$, s [m] being the average length of the injection cell, α_n, $n = 1, 2, ...$, are the roots of $\alpha\tan(\alpha l) = h$ [l/m], and 1 [m] is the average length of the sample. The average length of the injection cell (s) and the length of the sample (l) are both needed as input parameters.

Once the above mentioned parameters have been fixed, the theoretical model is fitted to the breakthrough curves by varying the effective diffusion coefficient D_e and the porosity ε_p. Another possibility is to infer the value of porosity from independent measurements, in which case the effective diffusion coefficient is the only parameter to be fitted.

Although measurements are carried out in the gas phase, the corresponding diffusion coefficients for the water-saturated case can be derived. This is based on the fact that in both cases, the diffusion equation is the same apart from the actual values of the diffusion coefficients. Significant changes in the pore space are not expected to occur upon drying of the samples.

For helium diffusing in free nitrogen gas at 22°C, the diffusion coefficient $D_e(N_2)$ is $6.75*10^{-5}$ m^2/s, and for helium diffusing in free water at 22°C the diffusion coefficient $D_e(H_2O)$ is $5.8*10^{-9}$ m^2/s. The ratio $D_e(H_2O)$ / $D_e(N_2)$ is therefore 1/11 600. Scaling of the measured diffusion coefficients by this factor should provide a good estimate of the corresponding coefficients for helium atoms diffusing in rock samples saturated with water. If other inert molecules are considered, their mass and size should also be taken into account. For typical molecules consisting of only a few atoms, the diffusion coefficient in free water is close to $2*10^{-9}$ m^2/s. Measurements can therefore be scaled to the diffusion coefficients of these heavier molecules in water-saturated samples by using an approximate scaling factor of 1/35 000 (Hartikainen et al. 1996b).

In practice the whole breakthrough curves of helium were measured and the results were fitted by model calculations. In these fits the effective diffusion

coefficient and the porosity of the sample were used as the fitting parameters. The decay part of the breakthrough curve determines the effective diffusion coefficient while porosity is decisive for the rising part of the curve. In most cases there is no ambiguity as to the value of the diffusion coefficient, but the early rise and the levelling off of the breakthrough curve may be sensitive to inhomogenities within the sample. These inhomogenities are not included in the model, and the calculated and measured curves usually have a slightly different form at short times. There is therefore no unique way to do the fitting there, and two different ways of fitting were used for a consistency check. The first method was to fit the model curve to the very beginning of the measured breakthrough curve (Figure 4.4-1.). Porosities defined in this way were labelled by ε_{p1}. The other method used was to fit the model curve at the turning point in the breakthrough curve (Figure 4.4-1.). Porosities defined in this way were labelled by ε_{p2}. One expects that if there are microcracks in the sample, ε_{p1} will underestimate the porosity. Otherwise the two values should be rather similar.

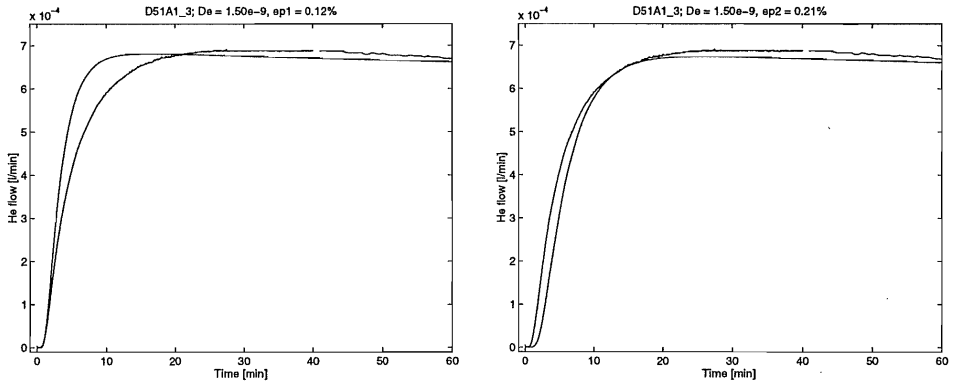

Figure 4.4-1. *Two different ways to determine the porosity.*

4.5 RESULTS

4.5.1 Sealing of the samples

To begin with one had to make sure that terostat sealing between the rock surface and the measuring chamber was He-tight. This test was carried out by comparing terostat sealing with sealing by He-tight epoxy resin. The measurements were done by using the through-diffusion method (Chapter 4.1). The results of these measurements are shown in Table 4.5-1. The first four measurements were done with terostat sealing. In the last two measurements the surface of the ring sample was covered with an epoxy resin. The space between the aluminium parts and the epoxy resin were filled with terostat. It is evident from these results that there is no detectable effect on the measured quantities caused by sealing.

Table 4.5-1.Results of the Terostat-Epoxy –comparison for ring sample D12.

Sealing	D_e [m^2/s]	ε_p [%]
Terostat	$5.75*10^{-9}$	0.20
	$5.30*10^{-9}$	0.15
	$5.10*10^{-9}$	0.15
	$5.00*10^{-9}$	0.16
Epoxy resin	$5.60*10^{-9}$	0.17
	$5.60*10^{-9}$	0.18

4.5.2 Ring samples

Two ring samples were measured and the average diffusion coefficient of sample D12 was $6.12 \cdot 10^{-9}$ m^2/s and that of sample D13 was $5.55 \cdot 10^{-9}$ m^2/s. The porosity of sample D12 was 0.16% and that of sample D13 0.15%. The data of six measurements are given in Table 4.5-2. Diffusion coefficients are also given for typical bigger molecules (M) in samples saturated by water (scaled by 1/35000). The measured and fitted breakthrough curves are shown in Appendix C.

Table 4.5-2. Porosities and effective diffusion coefficients of the ring samples.

Sample / Meas. no.	Porosity ε_p [%]	D_e [m^2/s] (He/N_2)	D_e [m^2/s] (M/H_2O)
D12 /1	0.18	$6.75 \cdot 10^{-9}$	$1.93 \cdot 10^{-13}$
/2	0.17	$6.05 \cdot 10^{-9}$	$1.73 \cdot 10^{-13}$
/3	0.13	$6.45 \cdot 10^{-9}$	$1.84 \cdot 10^{-13}$
/4	0.14	$6.20 \cdot 10^{-9}$	$1.77 \cdot 10^{-13}$
/5	0.18	$5.70 \cdot 10^{-9}$	$1.63 \cdot 10^{-13}$
/6	0.18	$5.55 \cdot 10^{-9}$	$1.59 \cdot 10^{-13}$
Average:	**0.16**	$\mathbf{6.12 \cdot 10^{-9}}$	$\mathbf{1.75 \cdot 10^{-13}}$
D13 /1	0.16	$6.50 \cdot 10^{-9}$	$1.86 \cdot 10^{-13}$
/2	0.16	$6.00 \cdot 10^{-9}$	$1.71 \cdot 10^{-13}$
/3	0.14	$4.60 \cdot 10^{-9}$	$1.31 \cdot 10^{-13}$
/4	0.13	$4.60 \cdot 10^{-9}$	$1.31 \cdot 10^{-13}$
/5	0.17	$6.00 \cdot 10^{-9}$	$1.71 \cdot 10^{-13}$
/6	0.14	$5.60 \cdot 10^{-9}$	$1.60 \cdot 10^{-13}$
Average:	**0.15**	$\mathbf{5.55 \cdot 10^{-9}}$	$\mathbf{1.59 \cdot 10^{-13}}$

4.5.3 Cubic samples

All cubic samples were measured by through diffusion of helium in the two main directions as shown in Figure 4.5-1. Both flow directions for each orientation were measured.

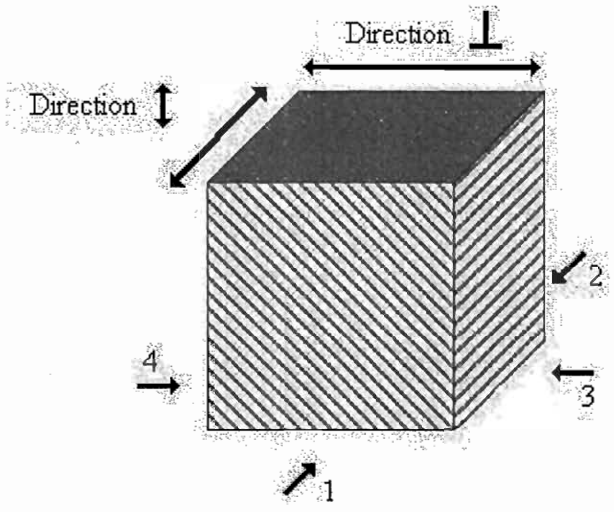

Figure 4.5-1*. The four measuring directions.*

The measured effective diffusion coefficient D_e (He/N_2) of the cubic samples varied between $0.54 \cdot 10^{-9}$ and $8.50 \cdot 10^{-9}$ m^2/s (Appendix D). The measured porosities ε_p by through-diffusion method of the samples were in the range 0.12 – 0.62% (Appendix D). There seems to be a rather clear orientation dependence in the measured diffusion coefficients due to the structure of the samples, and also in the connectivity of the pore space, as indicated by the apparent orientation dependence of the porosity. The averages of the measured values for each sample and direction are shown in Table 4.5-3. The all measured and fitted breakthrough curves with the determined parameters are shown in Appendix D.

The directions perpendicular to the structural orientation of the sample (directions 3 and 4) are labelled by ⊥ and those parallel to the structural orientation (directions 1 and 2) by ↕. The actual flow direction within either structural direction did not affect the measured values. Therefore the values for directions 1 and 2 (similarly for directions 3 and 4) have not been distinguished in calculating the averages (see Figure 4.5-1).

It can be seen from the results shown in Table 4.5-3 that the effective diffusion coefficients are larger for the samples with a disturbed zone (samples A) than for the intact samples (samples B). Also, the diffusion coefficients are smaller in direction ⊥ than in direction ↕, and thus there is evidence of structure dependent orientational effects. Porosities are also bigger in direction ↕ but there is no clear difference between samples A and

B. Porosities ε_{p1} and ε_{p2} are close to each other for the intact samples B, but differ somewhat for samples A with a disturbed zone. This is expected to be a result of inhomogeneties appearing in samples A.

The samples were first measured in the $\perp$ direction, after which they were further sawed before doing the measurements in direction $\updownarrow$.

Table 4.5-3. The effective diffusion coefficients and porosities for the cubic samples.

Sample	Direction	D_e [m^2/s] (He/N_2)	D_e [m^2/s] (M/H_2O)	ε_{p1} [%]	ε_{p2} [%]
D5.1					
A	$\perp$	$2.38 \cdot 10^{-9}$	$6.79 \cdot 10^{-14}$	0.22	0.34
	$\updownarrow$	$7.38 \cdot 10^{-9}$	$21.1 \cdot 10^{-14}$	0.30	0.54
B	$\perp$	$0.60 \cdot 10^{-9}$	$1.70 \cdot 10^{-14}$	0.15	0.19
	$\updownarrow$	$2.17 \cdot 10^{-9}$	$6.21 \cdot 10^{-14}$	0.28	0.29

Sample	Direction	D_e [m^2/s] (He/N_2)	D_e [m^2/s] (M/H_2O)	ε_{p1} [%]	ε_{p2} [%]
D14.2					
A	$\perp$	$2.03 \cdot 10^{-9}$	$5.80 \cdot 10^{-14}$	0.19	0.29
	$\updownarrow$	$4.17 \cdot 10^{-9}$	$11.9 \cdot 10^{-14}$	0.20	0.30
B	$\perp$	$0.79 \cdot 10^{-9}$	$2.26 \cdot 10^{-14}$	0.19	0.23
	$\updownarrow$	$2.16 \cdot 10^{-9}$	$6.16 \cdot 10^{-14}$	0.40	0.45

Sample	Direction	D_e [m^2/s] (He/N_2)	D_e [m^2/s] (M/H_2O)	ε_{p1} [%]	ε_{p2} [%]
D15.1					
A	$\perp$	$1.68 \cdot 10^{-9}$	$4.80 \cdot 10^{-14}$	0.13	0.25
	$\updownarrow$	$5.31 \cdot 10^{-9}$	$15.2 \cdot 10^{-14}$	0.22	0.38
B	$\perp$	$1.17 \cdot 10^{-9}$	$3.34 \cdot 10^{-14}$	0.25	0.29
	$\updownarrow$	$2.76 \cdot 10^{-9}$	$7.87 \cdot 10^{-14}$	0.31	0.39

5 PERMEABILITY MEASUREMENTS

5.1 MEASURING TECHNIQUES

The experimental set-up of permeability measurements is similar to that of the through-diffusion measurements.

The surface of the sample in the injection cell is exposed to an elevated pressure of helium. This is the inner surface of the central hole in the case of the ring samples and one of the rectangular faces in the case of the cubic samples. A constant pressure difference is maintained between the opposite surfaces. The outer surface of the sample is flushed with nitrogen, and the concentration of helium in the nitrogen is measured. The flow rate of helium through the sample is measured for several pressure differences. For each pressure difference, the flow rate is let to stabilize before reading its value. The purity of the helium used was 99.995% and that of the nitrogen 99.9%.

5.2 INTERPRETATION

In the case when a pressure difference exists across the sample, helium transport through the sample is mediated by diffusion and also by flow induced by the pressure gradient. According to Fick's and d'Arcy's laws for a compressible fluid, the volume flow of helium through the sample is then given by (Dullien 1979)

$$Q = Q_{diff} + \frac{KA}{\mu l}\frac{\left(p_2^2 - p_1^2\right)}{2p_1} \quad , \tag{5.2-1}$$

where Q [m^3/s] is the flow rate through the sample, Q_{diff} [m^3/s] is the flow rate due to diffusion only, K [m^2] is the permeability coefficient, A [m^2] is the cross-sectional area of the sample, μ [Pa s] is the dynamic viscosity of helium gas, l [m] is the length of the sample, p_2 [Pa] is the pressure of helium in the injection cell, and p_1 [Pa] is the pressure of helium at the outlet. The total flow rate through the sample is measured for several pressure differences, and the permeability coefficient is determined from a fit to the measured points by Equation (5.2-1) (Figure 5.2-1).

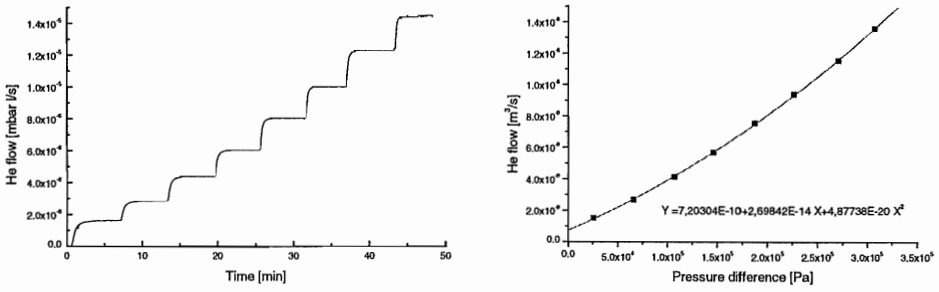

Figure 5.2-1. Permeability measurement and fitted curve.

The measured permeabilities, K [m^2], can be used to determine the hydraulic conductivities, K_H [m/s], of the samples. These are given by (Dullien 1979)

$$K_H = \frac{\rho g}{\mu} K, \qquad (5.2\text{-}2)$$

where ρ is the density of water (ρ = 997.08 kg/m^3 at 25°C (Kell 1967)), g is the acceleration of gravity at sea level (g = 9.81 m/s^2), and μ is the dynamic viscosity of water ($\mu = 8.9042*10^{-4}$ kg/ms at 25°C (Weast 1974-1975)).

5.3 RESULTS

5.3.1 Ring samples

The averages of the measured permeabilities and hydraulic conductivities, K_H, for the ring sample are shown in Table 5.3-1. The measured permeability coefficients of the ring samples varied between $4.61 \cdot 10^{-19}$ and $1.19 \cdot 10^{-18}$ m^2. The error in the permeability coefficients was within 10%. The measured and fitted permeability curves for the ring samples are shown in Appendix E.

Table 5.3-1. Measured permeabilities and hydraulic conductivities of the ring samples.

Sample	K [m^2]	K_H [m/s]
D12	$1.04 \cdot 10^{-18}$	$1.14 \cdot 10^{-11}$
D13	$5.25 \cdot 10^{-19}$	$5.77 \cdot 10^{-12}$

5.3.2 Cubic samples

The permeabilities of the cubic samples varied between $0.26 \cdot 10^{-19}$ and $8.83 \cdot 10^{-19}$ m^2. Permeabilities were larger for the samples with a disturbed zone, and larger in direction ↕ than in direction ⊥. The permeability coefficients did not correlate exactly with the diffusion coefficients. This means that there are some differences between the channels that play an important role in diffusion and in permeability. The average values of these quantities for each sample and direction are shown in Table 5.3-2. The measured and fitted permeability curves for the cubic samples are shown in Appendix F.

Table 5.3-2. Measured permeability coefficients and hydraulic conductivities of the cubic samples.

Sample	Direction	K [m^2]	K_H [m/s]
D5.1			
A	⊥	$2.92 \cdot 10^{-19}$	$3.21 \cdot 10^{-12}$
	↕	$6.62 \cdot 10^{-19}$	$7.27 \cdot 10^{-12}$
B	⊥	$0.35 \cdot 10^{-19}$	$0.38 \cdot 10^{-12}$
	↕	$3.03 \cdot 10^{-19}$	$3.33 \cdot 10^{-12}$

Sample	Direction	K [m^2]	K_H [m/s]
D14.2			
A	⊥	$5.44 \cdot 10^{-19}$	$5.98 \cdot 10^{-12}$
	↕	$7.50 \cdot 10^{-19}$	$8.24 \cdot 10^{-12}$
B	⊥	$0.26 \cdot 10^{-19}$	$0.29 \cdot 10^{-12}$
	↕	$3.16 \cdot 10^{-19}$	$3.47 \cdot 10^{-12}$

Sample	Direction	K [m^2]	K_H [m/s]
D15.1			
A	⊥	$4.12 \cdot 10^{-19}$	$4.53 \cdot 10^{-12}$
	↕	$8.83 \cdot 10^{-19}$	$9.70 \cdot 10^{-12}$
B	⊥	$0.73 \cdot 10^{-19}$	$0.80 \cdot 10^{-12}$
	↕	$3.68 \cdot 10^{-19}$	$4.04 \cdot 10^{-12}$

6 CONCLUSIONS

Previous studies (Hartikainen et al. 1995b, Autio 1996, Autio&Siitari-Kauppi 1997) have shown that there is a disturbed zone caused by boring adjacent to the experimental full scale deposition holes in the Research Tunnel at Olkiluoto. The properties of the disturbed zone in a direction perpendicular to the disturbed surface have previously been measured using also He-gas methods (Autio et al. 1998, Hartikainen et al. 1995b).

In this study the degree of disturbance was established in terms of porosity, effective diffusion coefficient and permeability parallel to the disturbed surface. The directions parallel to the disturbed surface are obviously of more importance for migration than the direction perpendicular to it, because there is a continuous disturbed zone of microfracturing and porosity parallel to the surface forming a continuous migration pathway. The porosity of disturbed rock samples obtained by using He-pycnometry (0.45%) was clearly higher than that of the undisturbed ones (0.24%). By assuming the depth of approximately 6 mm for the disturbed zone, found in the previous similar analyses, this means that the average porosity of the actual zone was about 1-2%. The permeabilities and diffusion coefficients obtained for the disturbed rock samples were also clearly higher than those obtained for the undisturbed ones. The ratio between the average permeabilities of the disturbed and undisturbed rock samples was 3.2, and the ratio between the diffusion coefficients was 3.1, even for the relatively large samples used (so that the disturbed zone only comprised a small part of sample A).

The permeabilities and diffusion coefficients were also clearly oriented, being larger in the direction of the schistosity of the rock than at an angle of approximately 45° to the schistocity. The ratio between the average diffusion coefficients in these two directions (2.8) was the same in both the disturbed and the undisturbed rock samples, whereas the ratio between the average permeabilities was larger in the undisturbed (7.4) than in the disturbed rock samples (1.8). The averages of the measured values for the cubic samples are shown in Table 6-1. The original data are given in Appendices D and F.

Table 6-1. The averages of the measured values for the cubic samples.

Direction	Sample	D_e [m^2/s] (He/N_2)	ε_{p1} [%]	ε_{p2} [%]	K [m^2]
Total	**A**	$3.83 \cdot 10^{-9}$	0.21	0.35	$5.91 \cdot 10^{-19}$
	B	$1.61 \cdot 10^{-9}$	0.26	0.31	$1.87 \cdot 10^{-19}$
↕	**A**	$5.62 \cdot 10^{-9}$	0.24	0.41	$7.65 \cdot 10^{-19}$
	B	$2.36 \cdot 10^{-9}$	0.33	0.38	$3.29 \cdot 10^{-19}$
⊥	**A**	$2.03 \cdot 10^{-9}$	0.18	0.29	$4.16 \cdot 10^{-19}$
	B	$0.85 \cdot 10^{-9}$	0.19	0.24	$0.45 \cdot 10^{-19}$

The values obtained for permeability and diffusion coefficient depend on the penetration of the epoxy based sealing material in the pores and fractures in the disturbed surface, preventing rapid gas flow along the immediate surface layer. The degree of penetration of epoxy in the disturbed surface of rock samples will later be quantitatively studied by fluoroscene microscopy.

Another conclusion which can be drawn from the present analysis is that the structure of rock induces marked orientation dependence in the migration properties. In the samples with a disturbed zone, there was a difference in the diffusitivity and permeability in the two main directions by a factor of $2-4$. In the intact samples, however, there was an order of magnitude difference in the permeability, while in the diffusitivity the difference was again a factor of two or three. In the disturbed zone orientational effects were weaker.

In through-diffusion measurements one should thus pay attention to the oritentational effects due to the structure of rock. Otherwise it is not possible to relate the measured values with representative averages. It is obvious that the ring geometry provides a convenient way to directly measure values which are averages over all possible migration directions.

REFERENCES

Autio, J., Characterization of the excavation disturbance caused by boring of the experimental full scale deposition holes at TVO-Research Tunnel, Report POSIVA-96-09, Posiva Oy, Helsinki and similar report TR 97-24 in SKB's (Svensk Kärnbräslehantering AB) report series, 1996

Autio, J., Kirkkomäki, T, Boring of full scale deposition holes using a novel dry blind boring method. Report POSIVA-96-07, Posiva Oy, Helsinki and similar report PR D-96-030 in SKB's (Svensk Kärnbräslehantering AB) report series, 1996

Autio, J., Siitari-Kauppi, M., in Scientific Basis for Nuclear Waste Management XXI, edited by I.G. McKinley&C. McCombie. (Mater.Res.Soc.Proc 506 , Warrendale, PA,1997) pp. 597-604

Autio, J., Siitari-Kauppi, M., Timonen, J., Hartikainen, K.& Hartikainen, J., determination of the porosity, permeability and diffusitivity of rock in the excavation-disturbed zone around full-scale deposition holes using the ^{14}C-PMMA and He-gas methods. Contam. Hydr. 763, (1998)

Carslaw, H.S., Jaeger, J.C., Conduction of Heat in Solids, 2nd. Ed., Oxford University Press, Oxford, 1959

Dullien, F.A.L., Porous Media Fluid Transport and Pore Structure,Academic Press, Inc., San Diego, California, 1979

Hartikainen, K., Väätäinen, K., Hautojärvi, A., and Timonen, J., in Scientific Basis for Nuclear Waste Management XVII, edited by A. Barkatt & R. Van Konynenburg (Mater.Res.Soc. Proc., Pittsburgh, PA, 1994) pp. 821-826

Hartikainen, K., Hautojärvi, A., Pietarila, H. and Timonen, J., in Scientific Basis for Nuclear Waste Management XVIII, edited by T. Murakami and R.C. Ewing (Mater. Res. Soc. Proc., Pittsburgh, PA, 1995a) pp. 435-440

Hartikainen, K., Hautojärvi, A., Pietarila, H. and Timonen, J., Permeability and diffusivity measurements with the He-gas method of disturbed zone in rock samples cored from the full-scale experimental deposition holes in the TVO research tunnel, Report YJT-95-19, Nuclear Waste Commission of Finnish Power Companies, and similar report AR D-95-018 in SKB's report series, 1995b

Hartikainen, K., Pietarila, H., Rasilainen, K., Nordman, H., Ruskeenniemi, T., Hölttä, P., Siitari-Kauppi, M., and Timonen, J., Characterization of the altered zone around a fracture in Palmottu natural analogue, pp. 839-846 in Scientific Basis for Nuclear Waste Management XIX, W. M. Murphy and D. A. Knecht (eds.), MRS, Pittsburgh, 1996a

Hartikainen, J., Hartikainen, K., Hautojärvi, A., Kuoppamäki, K. and Timonen, J., Helium gas methods for rock characteristics and matrix diffusion. Report Posiva-96-22. Posiva Oy, Helsinki, 1996b

Kell G. S., Precise Presentation of Volume Properties of Water at One Atmosphere, Journal of Chemical and Engineering Data, Vol.12 (1967) pp.66-69

Taylor, J.R., An Introduction to Error Analysis, 2nd. Ed., 1997

Väätäinen, K., Timonen, J., Hautojärvi, A., in Symp. Scientific Basis for Nuclear Waste Management XVI, edited by C.G. Interrante & R.T. Pabalan (Mater. Res. Soc. Proc., Pittsburgh, PA, 1993) pp. 851-856

Weast, R.C., (ed.), Handbook of Chemistry and Physics, 55th. Ed., p. F49, Chemical Rubber Comppany Press, Cleveland, Ohio, 1974-1975

Appendix A

The drying curves for the cubic samples and test samples

D 5.1 drying curve

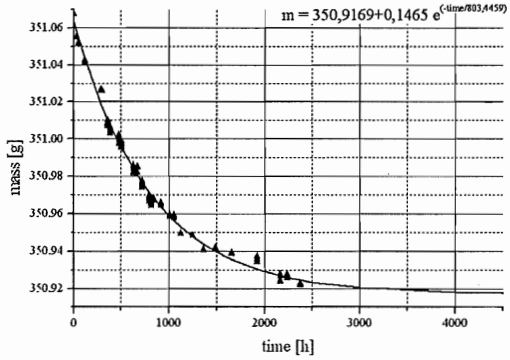

D 14.2 drying curve

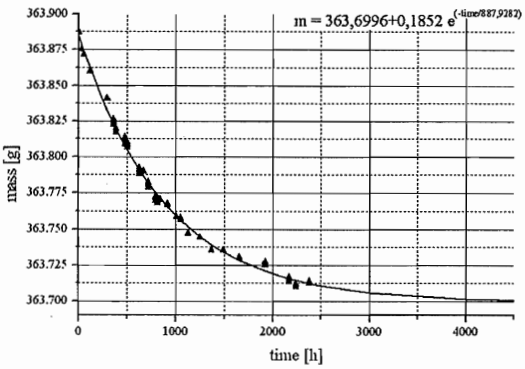

D 5.1 A drying curve

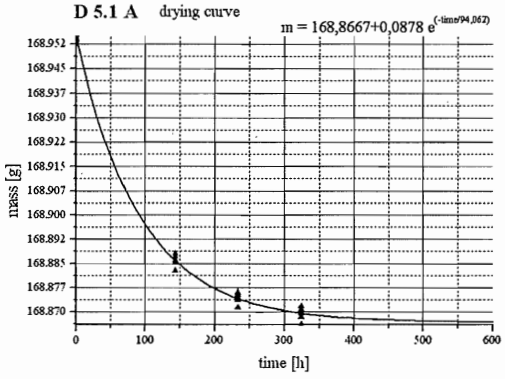

D 14.2 A drying curve

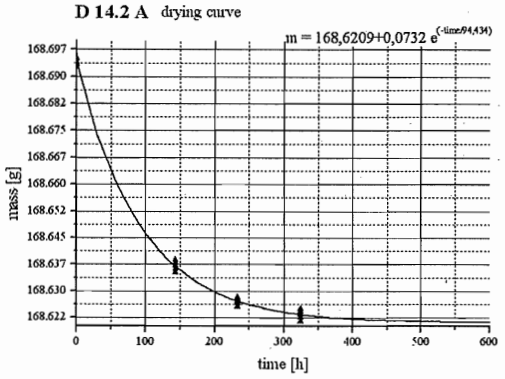

D 5.1 B drying curve

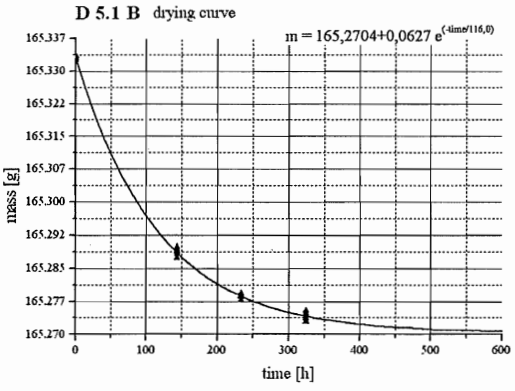

D 14.2 B drying curve

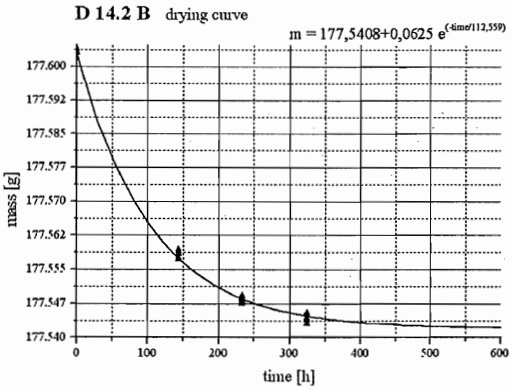

Appendix A

The drying curves for the cubic samples and test samples

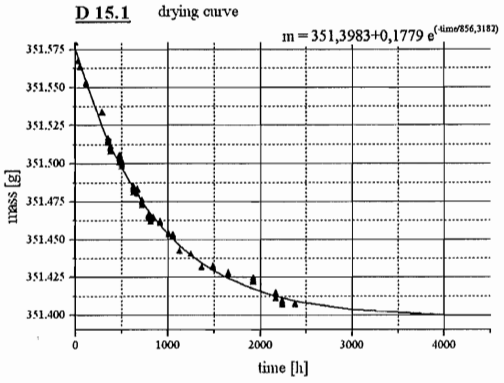

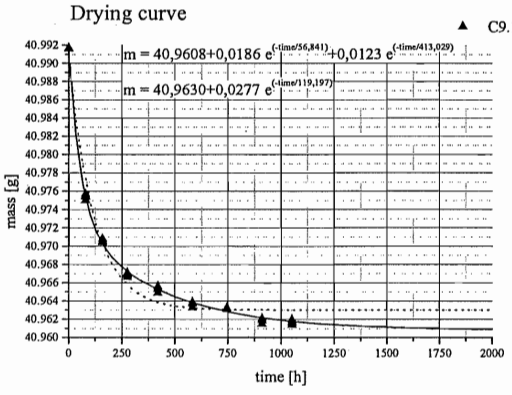

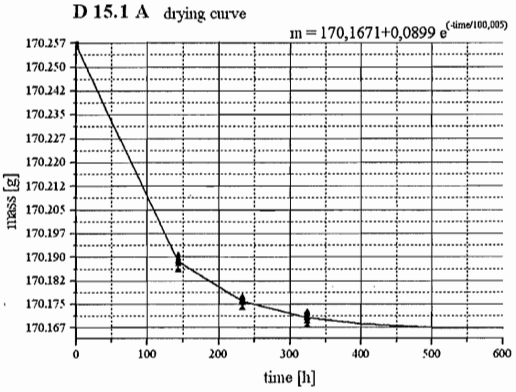

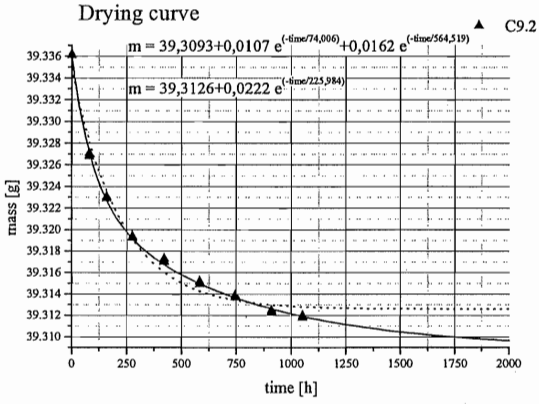

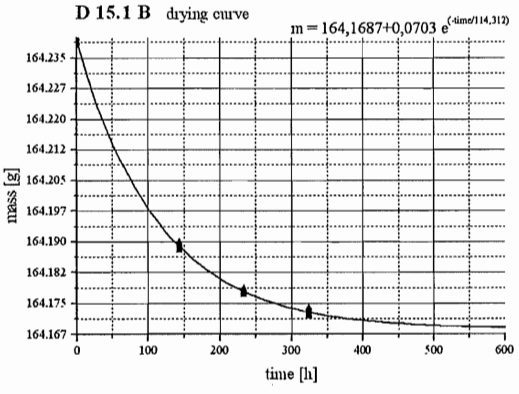

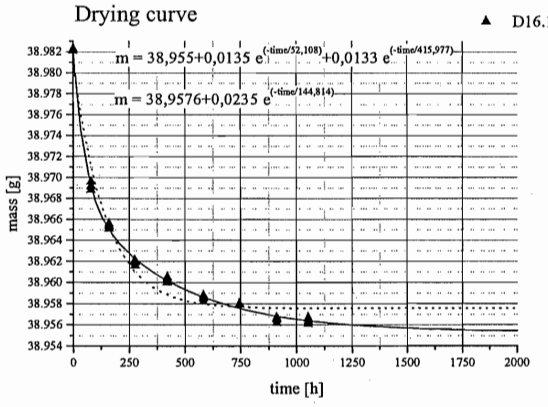

Appendix A

The drying curves for the cubic samples and test samples

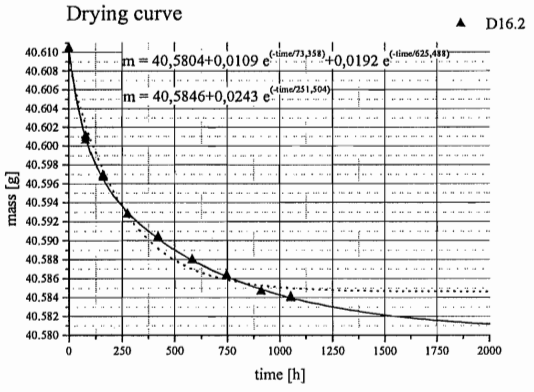

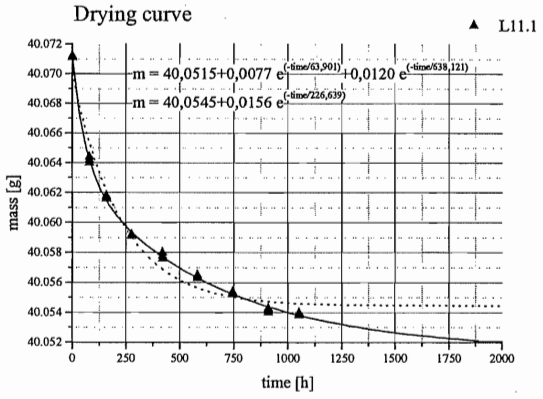

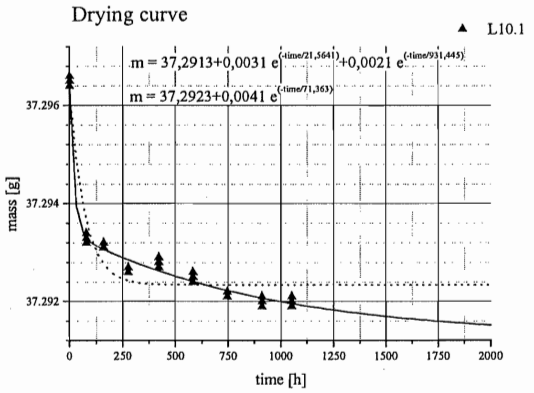

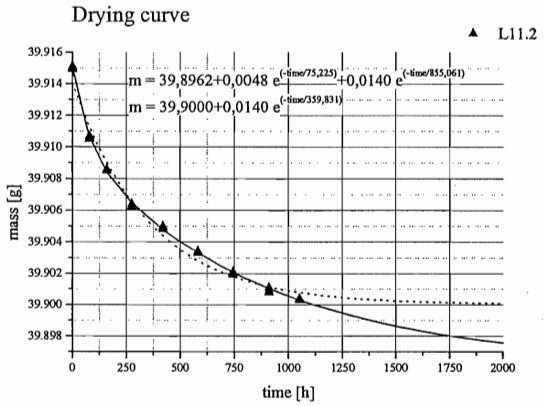

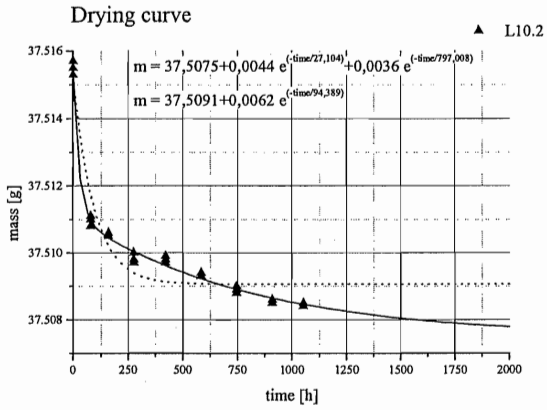

Appendix B

The bulk volume determinations

D 5.1 bulk volume determination

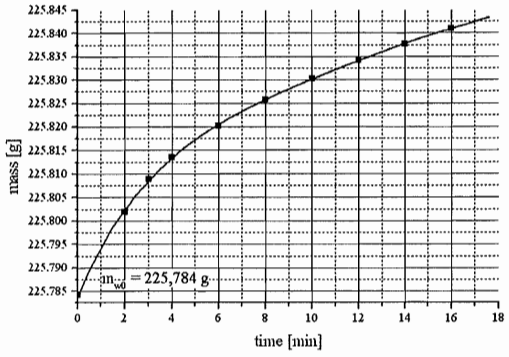

D 14.2 Bulk volume determination

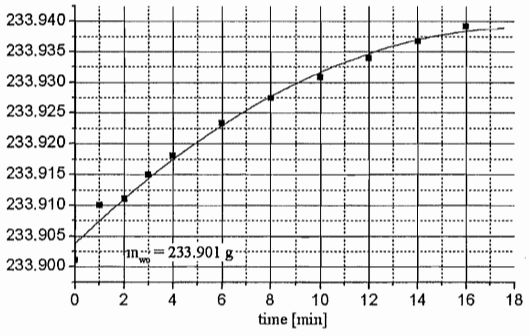

D 5.1 A bulk volume determination

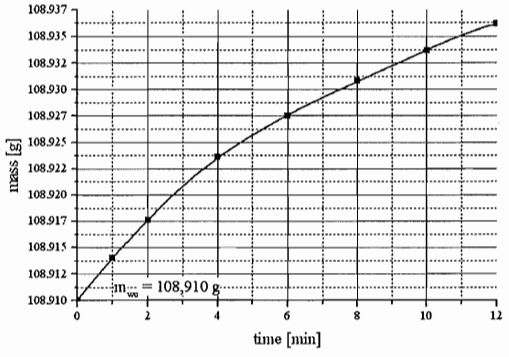

D 14.2 A bulk volume determination

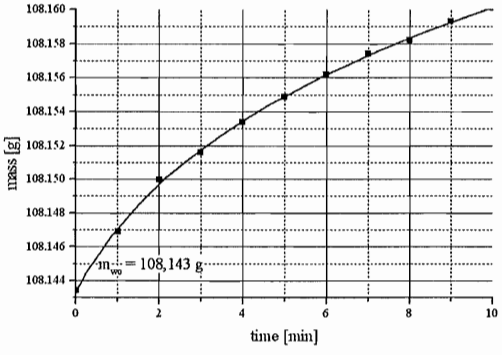

D 5.1 B bulk volume determination

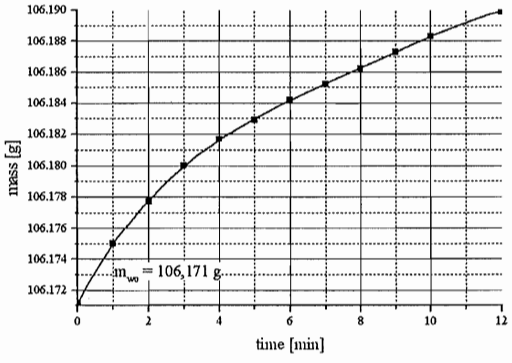

D 14.2 B bulk volume determination

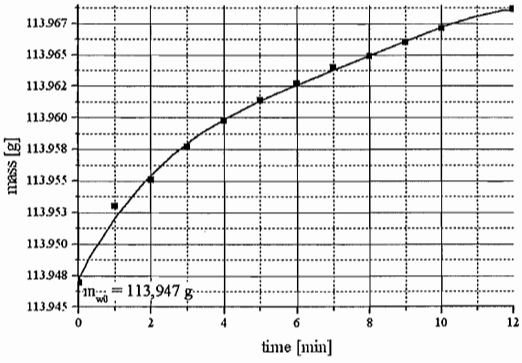

Appendix B

The bulk volume determinations

D 15.1 bulk volume determination

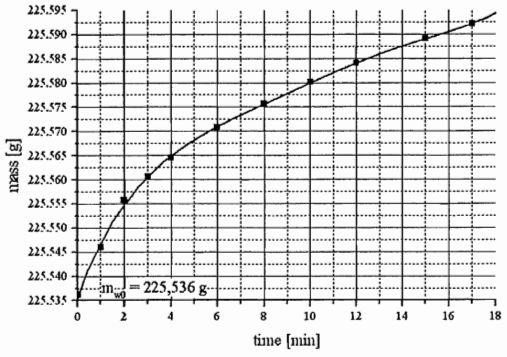

D 15.1 A bulk volume determination

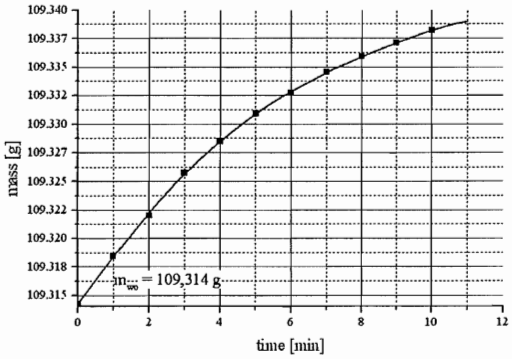

D 15.1 B bulk volume determination

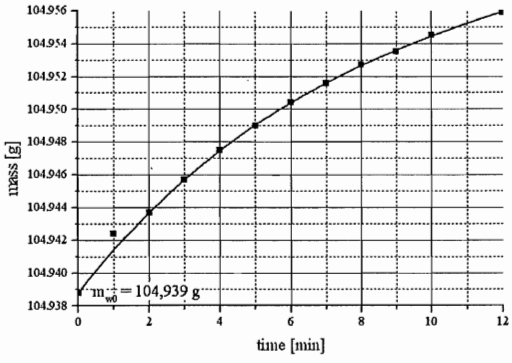

Appendix C

Diffusivity measurements on the ring samples

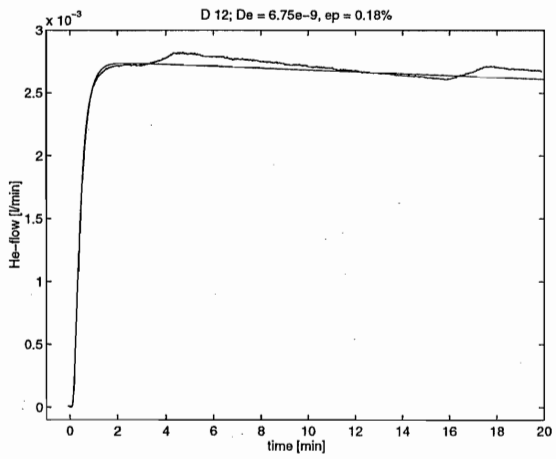

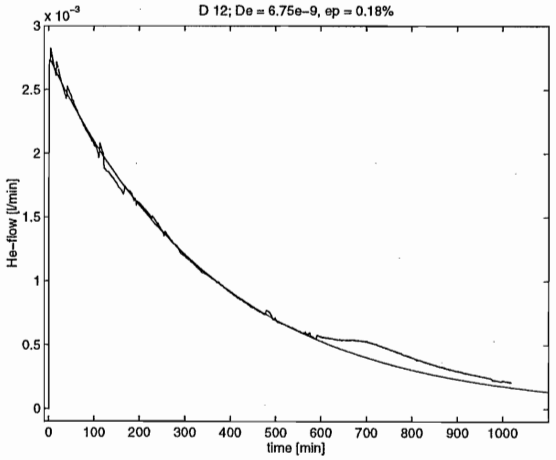

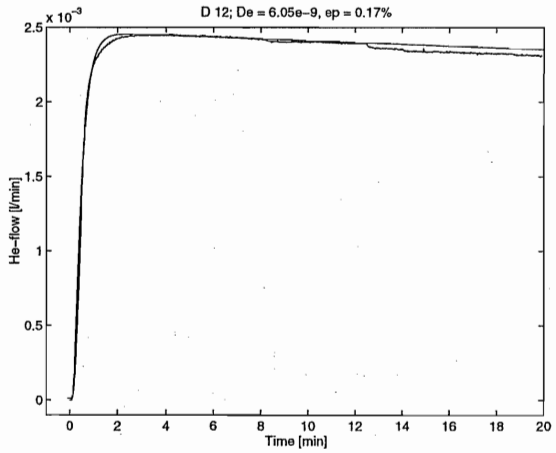

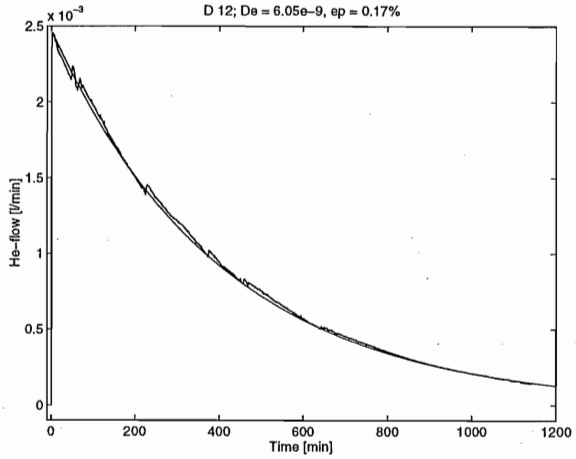

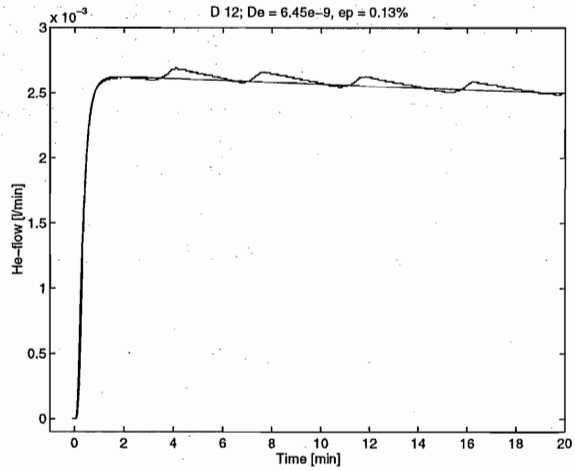

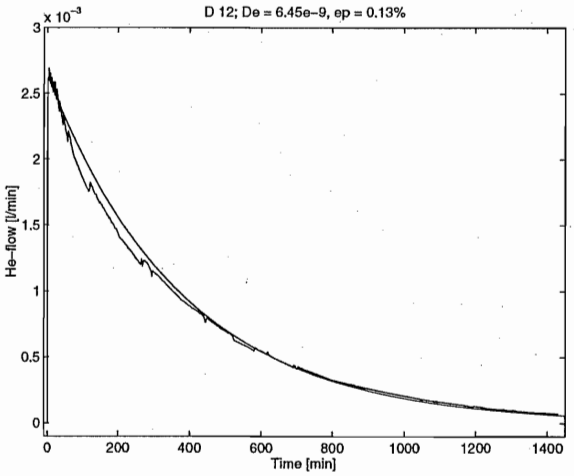

Appendix C

Diffusivity measurements on the ring samples

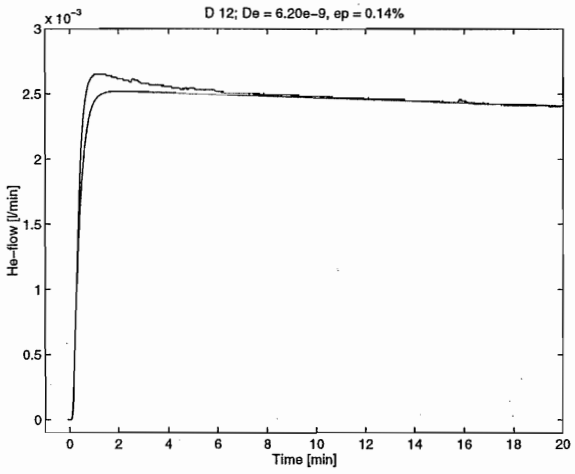

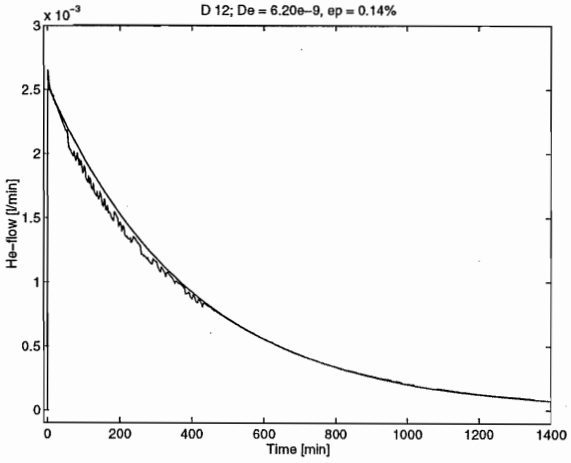

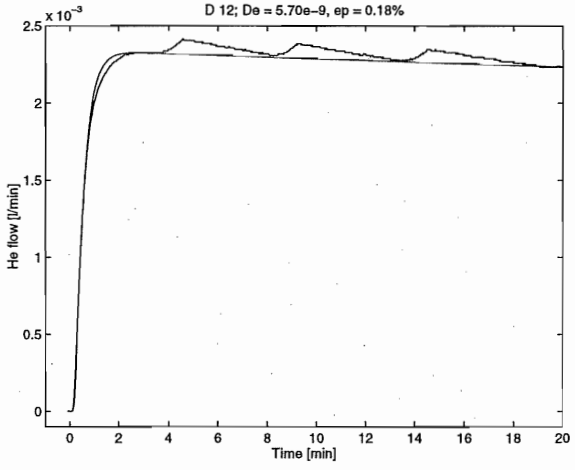

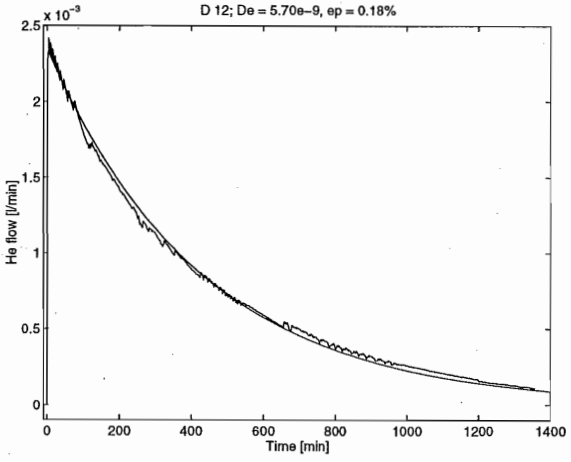

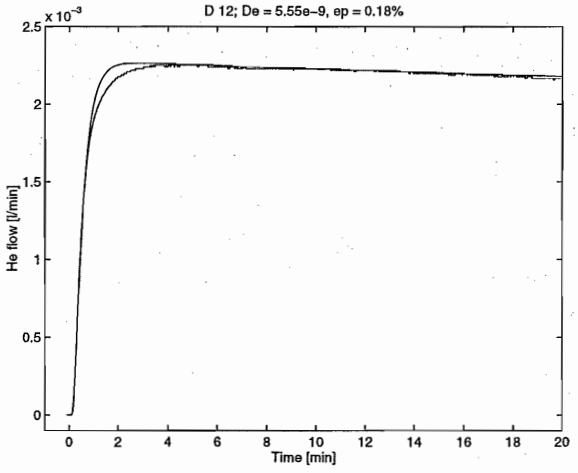

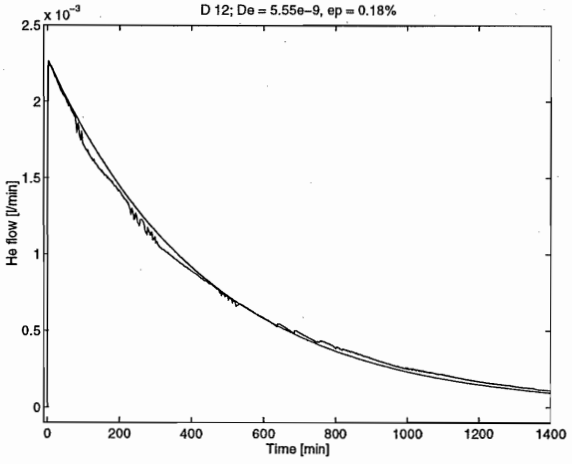

Appendix C

Diffusivity measurements on the ring samples

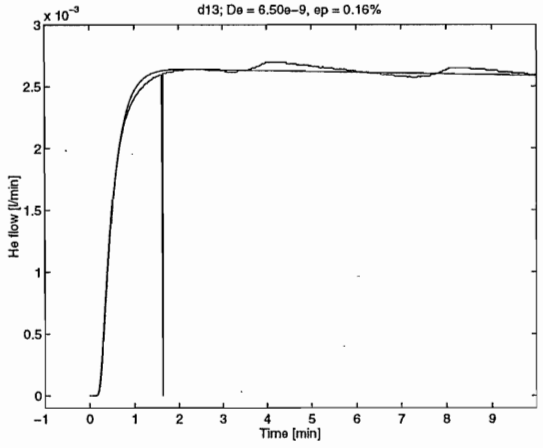

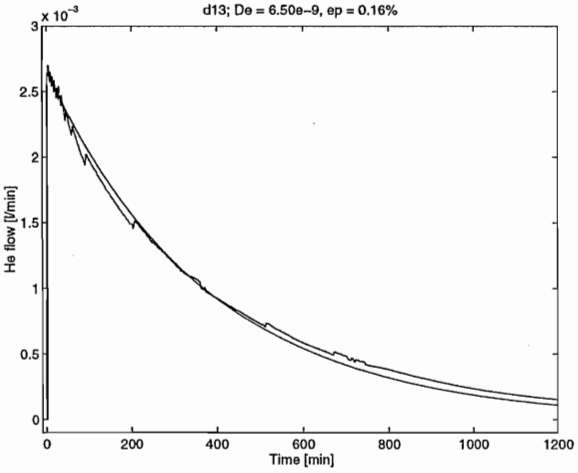

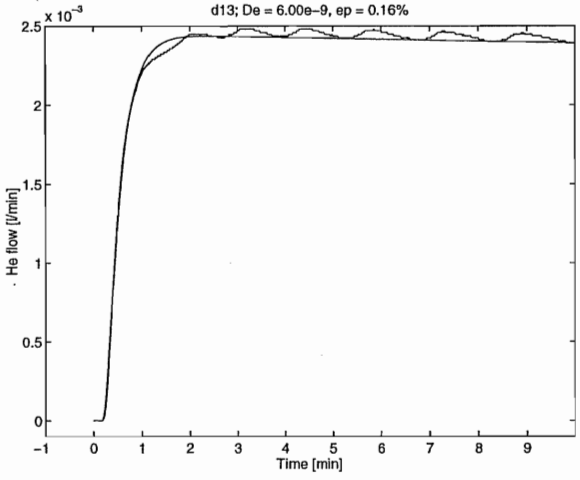

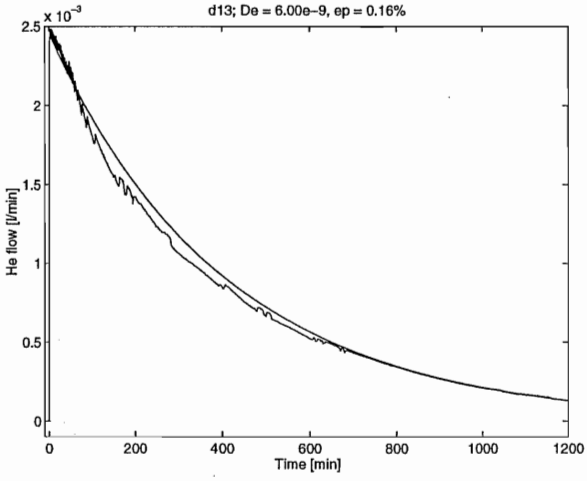

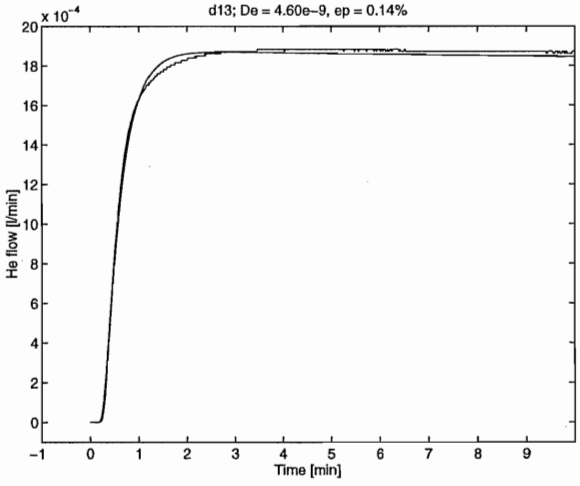

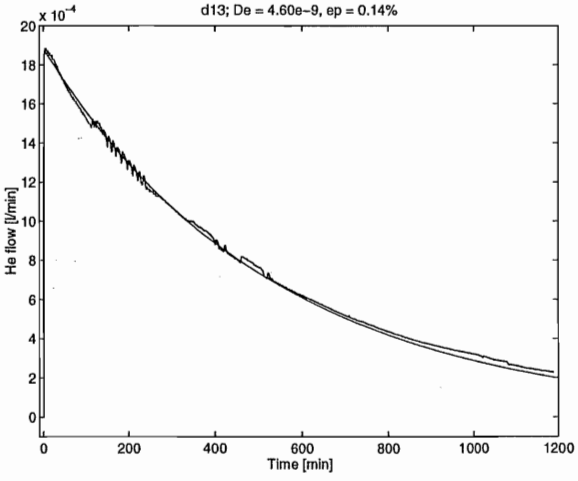

Appendix C

Diffusivity measurements on the ring samples

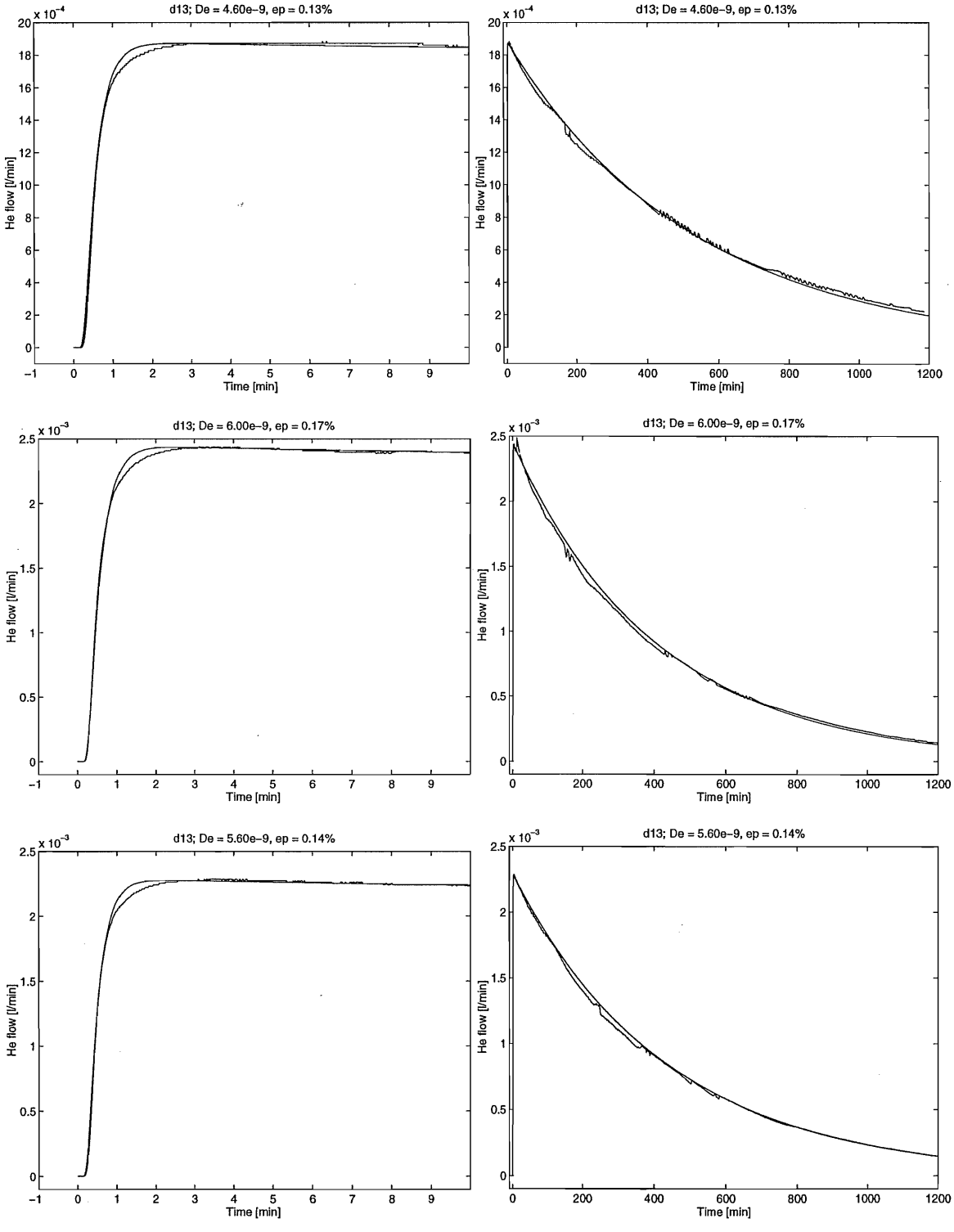

Appendix D

Diffusivity measurements on the cubic samples

D 5.1 A ⊥/ 1

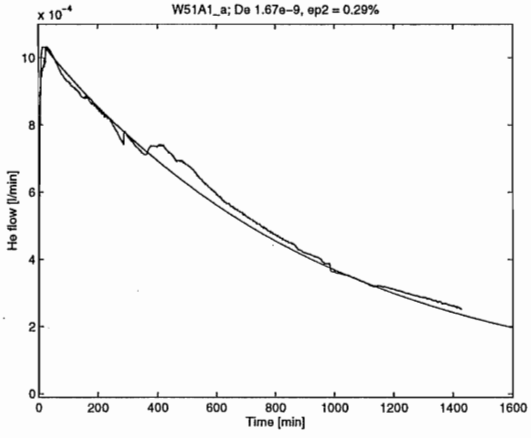

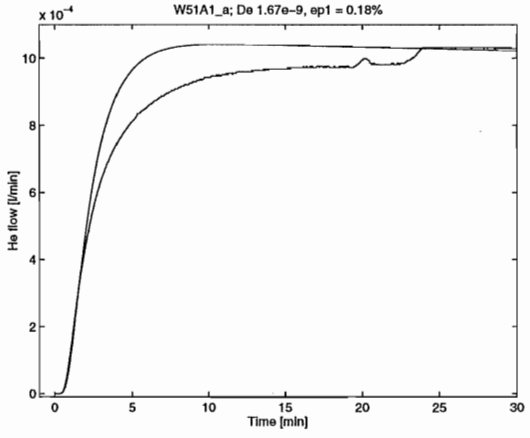

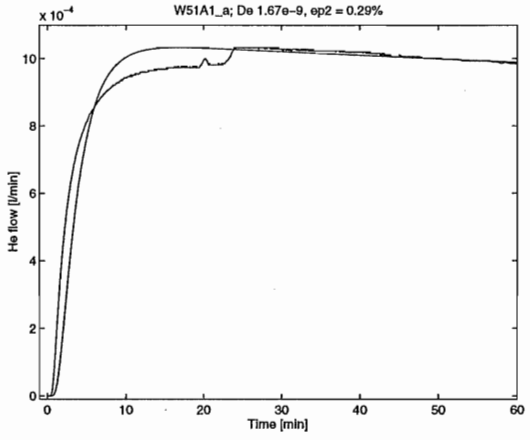

D 5.1 A ⊥/ 2

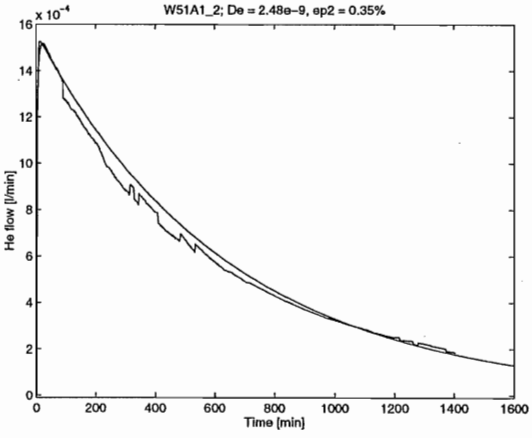

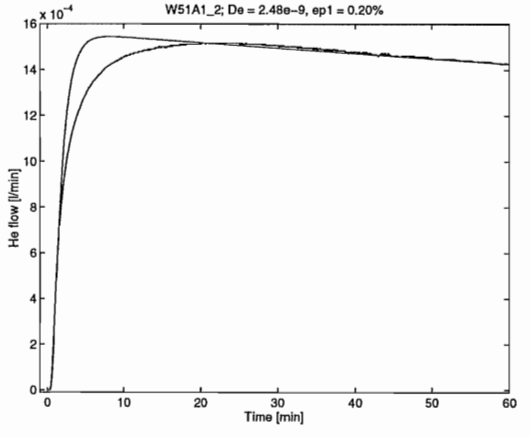

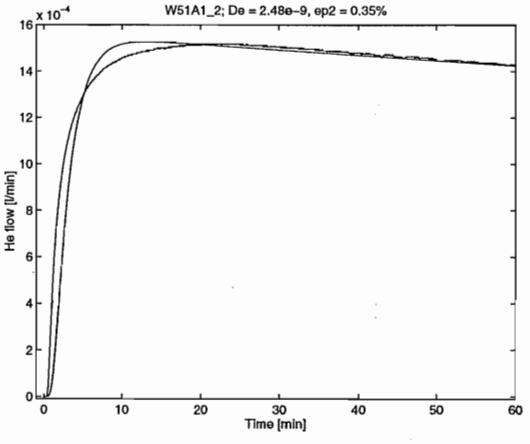

Appendix D

Diffusivity measurements on the cubic samples

D 5.1 A ⊥/ 3

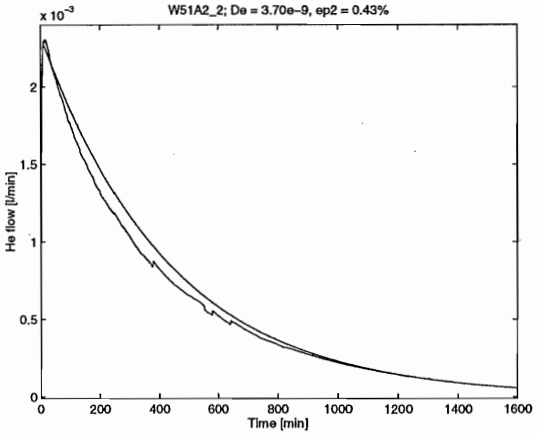

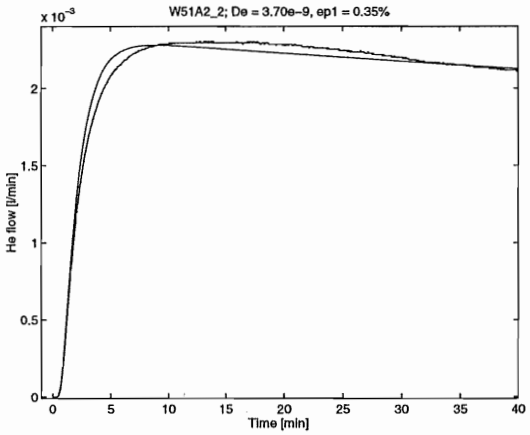

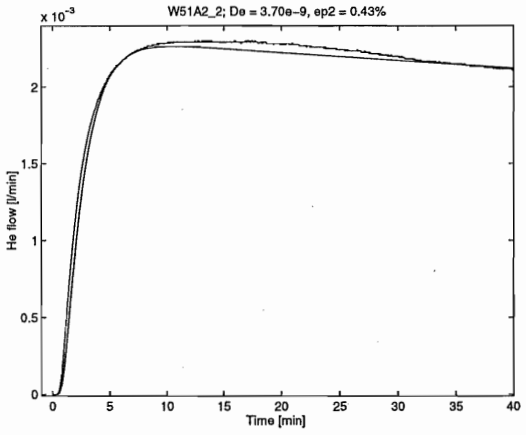

D 5.1 A ⊥/ 4

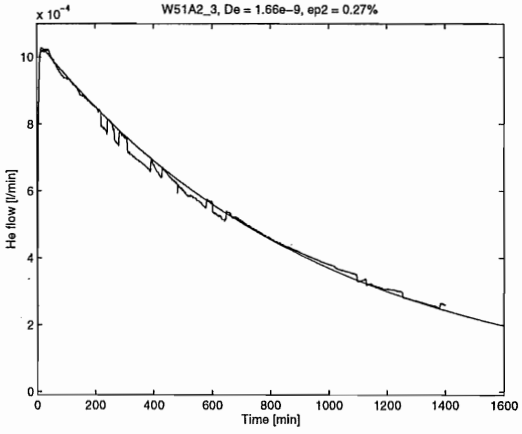

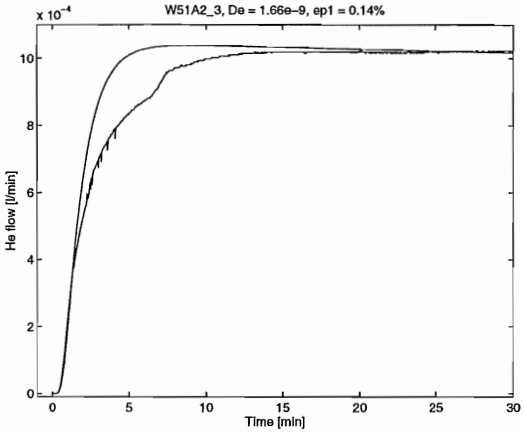

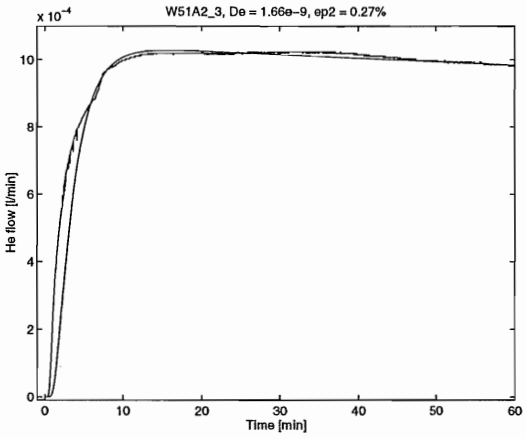

Appendix D

Diffusivity measurements on the cubic samples

D 5.1 A ↕/ 1

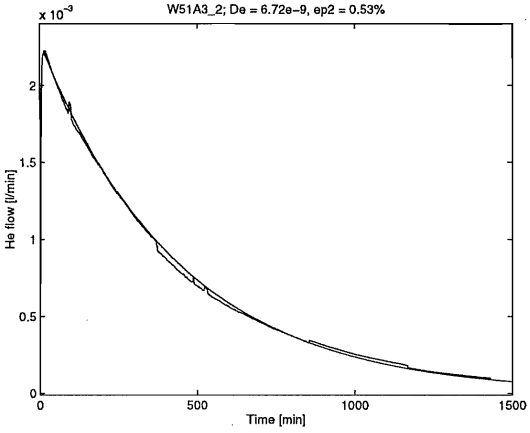

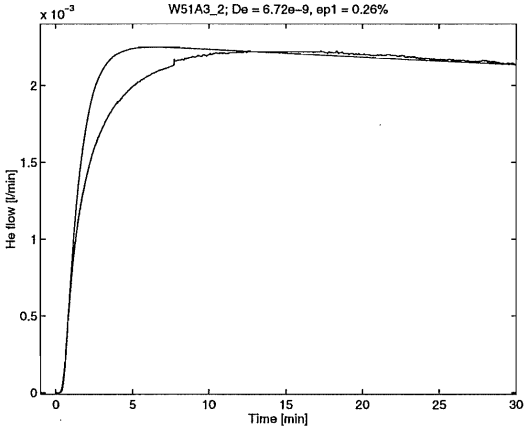

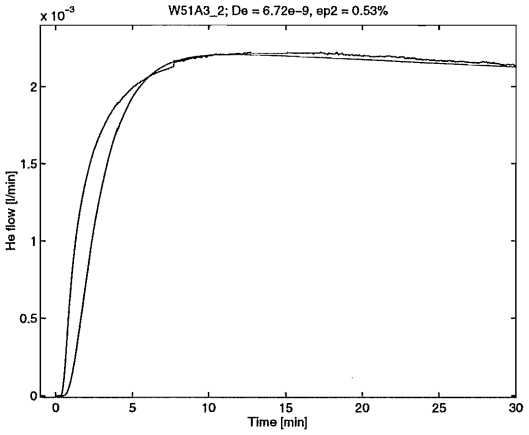

D 5.1 A ↕/ 2

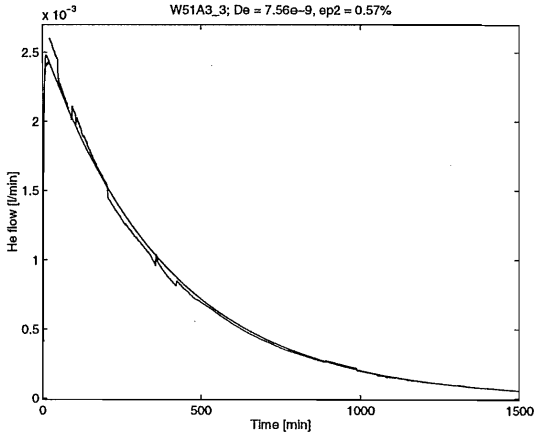

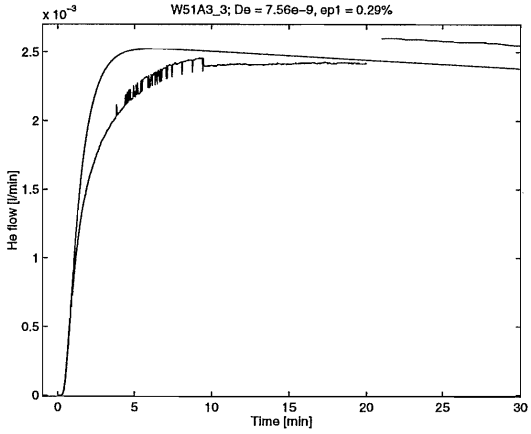

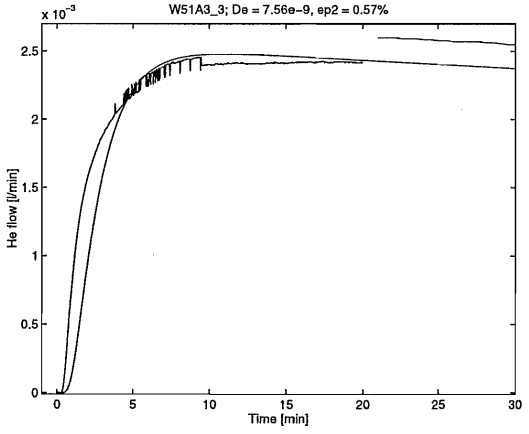

Appendix D

Diffusivity measurements on the cubic samples

D 5.1 A ↕/ 3

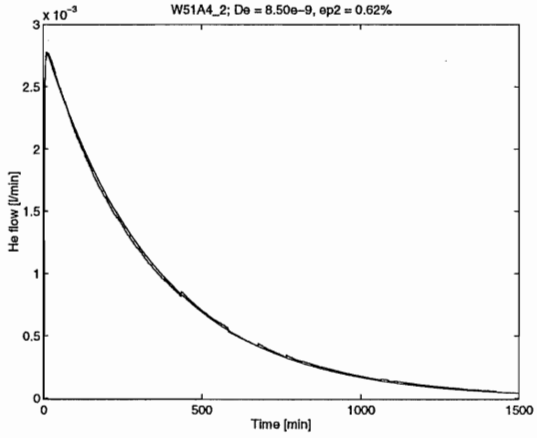

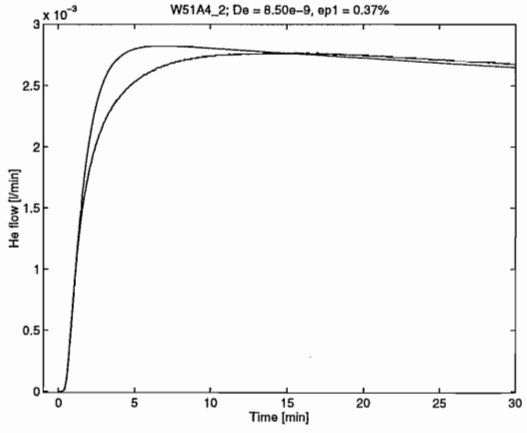

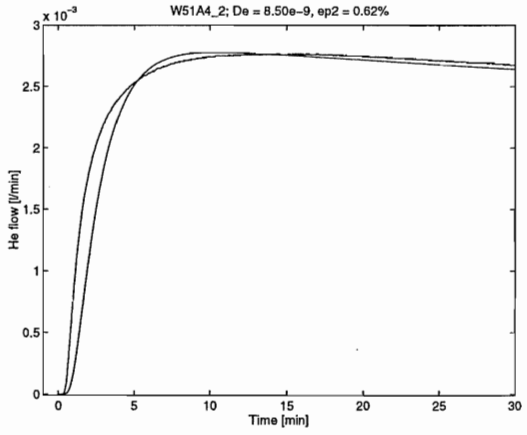

D 5.1 A ↕/ 4

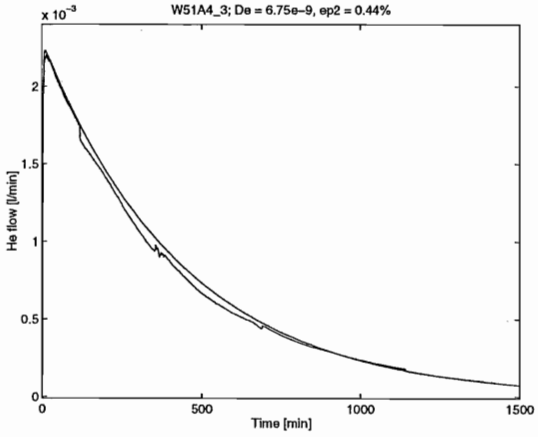

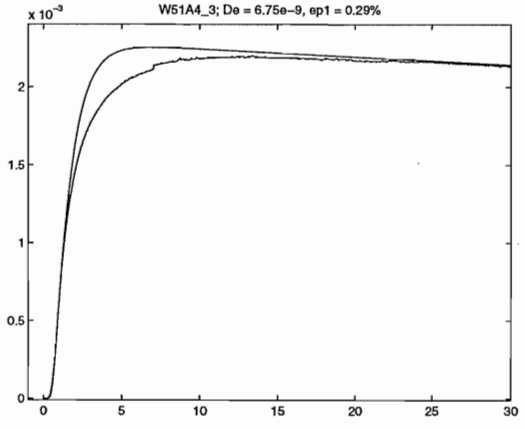

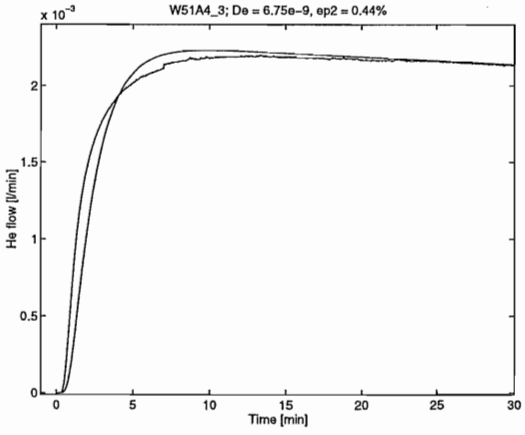

Appendix D

Diffusivity measurements on the cubic samples

D 5.1 B ⊥/ 1

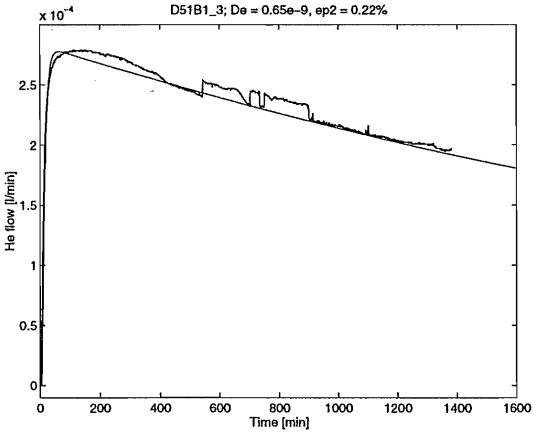

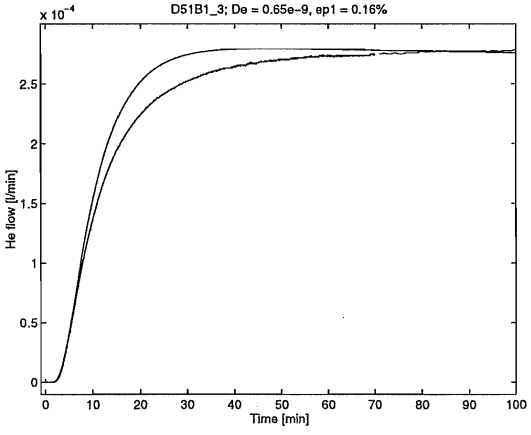

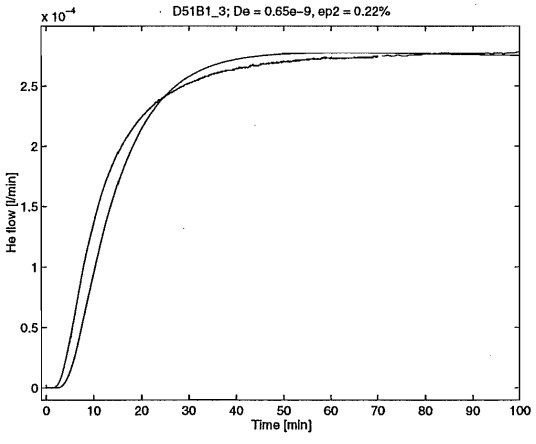

D 5.1 B ⊥/ 2

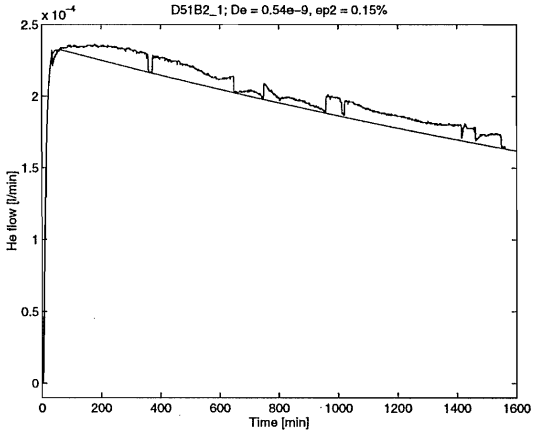

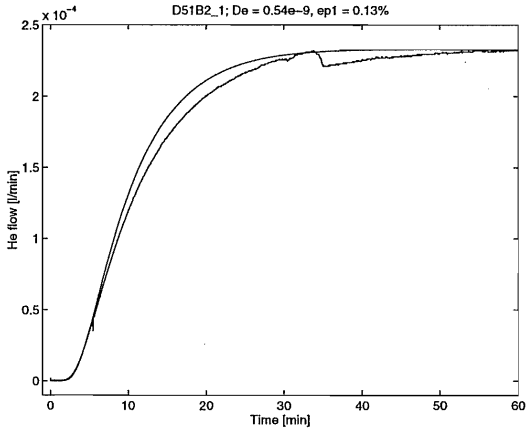

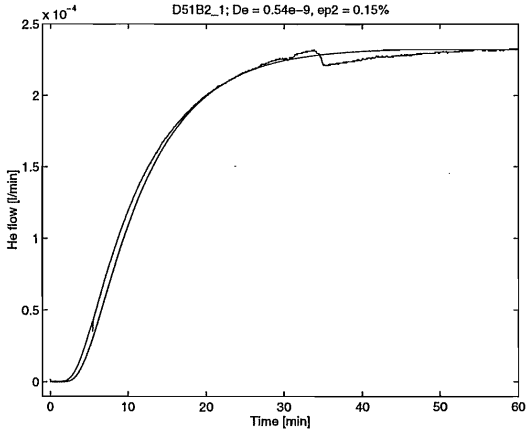

Appendix D

Diffusivity measurements on the cubic samples

D 5.1 B ↕/ 1

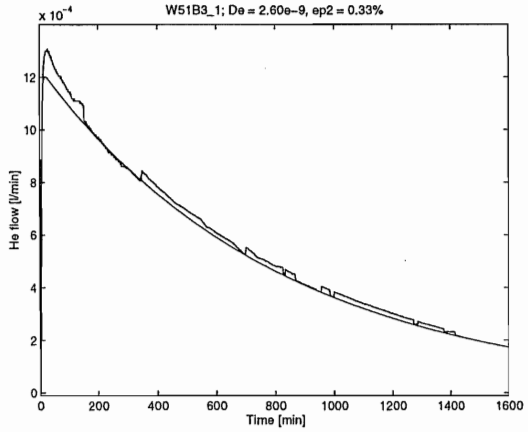

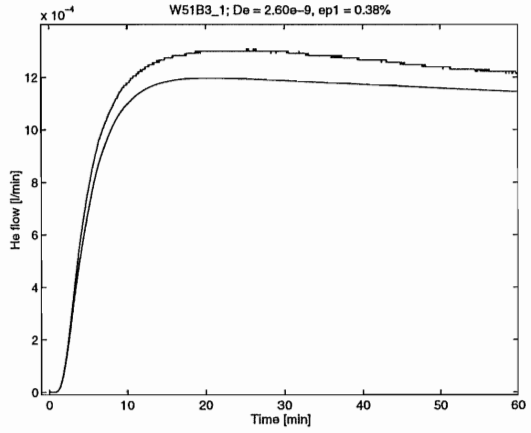

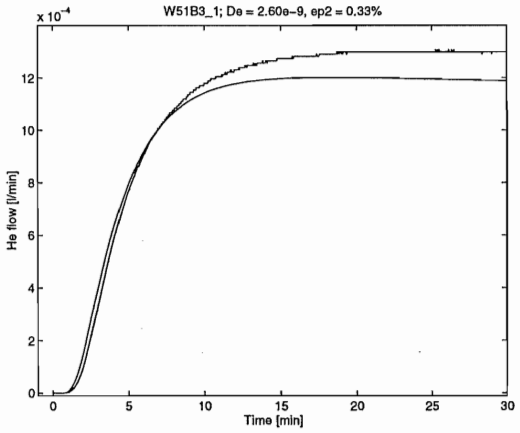

D 5.1 B ↕/ 2

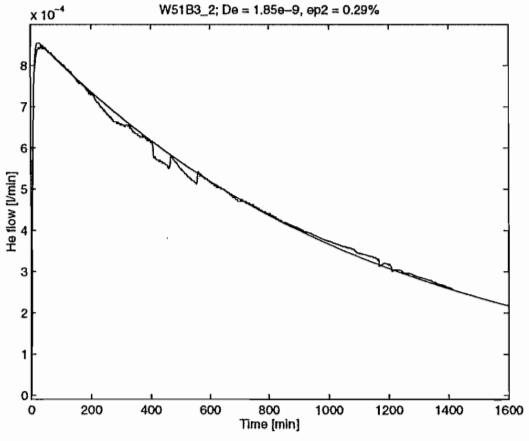

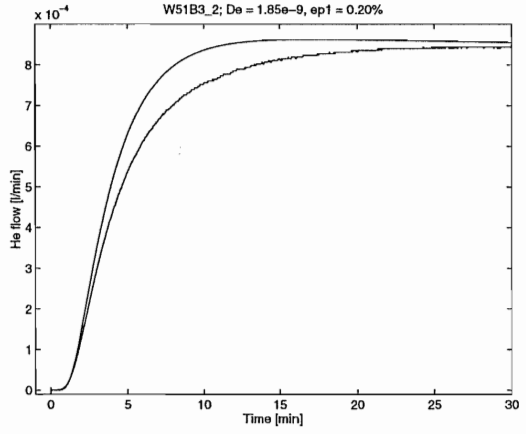

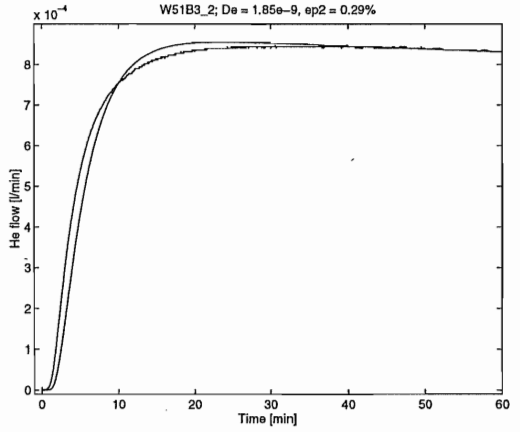

Appendix D

Diffusivity measurements on the cubic samples

D 5.1 B ↕/ 3

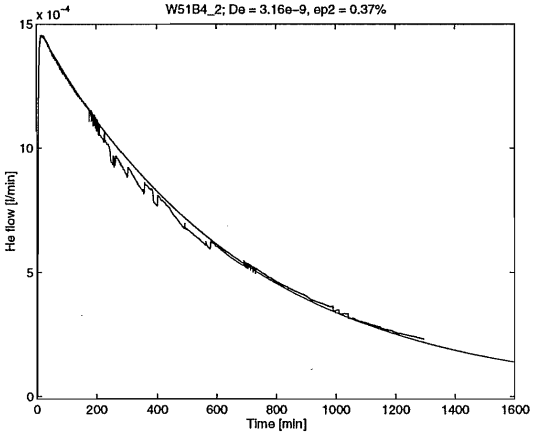

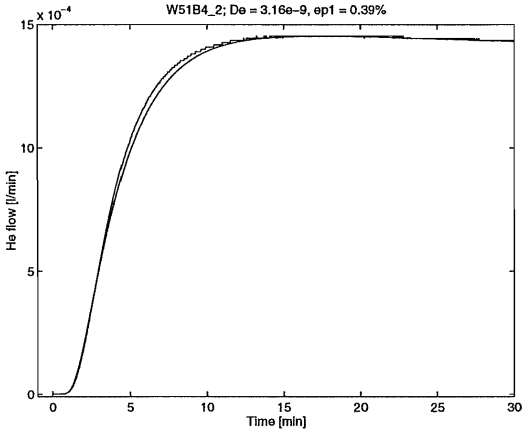

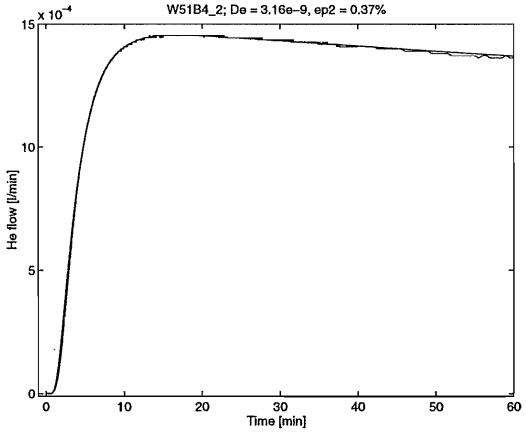

D 5.1 B ↕/ 4

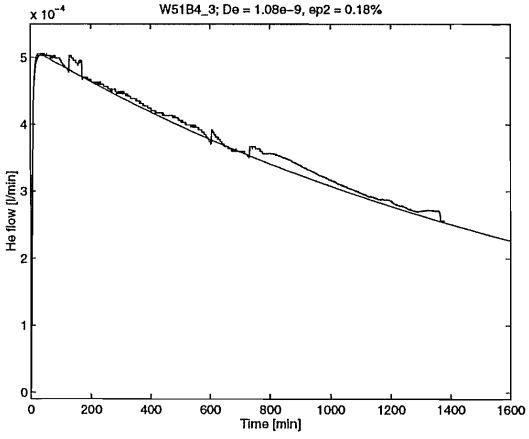

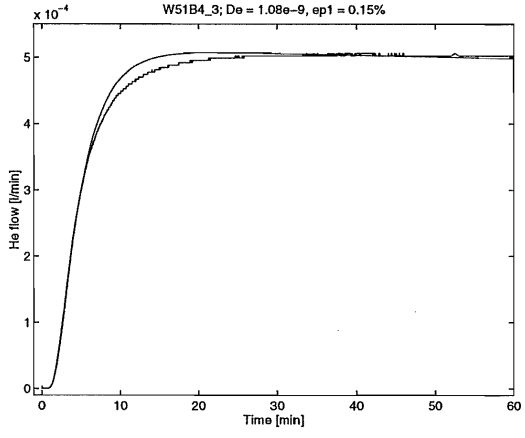

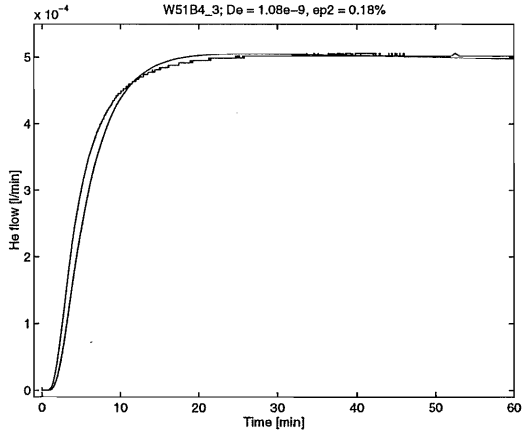

Appendix D

Diffusivity measurements on the cubic samples

D 14.2 A ⊥/ 1

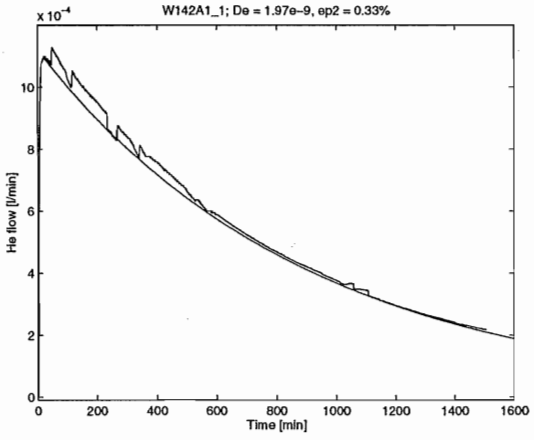

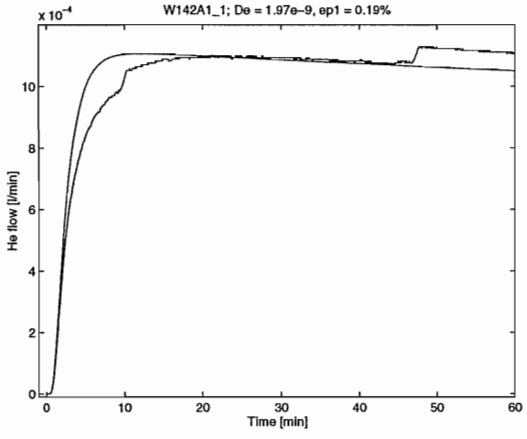

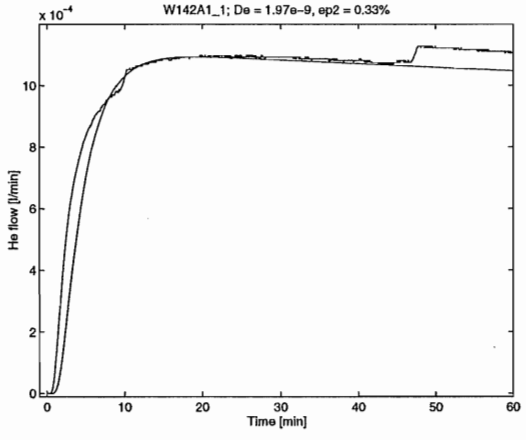

D 14.2 A ⊥/ 2

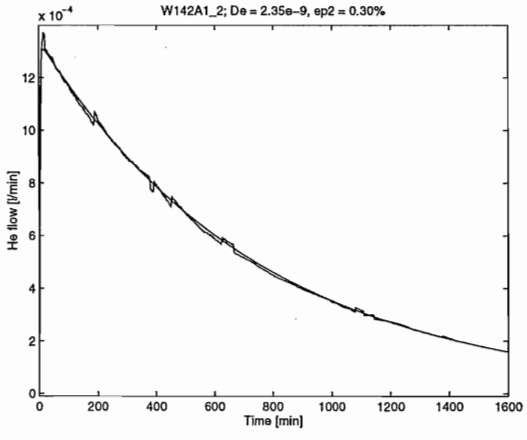

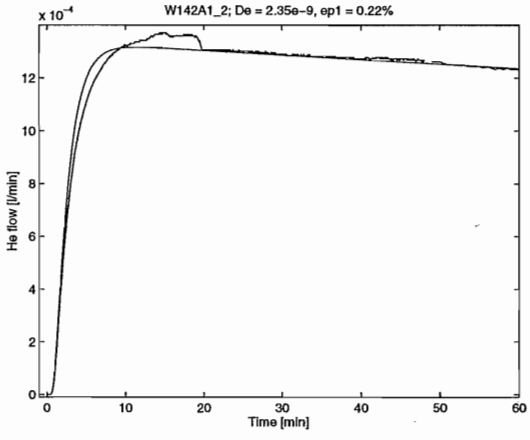

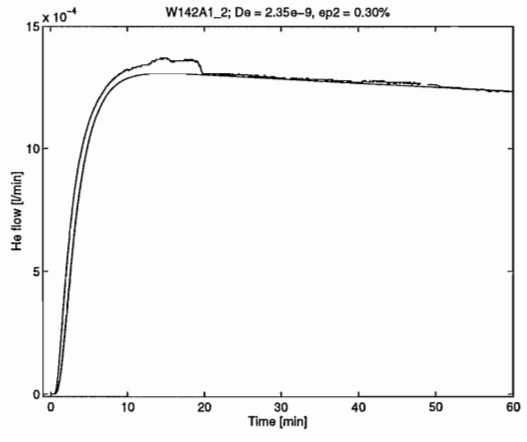

Appendix D

Diffusivity measurements on the cubic samples

D 14.2 A ⊥/ 3

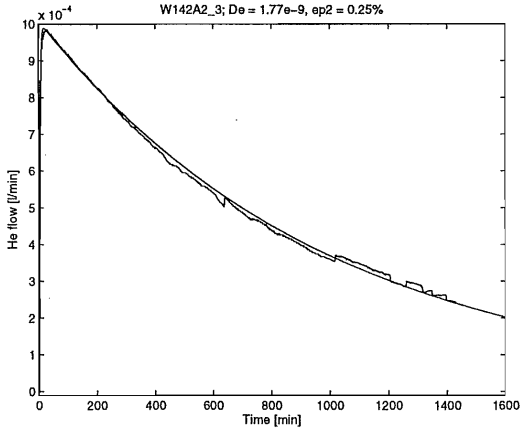

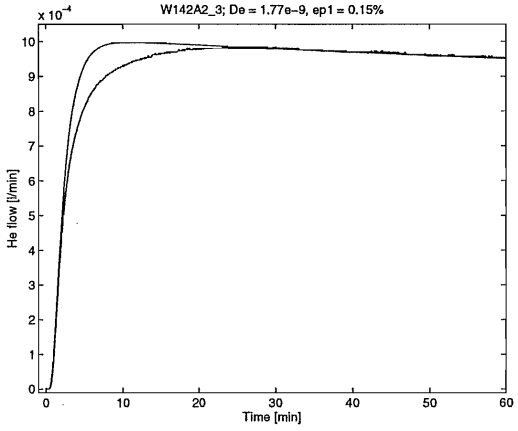

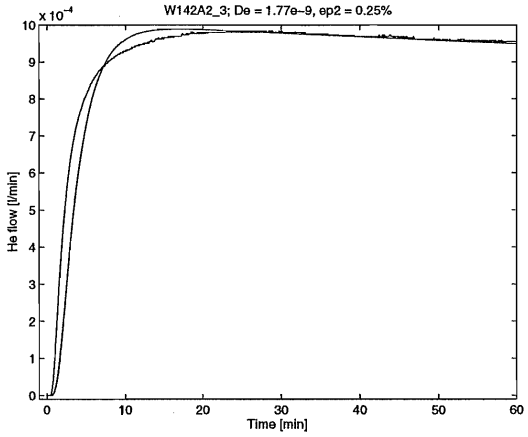

D 14.2 A ↕/ 1

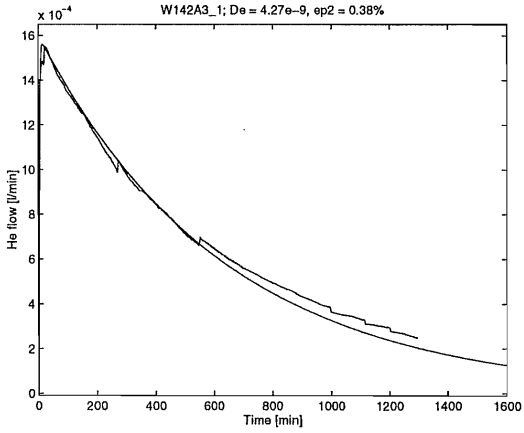

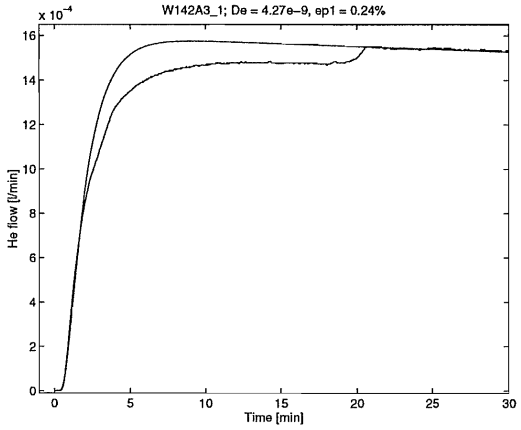

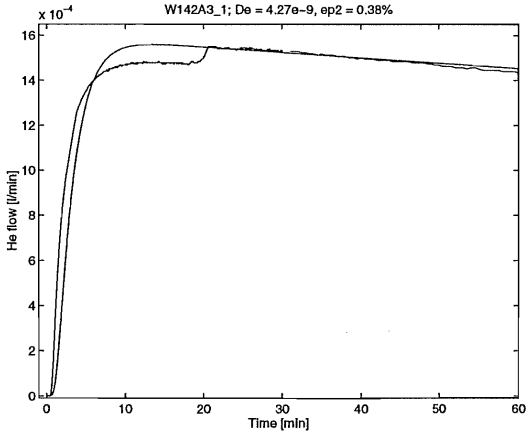

Appendix D

Diffusivity measurements on the cubic samples

D 14.2 A ↕/ 2

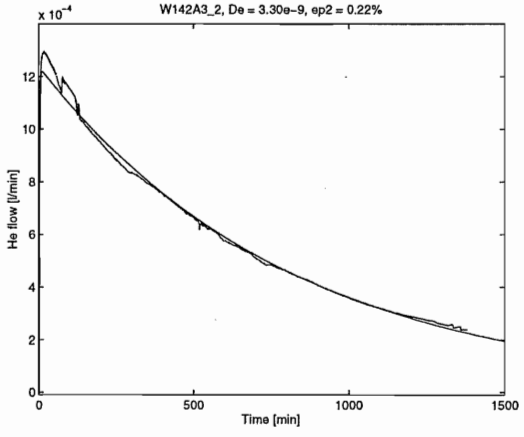

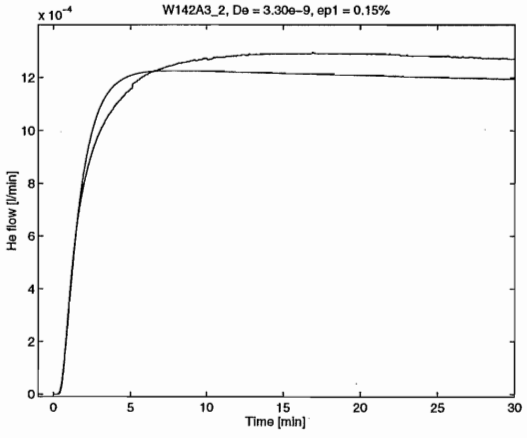

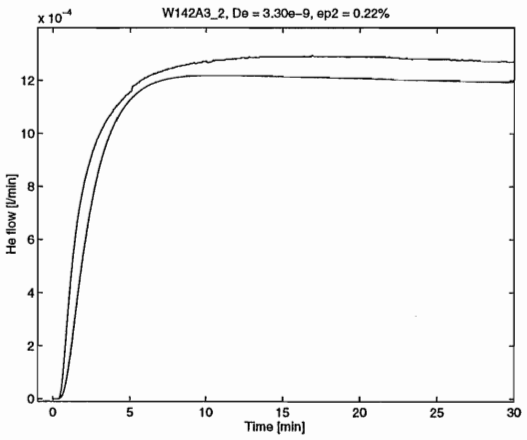

D 14.2 A ↕/ 3

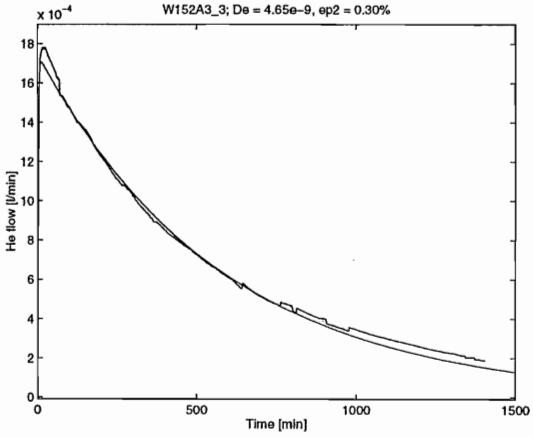

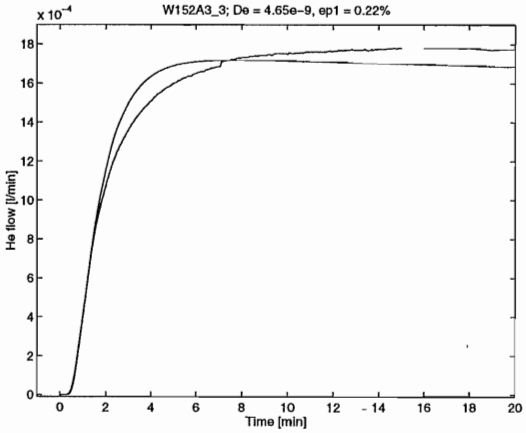

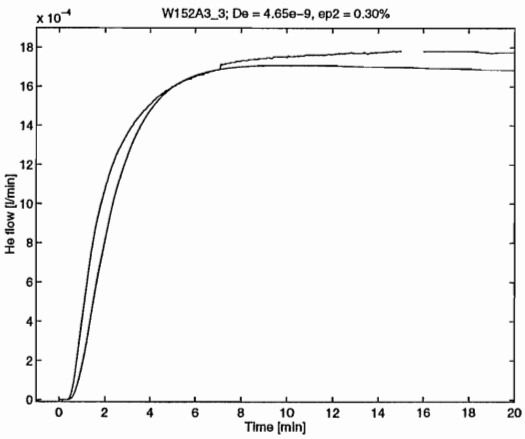

Appendix D

Diffusivity measurements on the cubic samples

D 14.2 A ↕/ 4

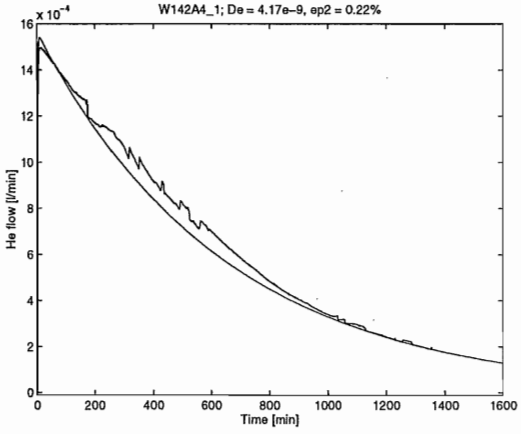

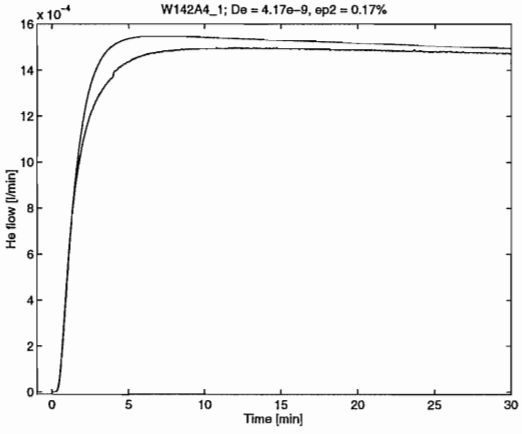

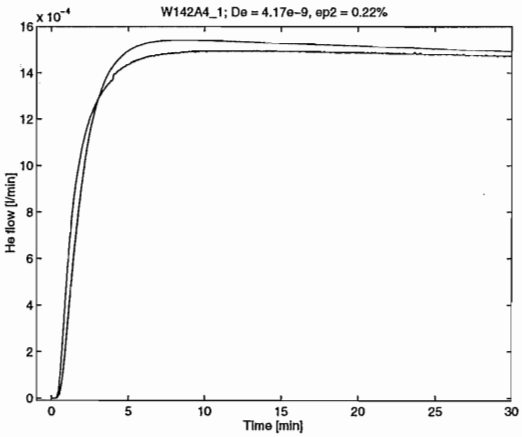

D 14.2 A ↕/ 5

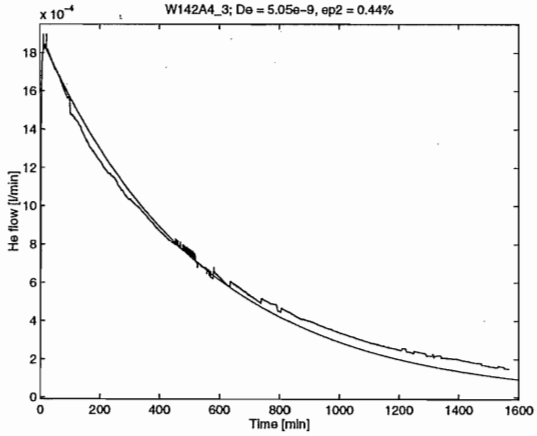

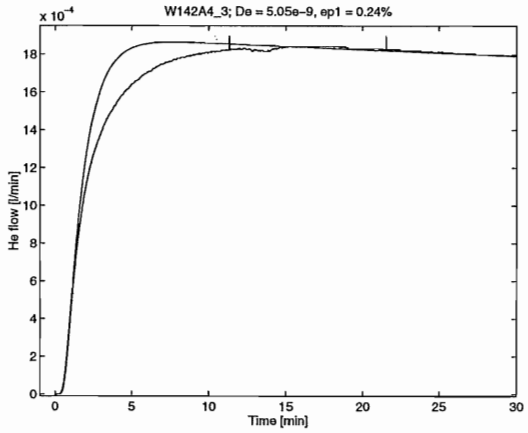

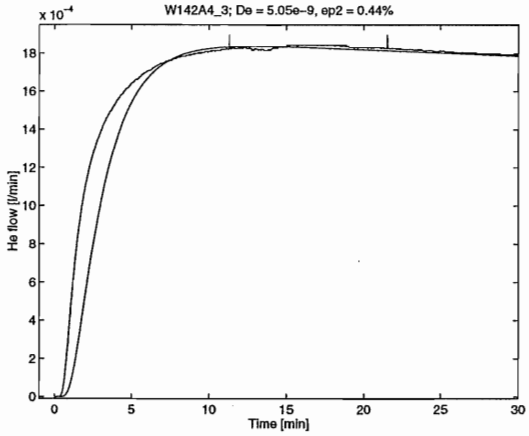

Appendix D

Diffusivity measurements on the cubic samples

D 14.2 A ↕/ 6

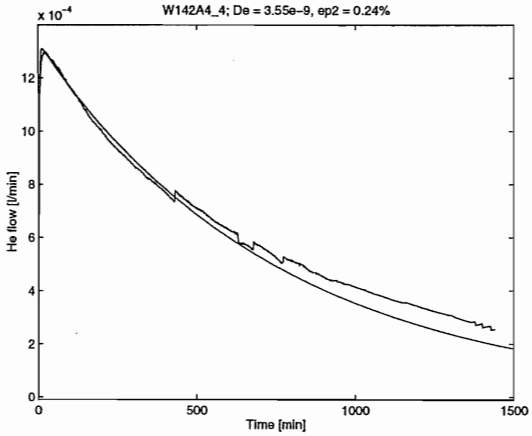

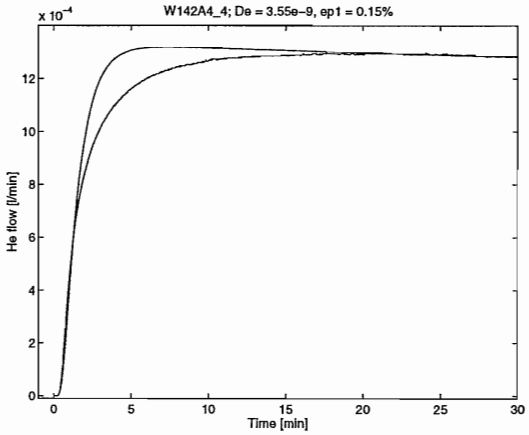

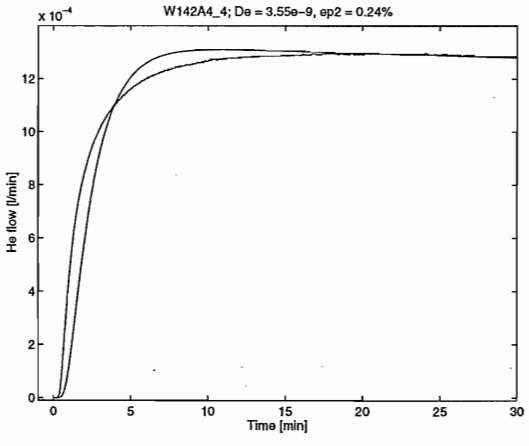

D 14.2 B ⊥/ 1

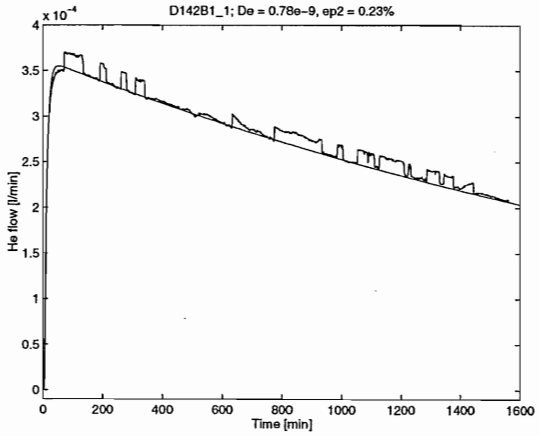

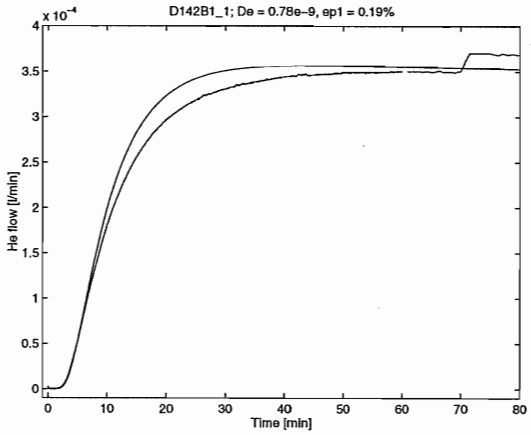

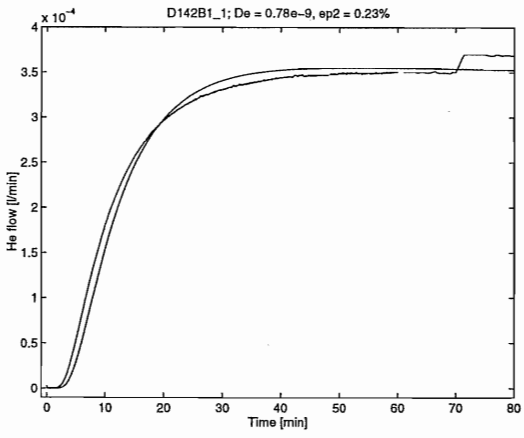

Appendix D

Diffusivity measurements on the cubic samples

D 14.2 B ⊥/ 2

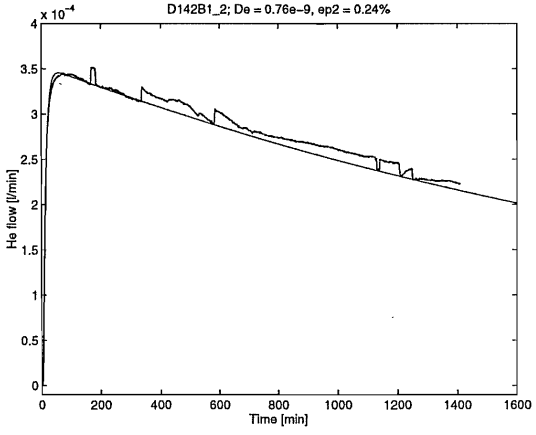

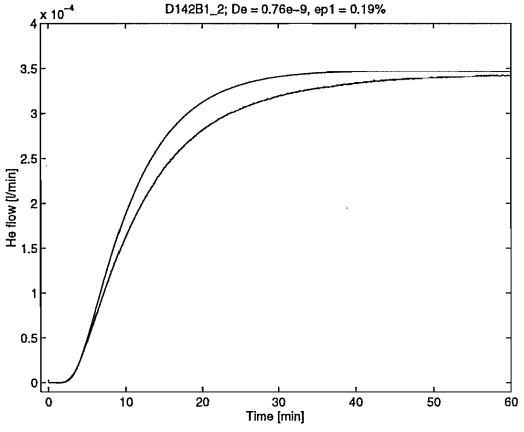

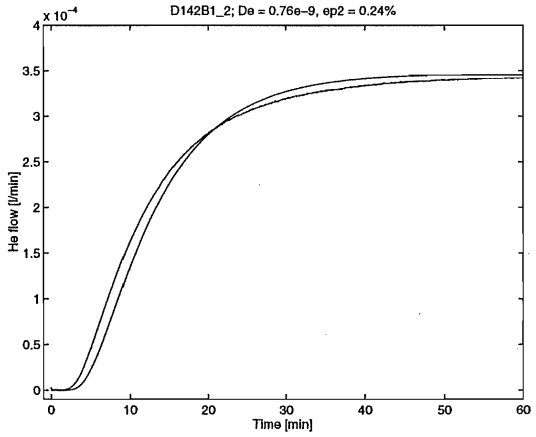

D 14.2 B ⊥/ 3

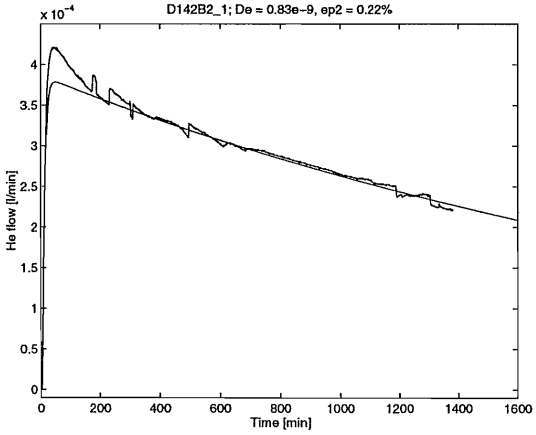

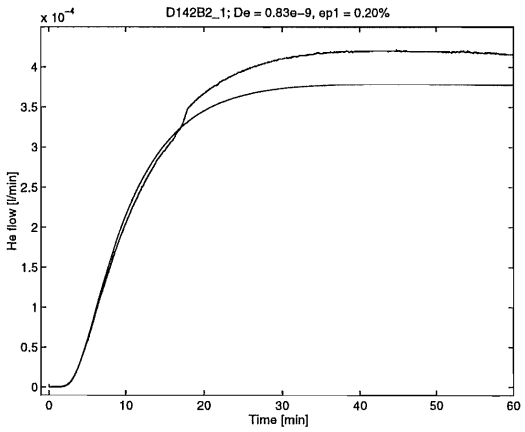

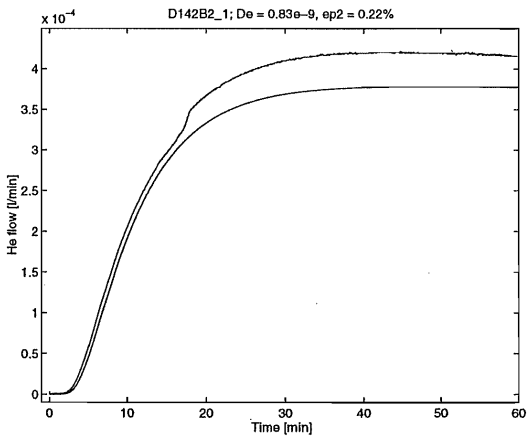

Appendix D

Diffusivity measurements on the cubic samples

D 14.2 B ↕/ 1

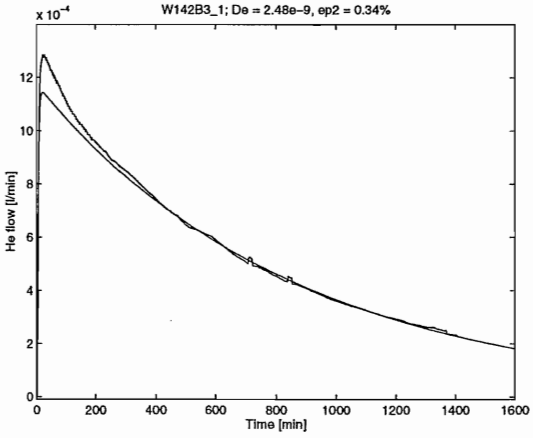

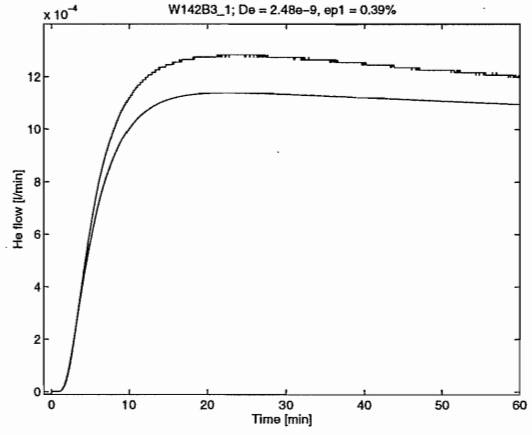

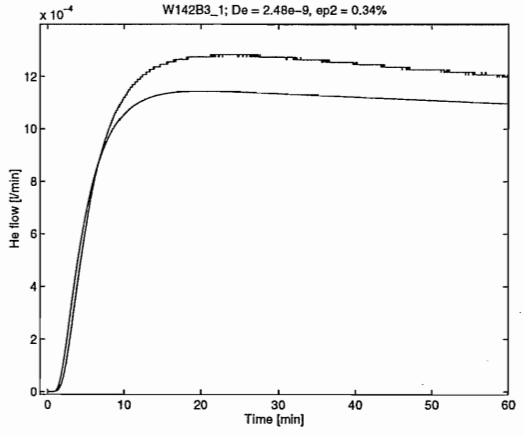

D 14.2 B ↕/ 2

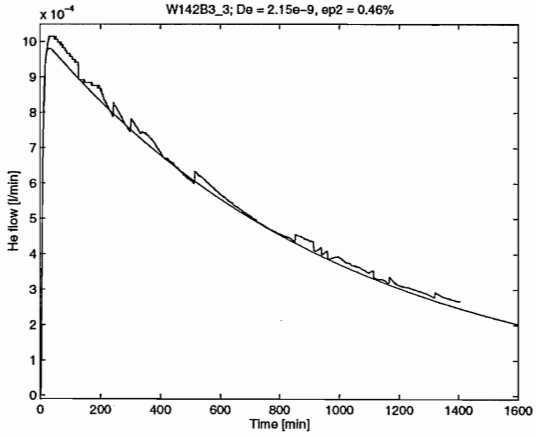

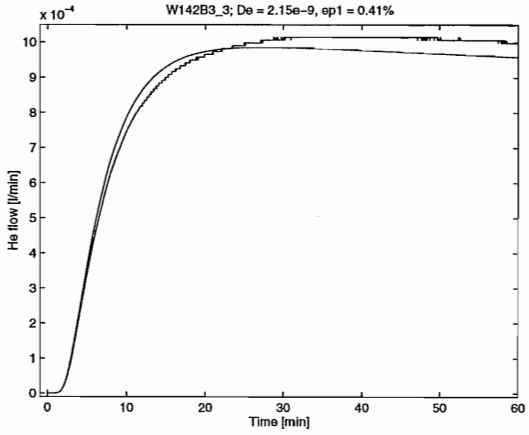

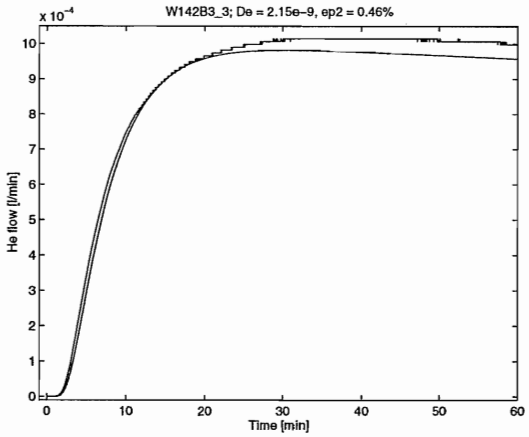

Appendix D

Diffusivity measurements on the cubic samples

D 14.2 B ↕/ 3

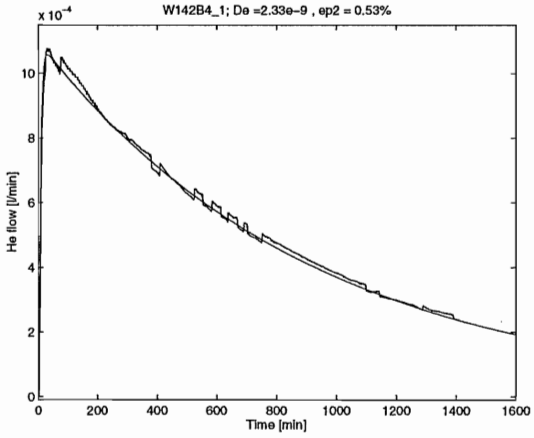

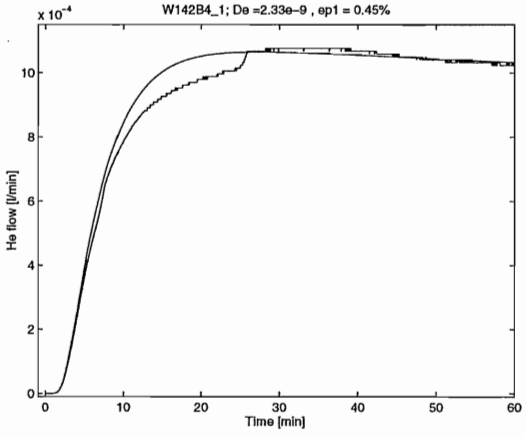

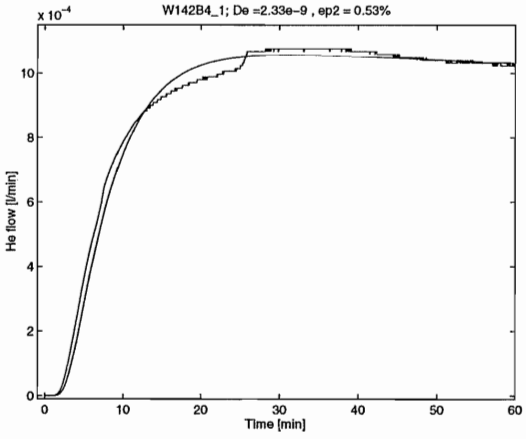

D 14.2 B ↕/ 4

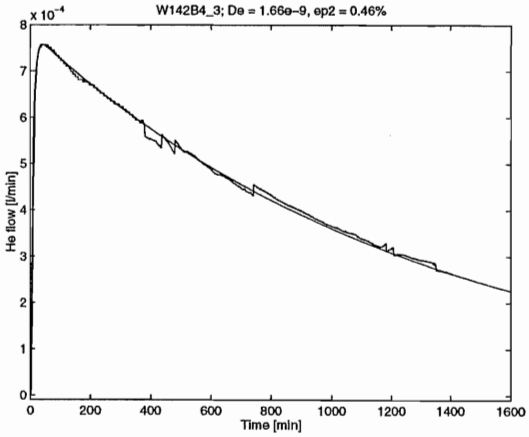

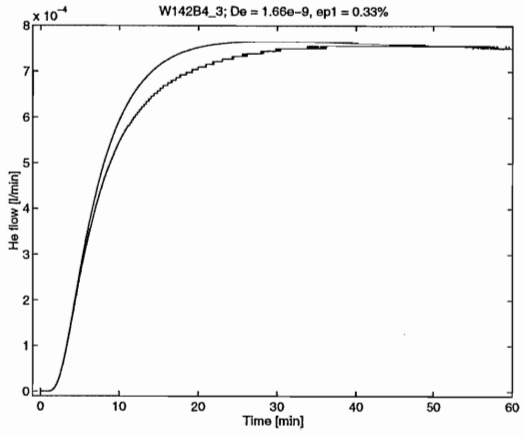

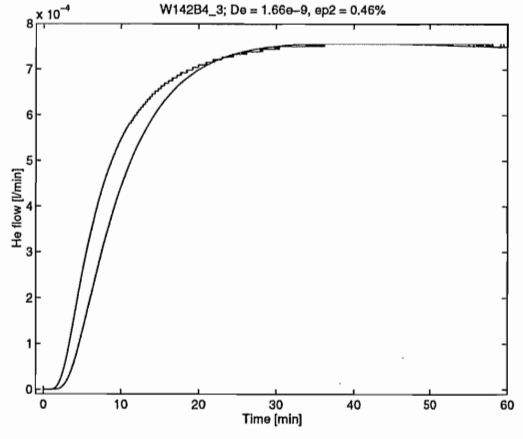

Appendix D

Diffusivity measurements on the cubic samples

D 15.1 A ⊥/ 1

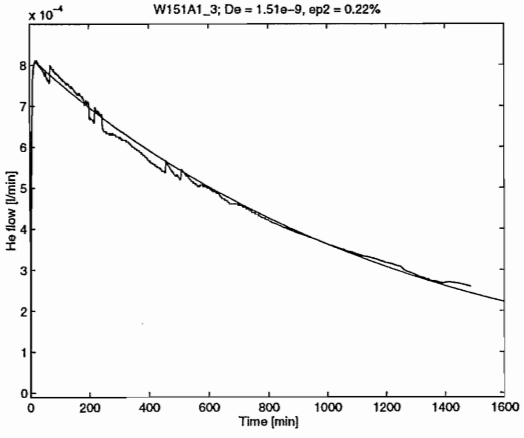

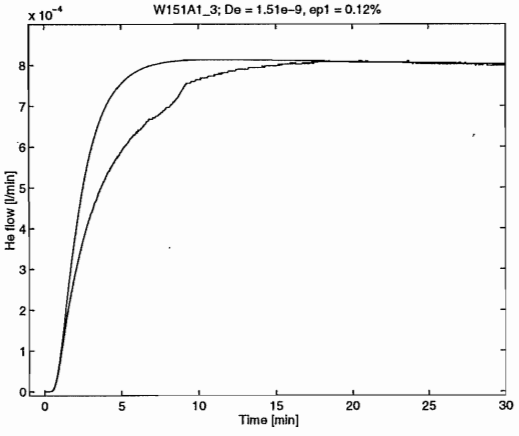

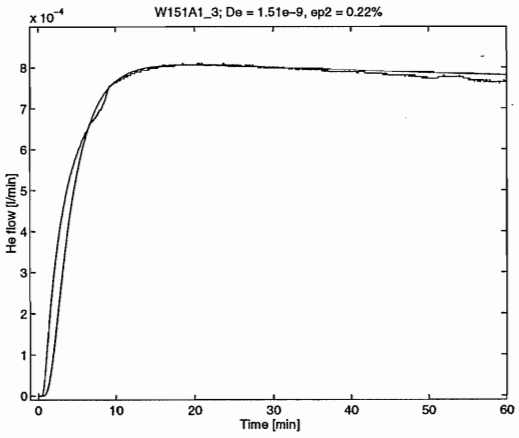

D 15.1 A ⊥/ 2

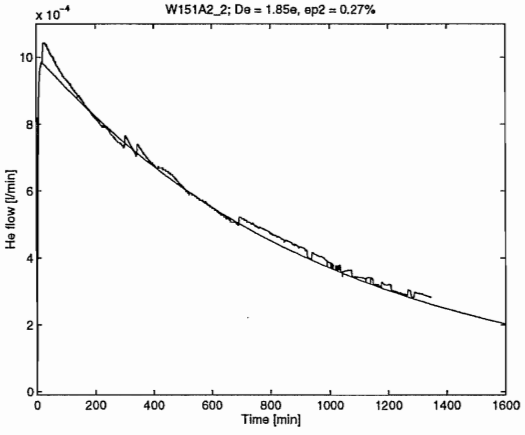

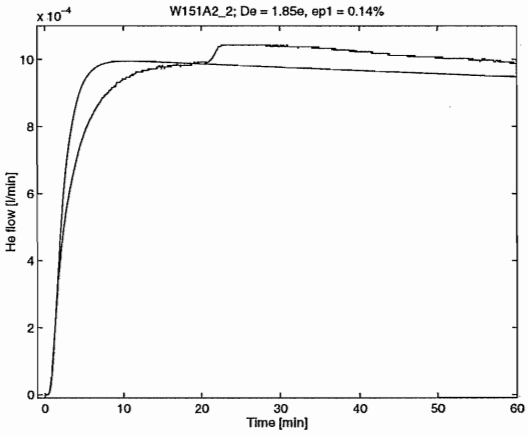

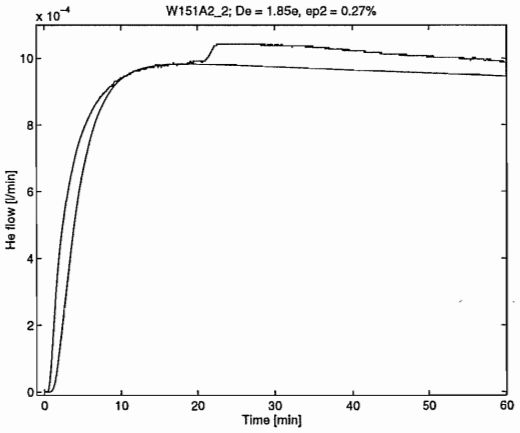

Appendix D

Diffusivity measurements on the cubic samples

D 15.1 A ↕/ 1

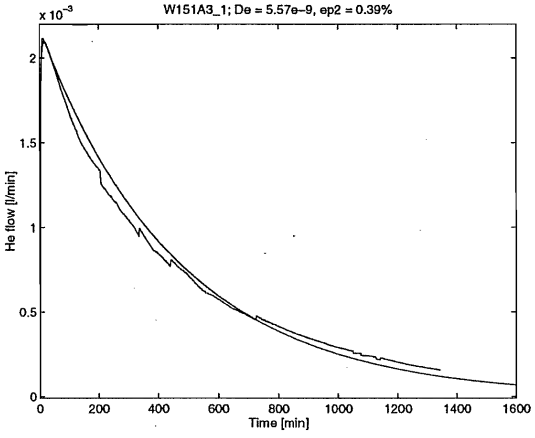

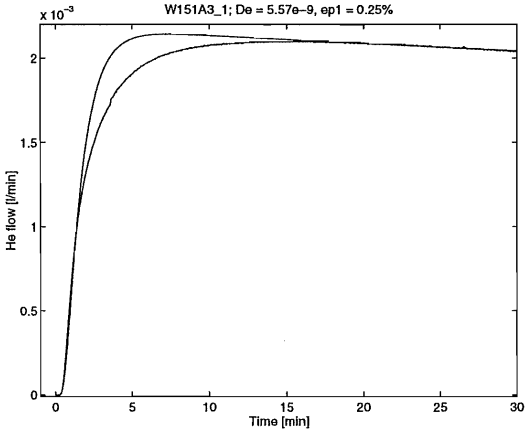

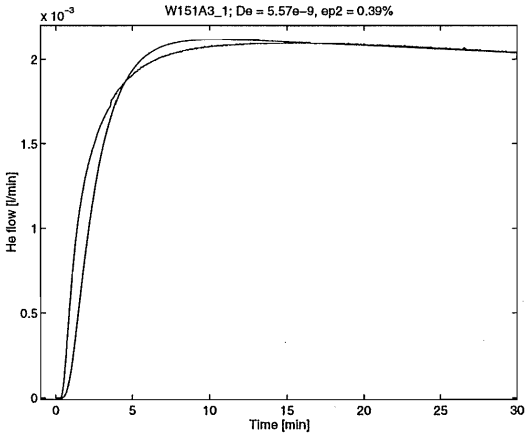

D 15.1 A ↕/ 2

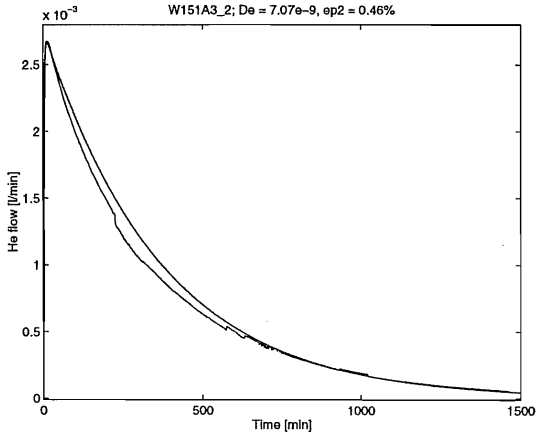

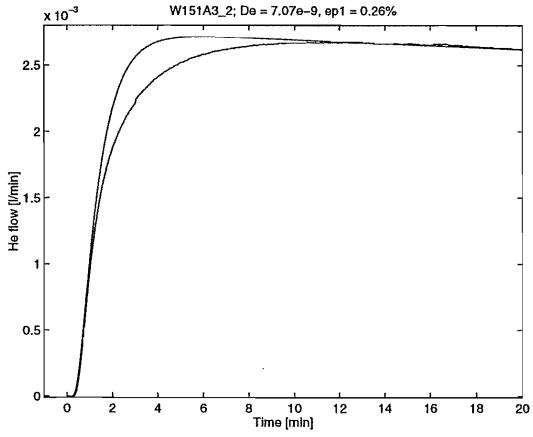

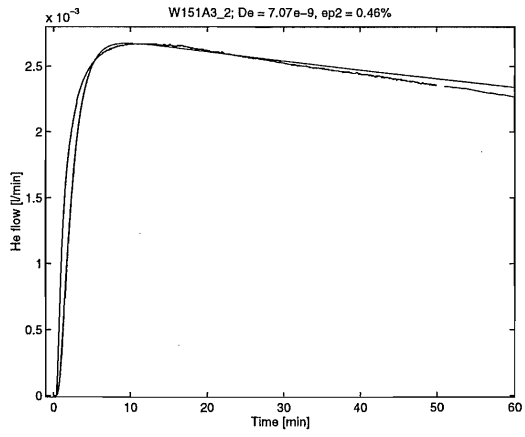

Appendix D

Diffusivity measurements on the cubic samples

D 15.1 A ↕/ 3

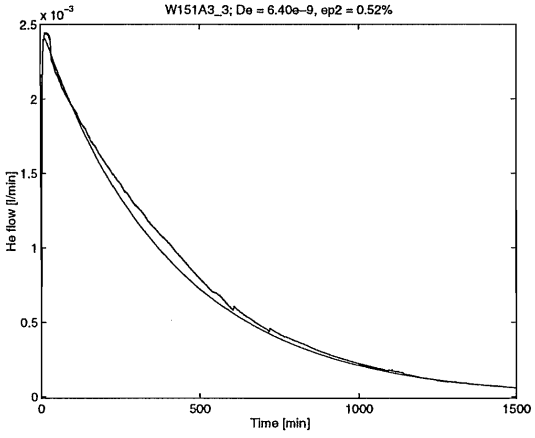

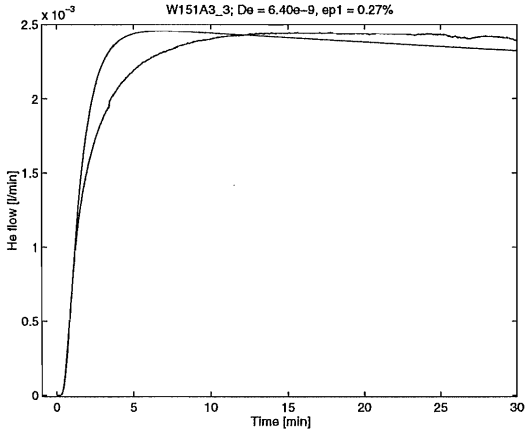

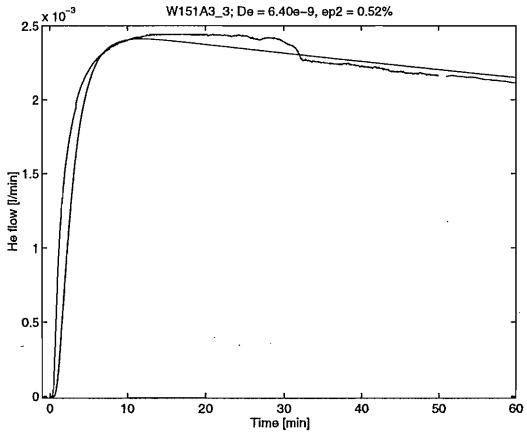

D 15.1 A ↕/ 4

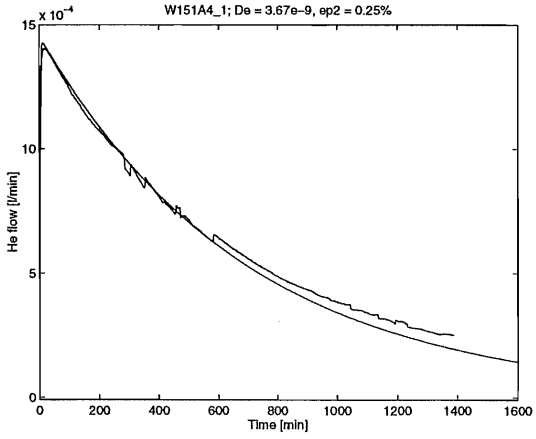

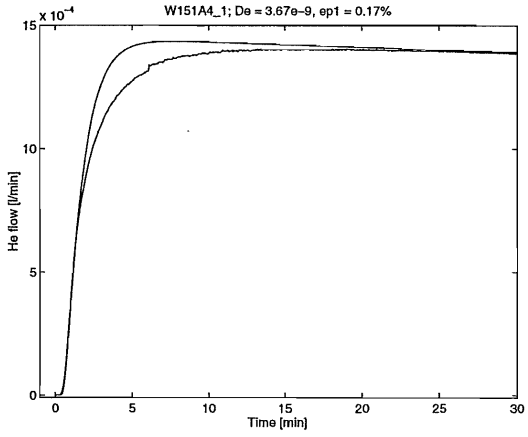

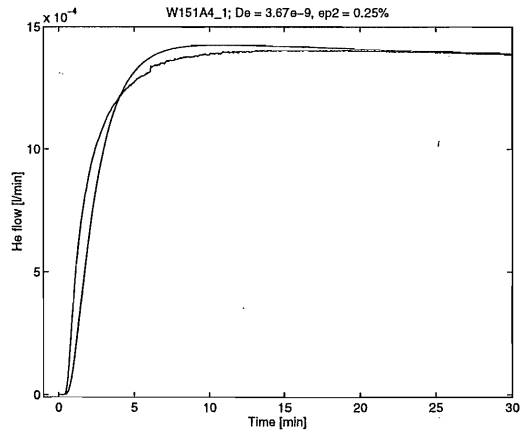

Appendix D

Diffusivity measurements on the cubic samples

D 15.1 A ↕/ 5

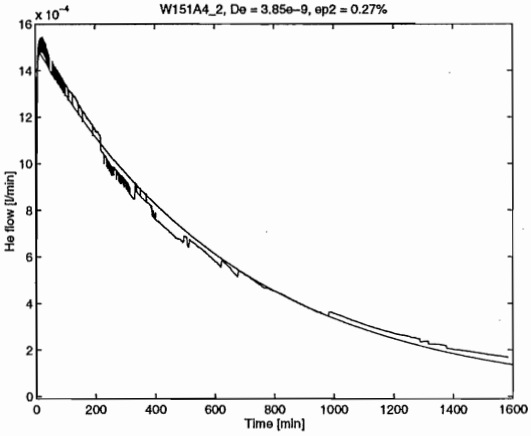

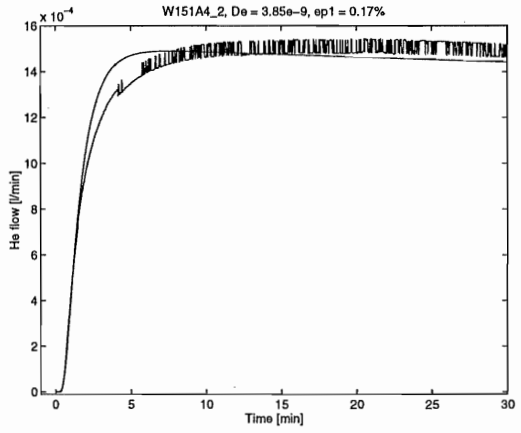

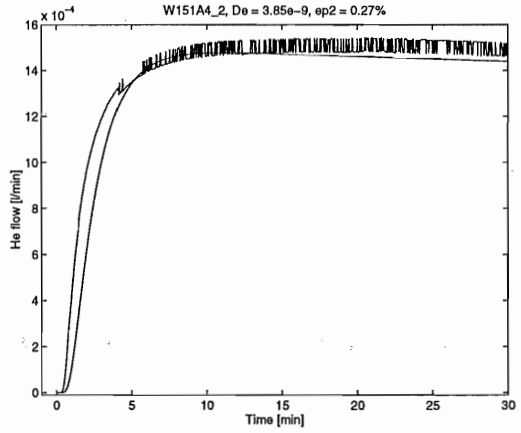

D 15.1 B ⊥/ 1

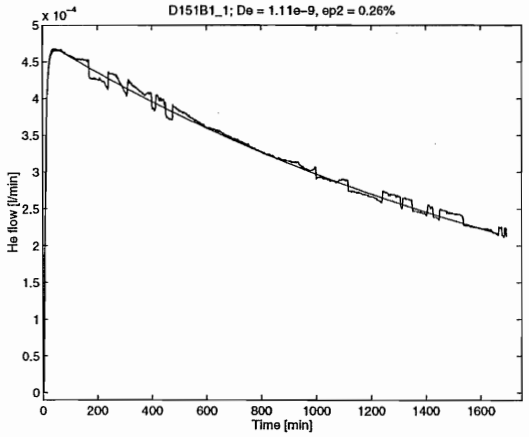

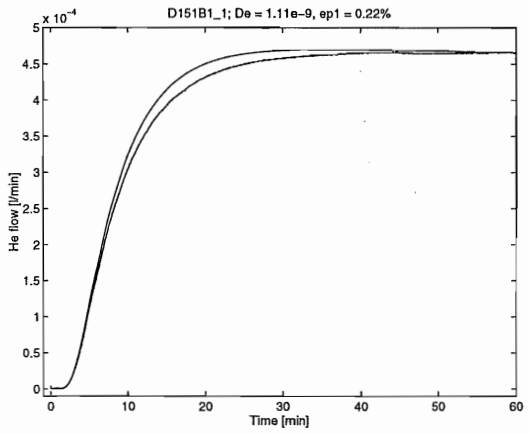

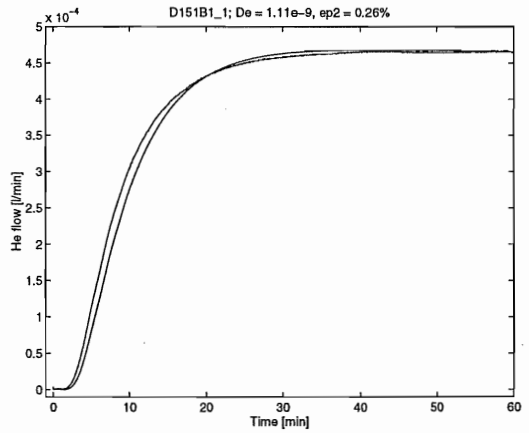

Appendix D

Diffusivity measurements on the cubic samples

D 15.1 B ⊥/ 2

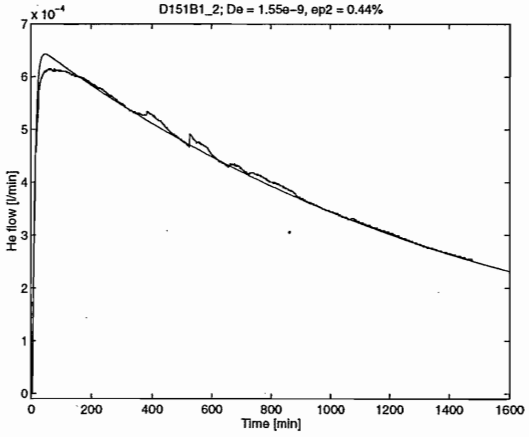

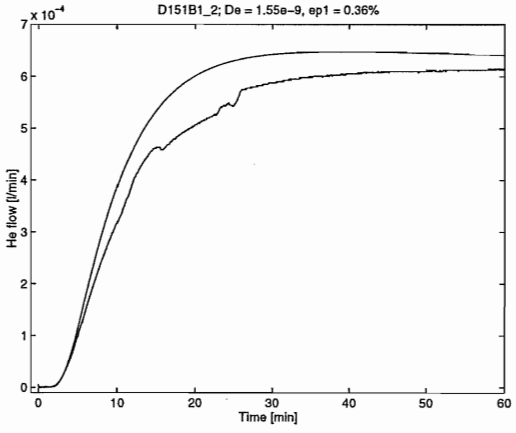

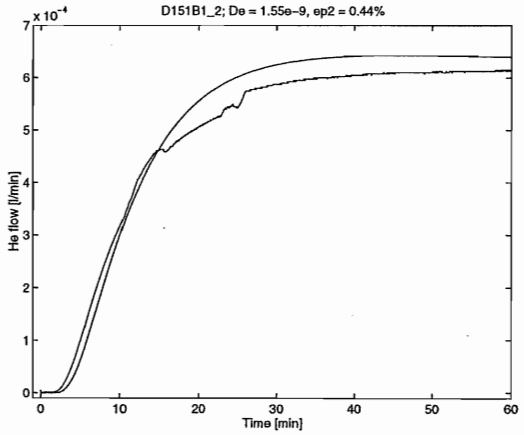

D 15.1 B ⊥/ 3

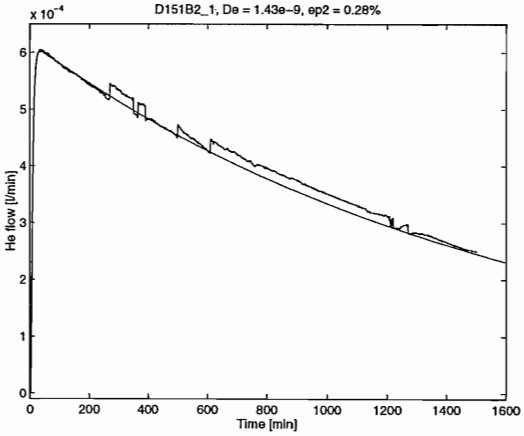

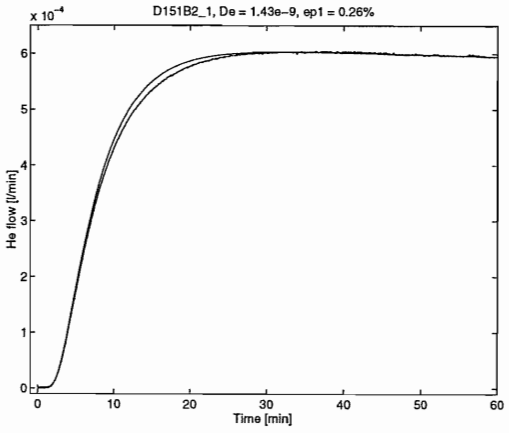

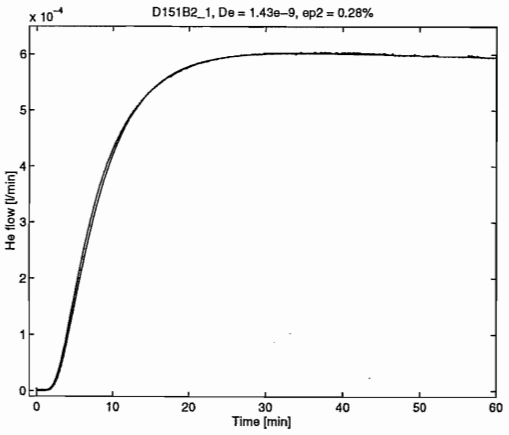

Appendix D

Diffusivity measurements on the cubic samples

D 15.1 B ⊥/ 4

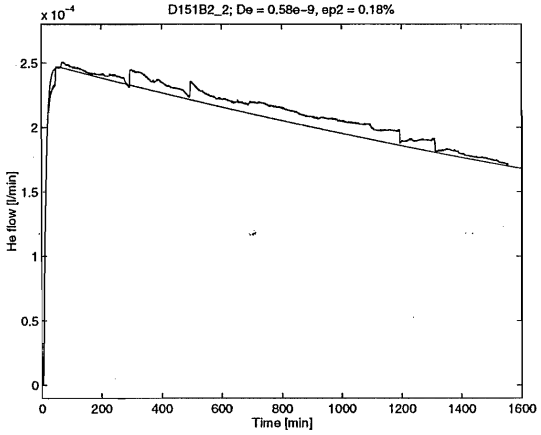

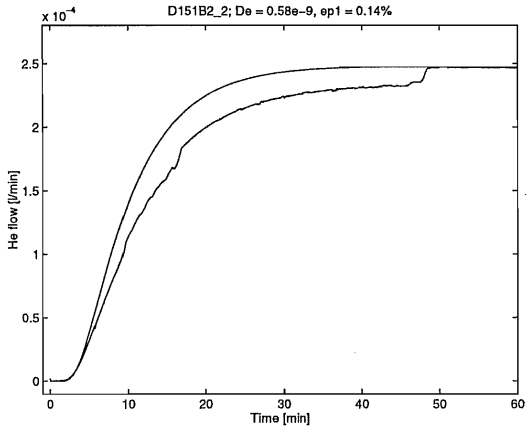

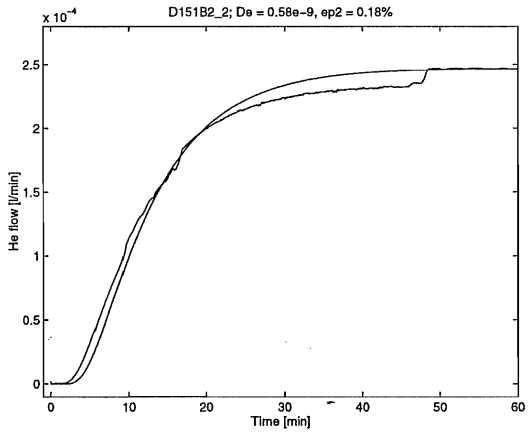

D 15.1 B ↕/ 1

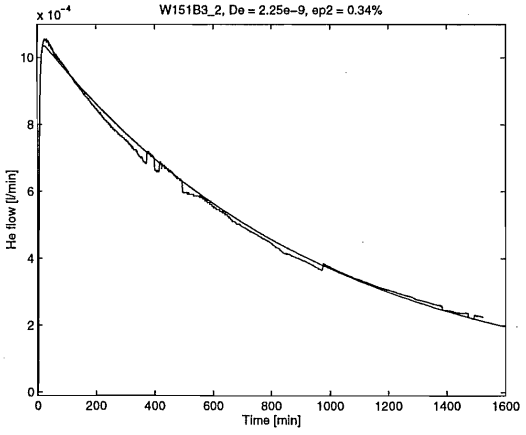

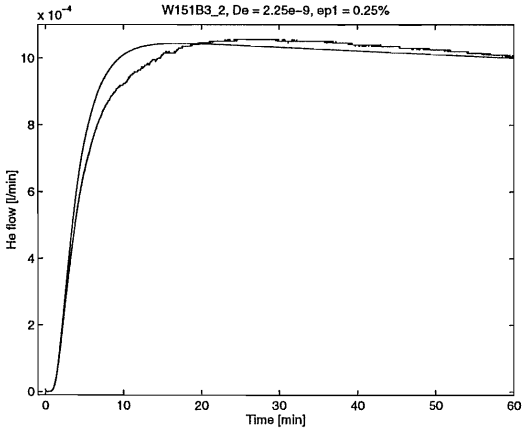

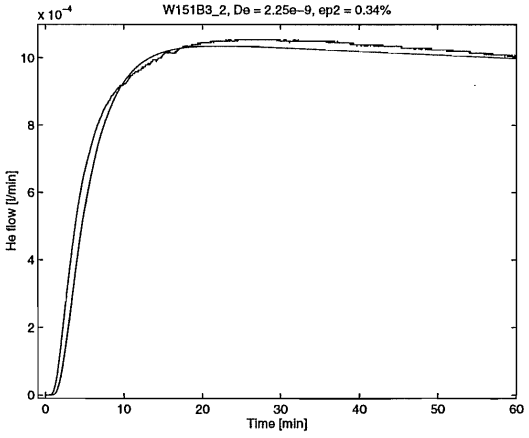

Appendix D

Diffusivity measurements on the cubic samples

D 15.1 B ↕/ 2

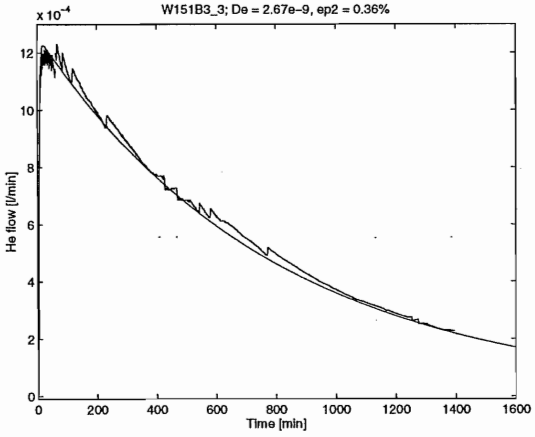

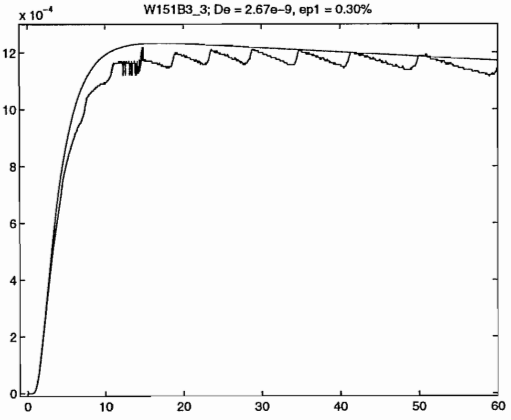

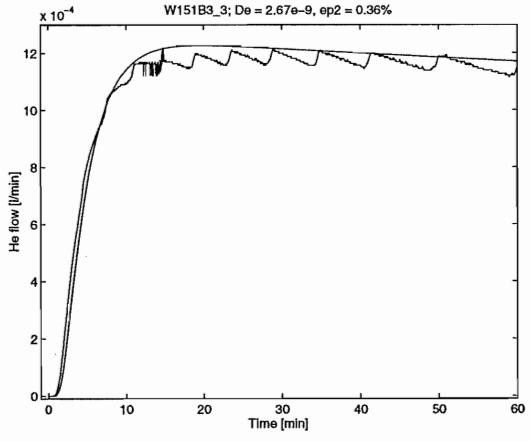

D 15.1 B ↕/ 3

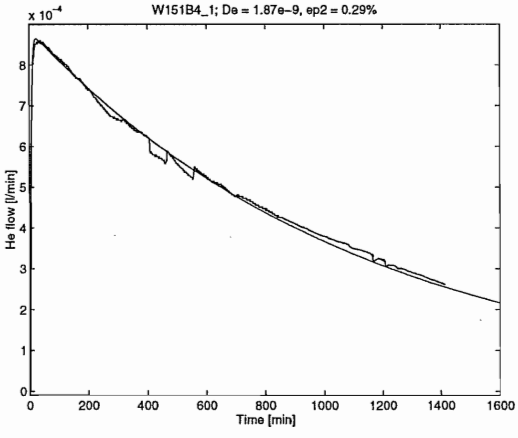

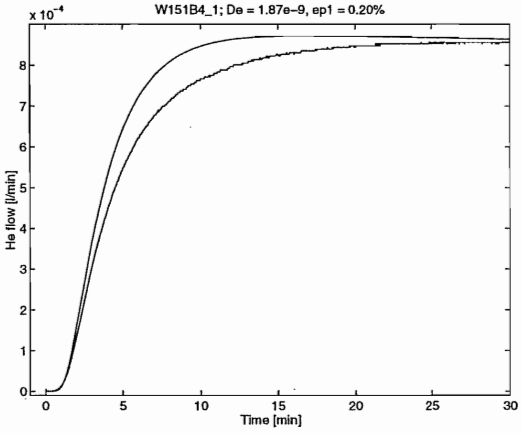

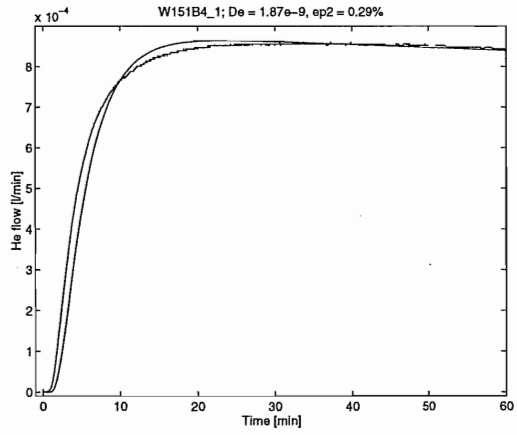

Appendix D

Diffusivity measurements on the cubic samples

D 15.1 B ↕/ 4

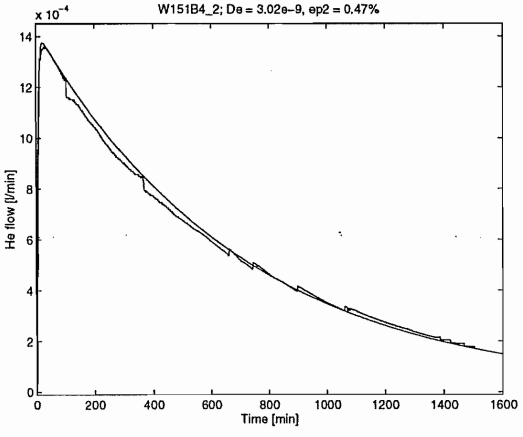

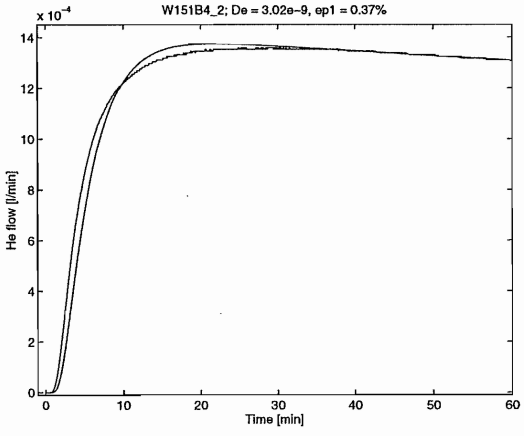

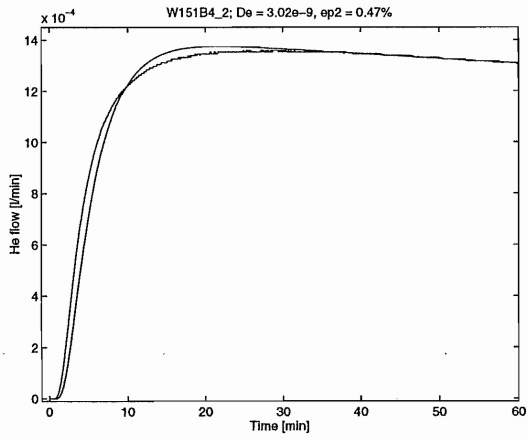

D 15.1 B ↕/ 5

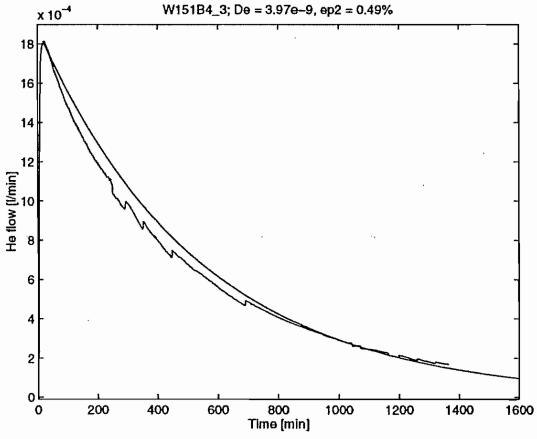

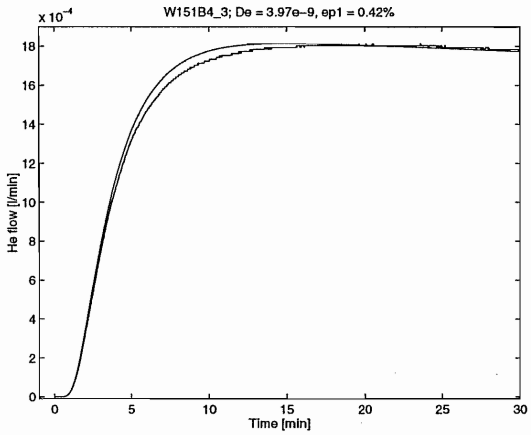

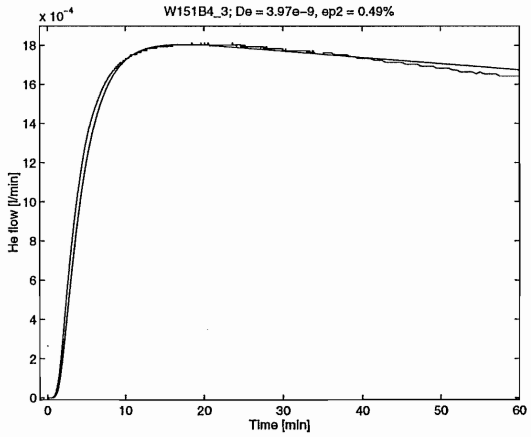

Appendix E

Permeability measurements on the ring samples

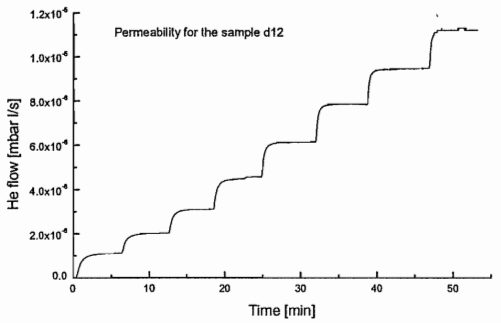

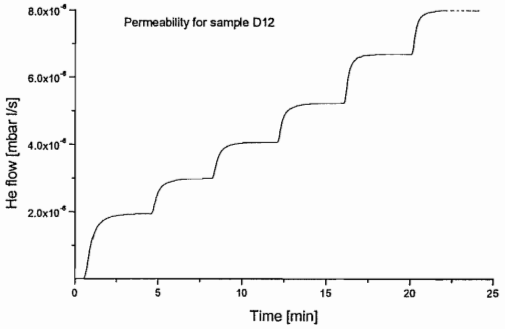

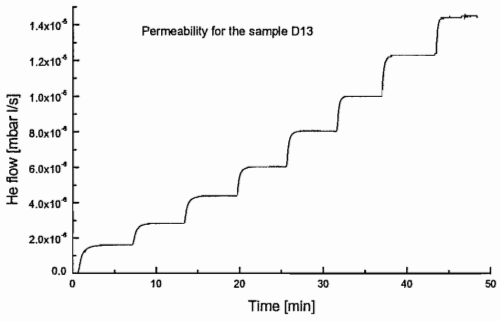

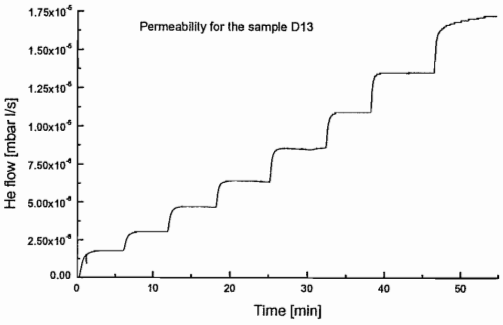

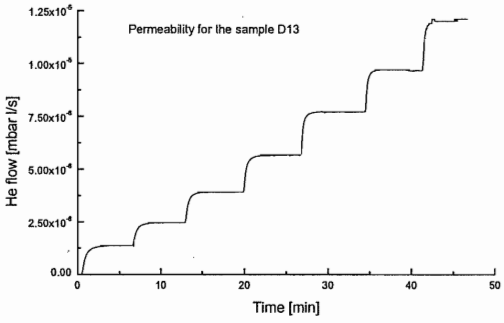

Appendix E

Permeability measurements on the ring samples

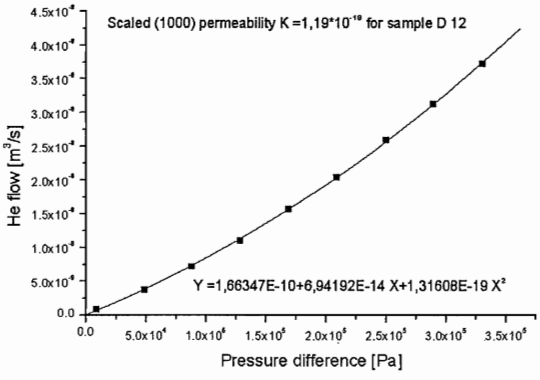

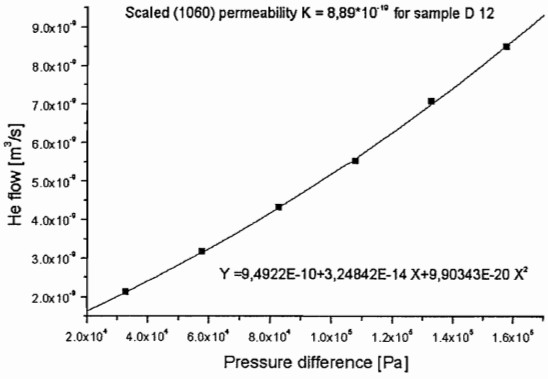

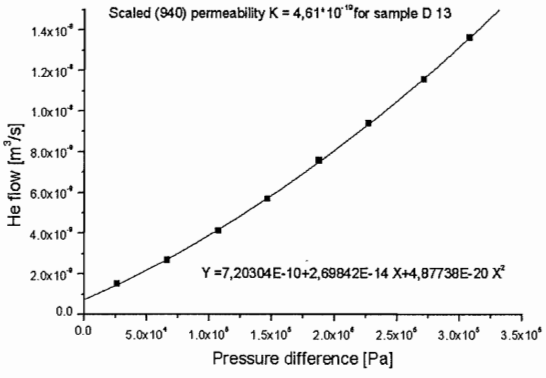

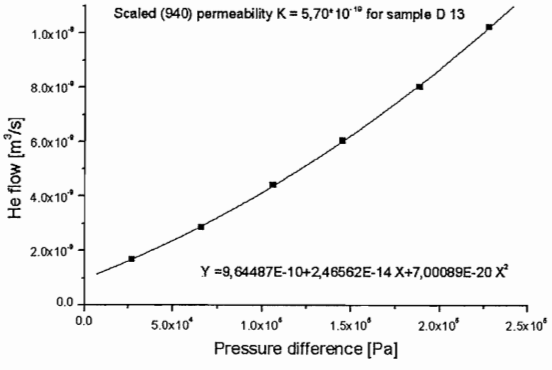

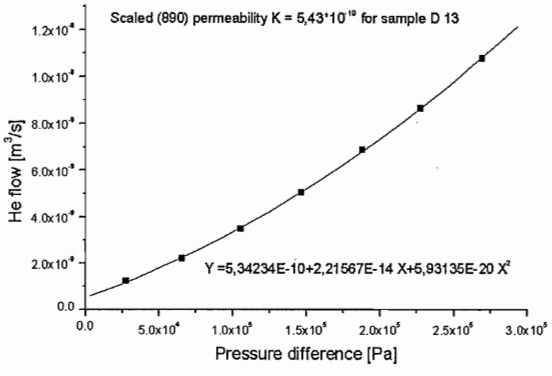

Appendix F

Permeability measurements on the cubic samples

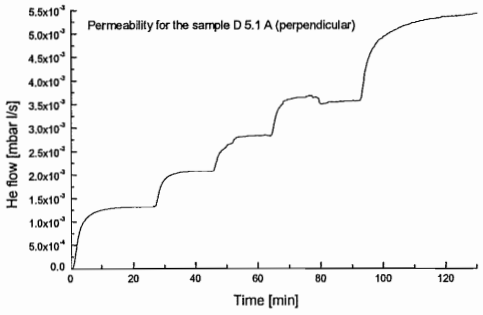

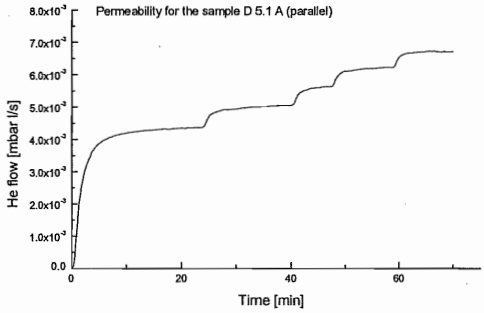

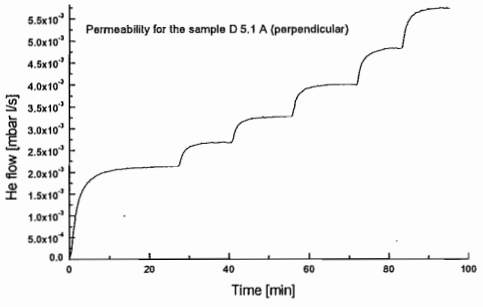

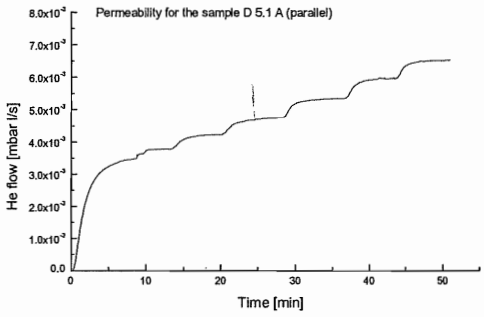

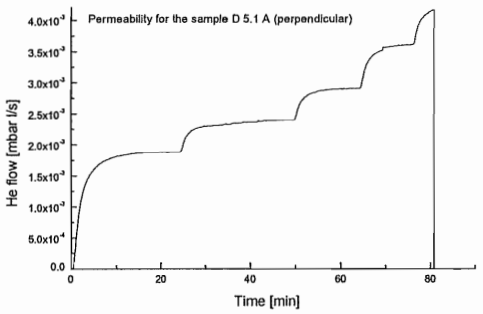

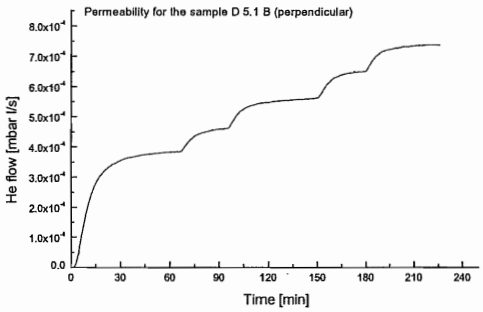

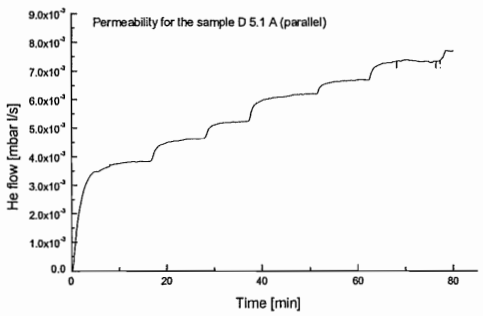

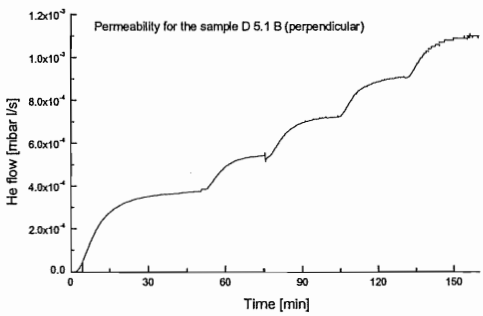

Permeability measurements on the cubic samples

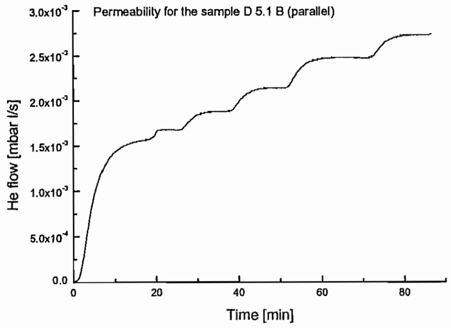

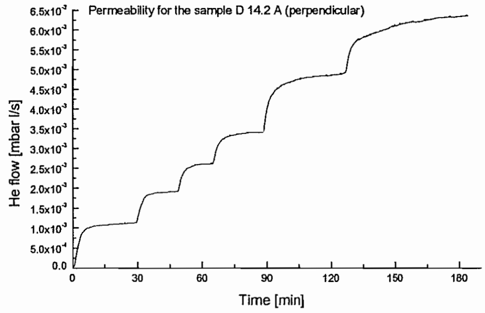

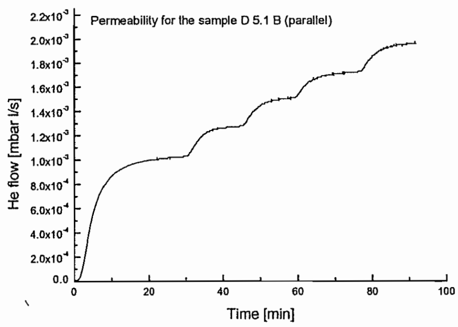

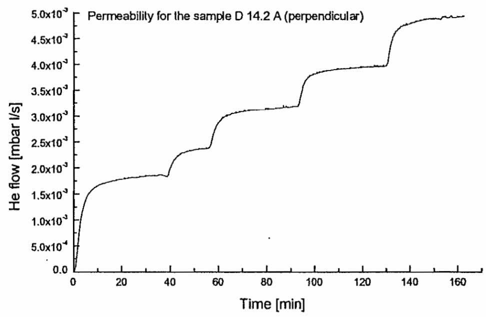

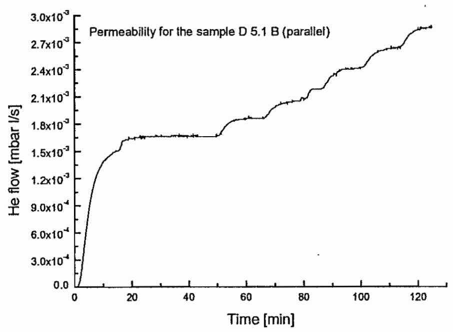

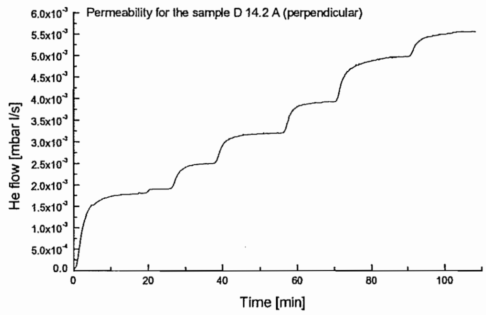

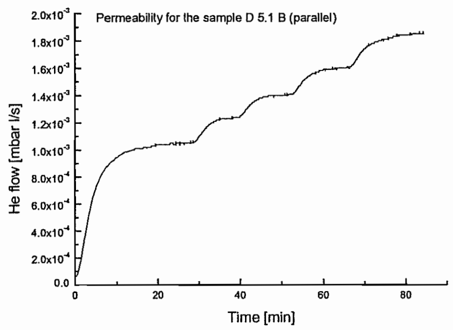

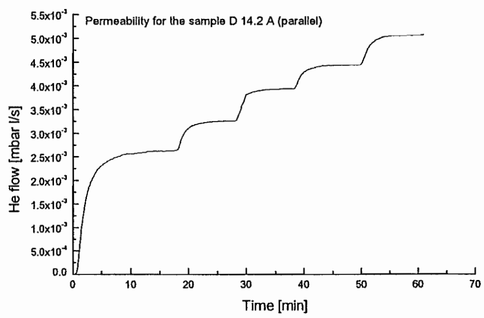

Appendix F

Permeability measurements on the cubic samples

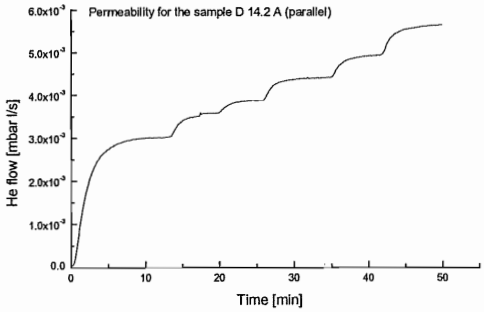

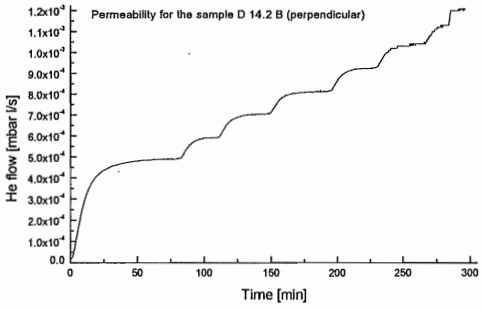

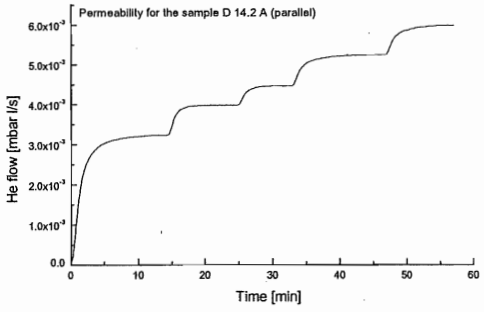

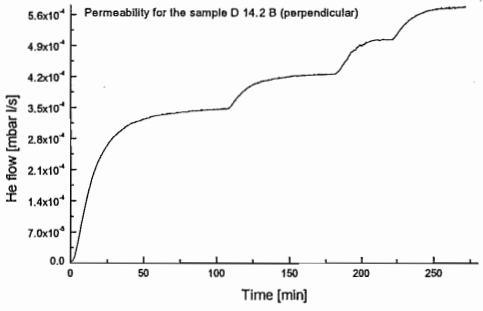

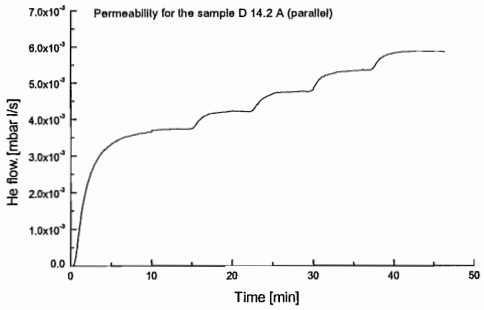

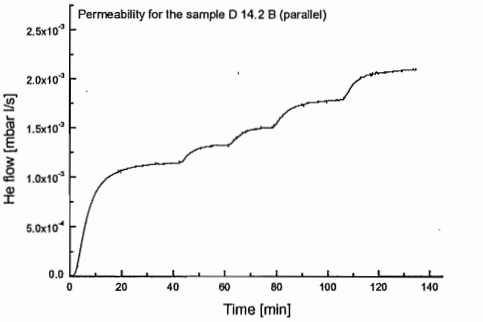

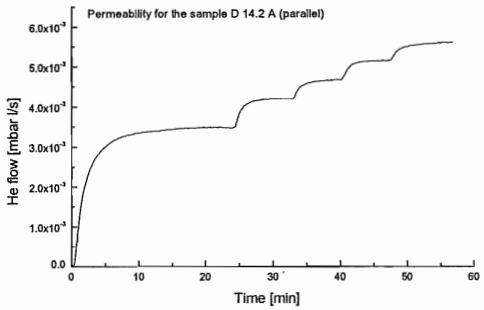

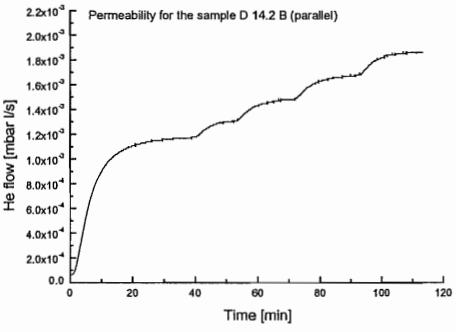

Permeability measurements on the cubic samples

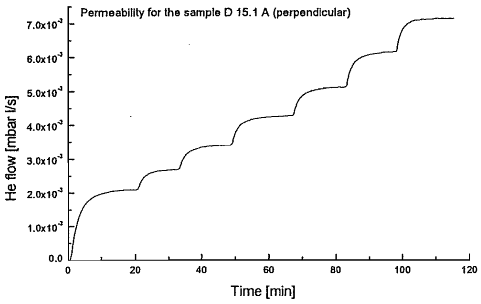

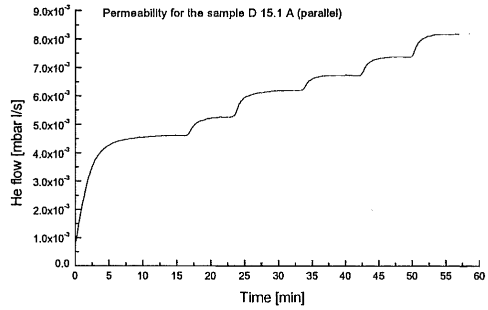

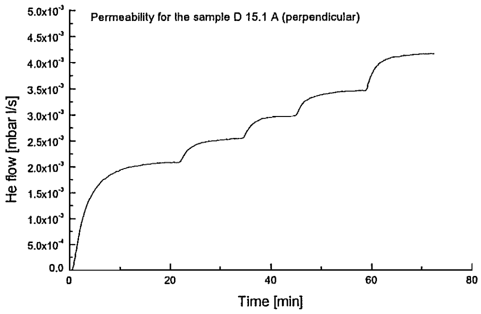

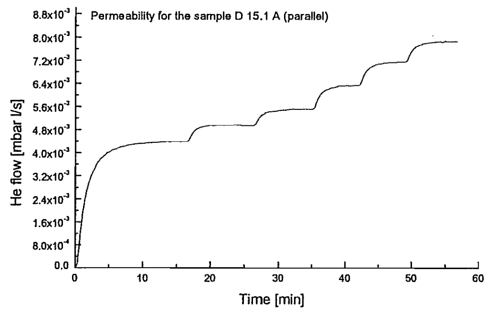

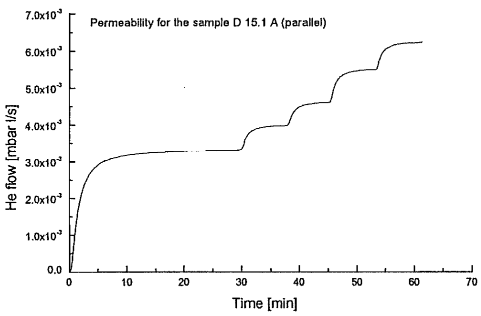

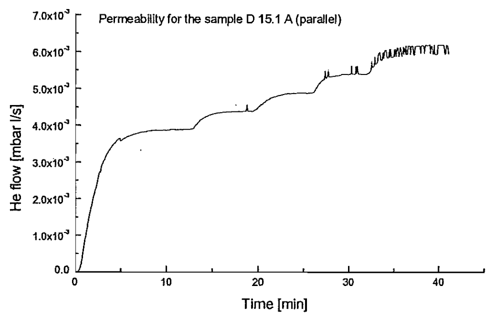

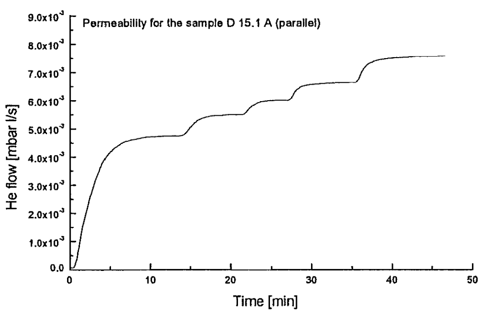

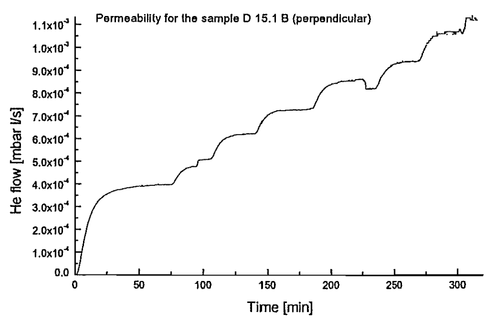

Appendix F

Permeability measurements on the cubic samples

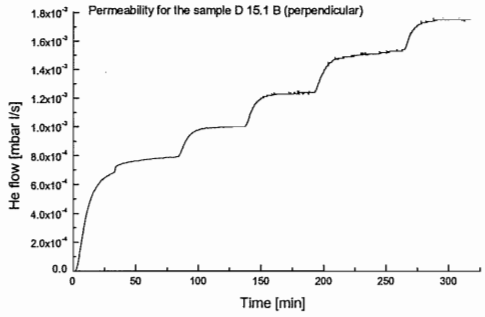

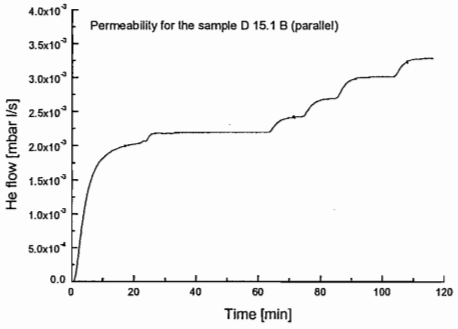

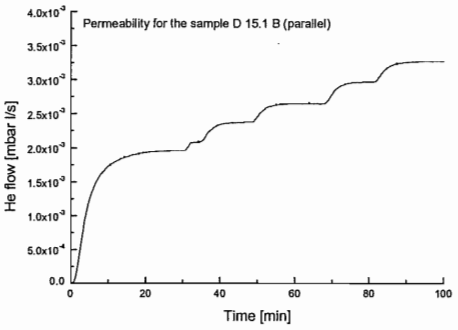

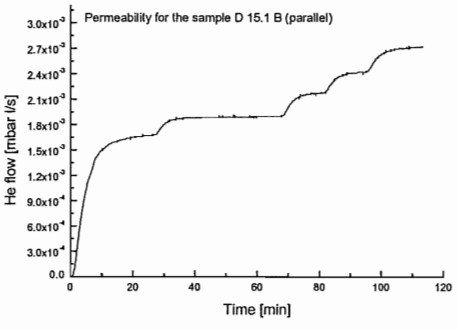

Appendix F

Permeability measurements on the cubic samples

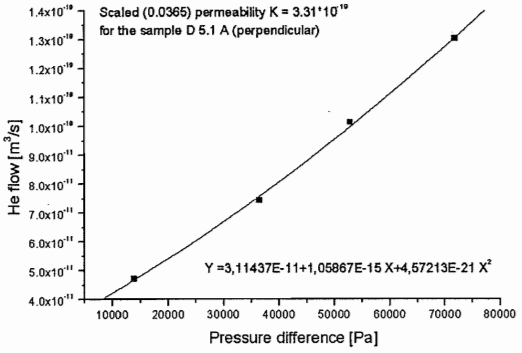

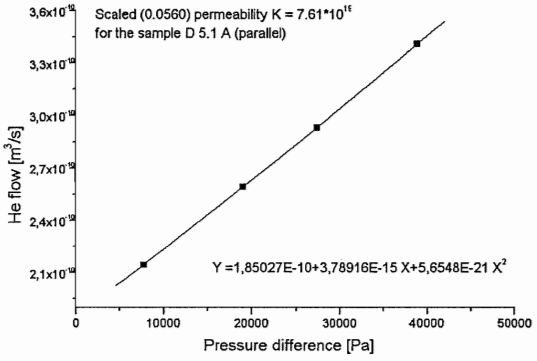

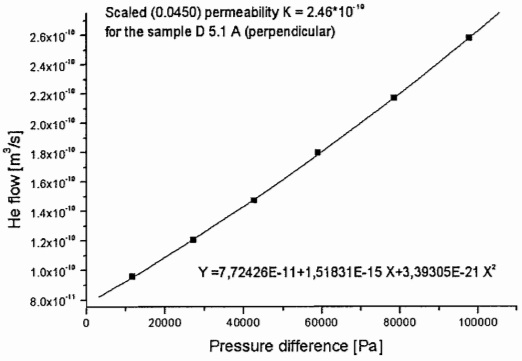

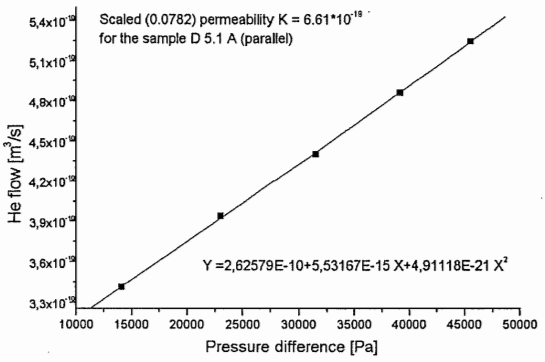

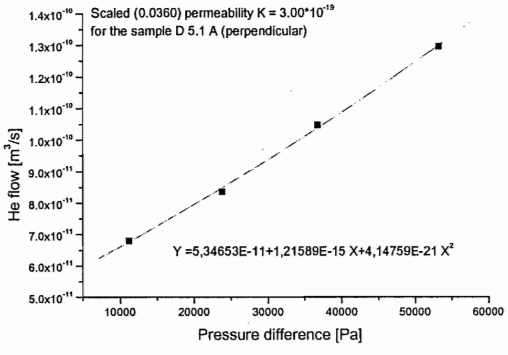

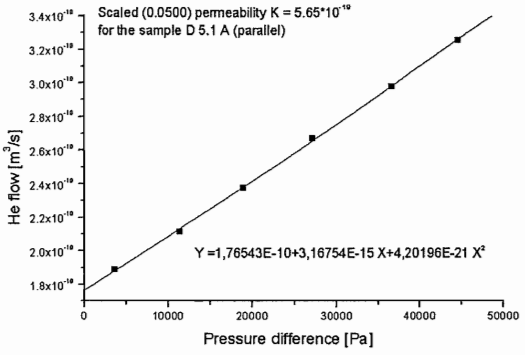

Appendix F

Permeability measurements on the cubic samples

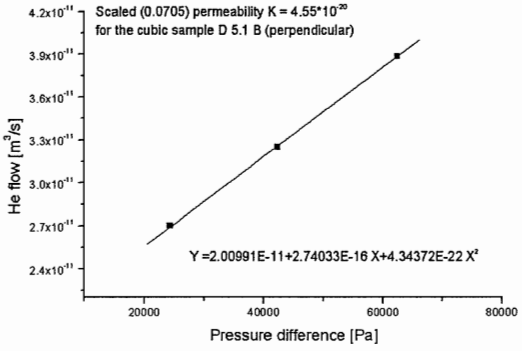

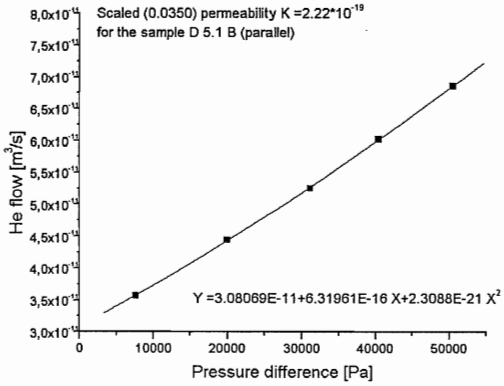

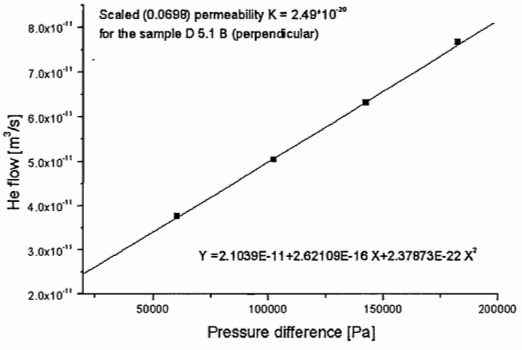

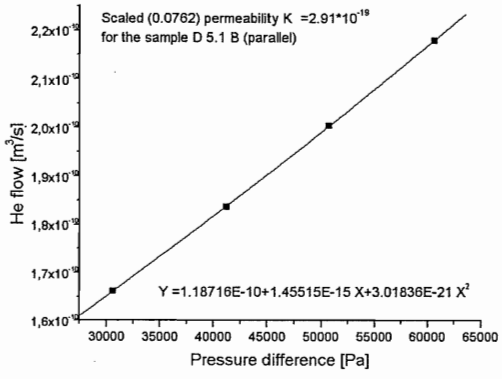

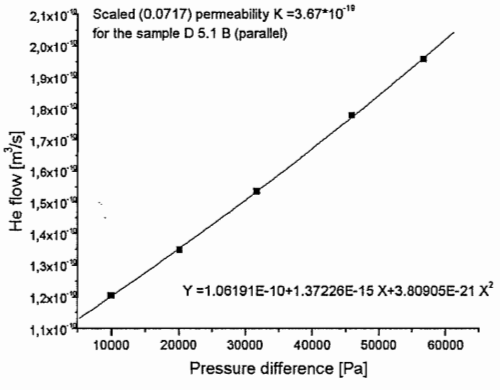

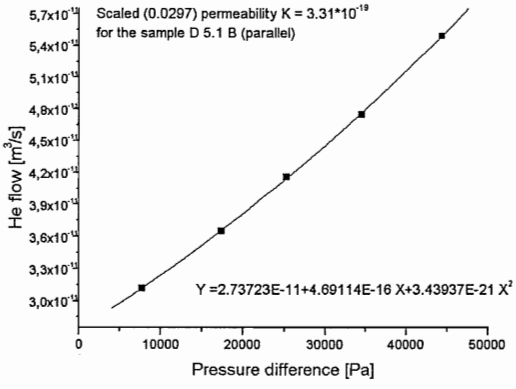

Appendix F

Permeability measurements on the cubic samples

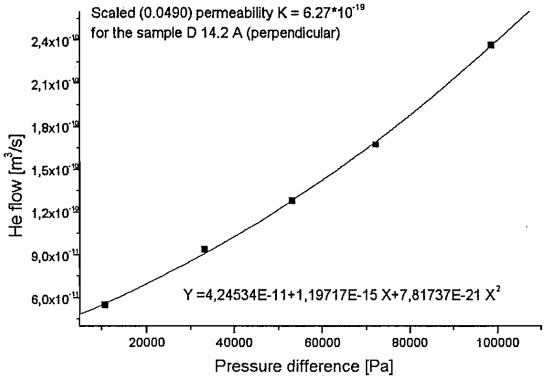

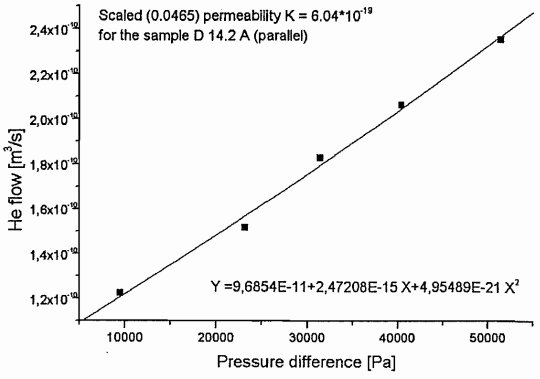

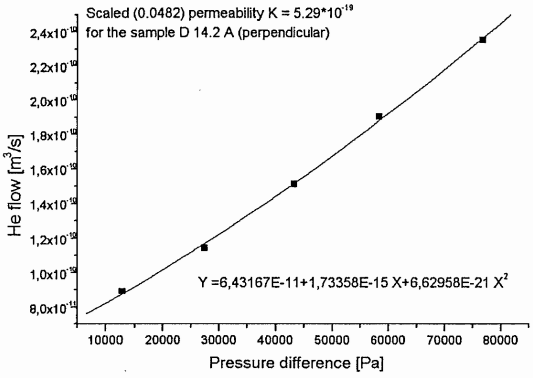

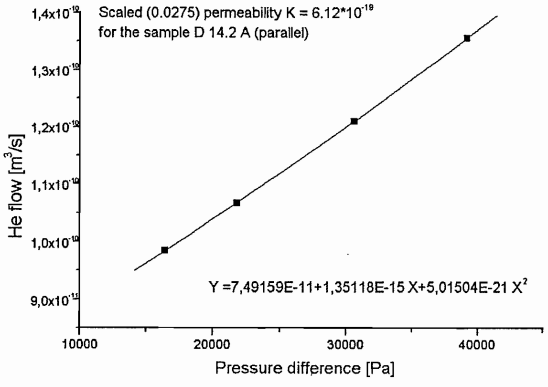

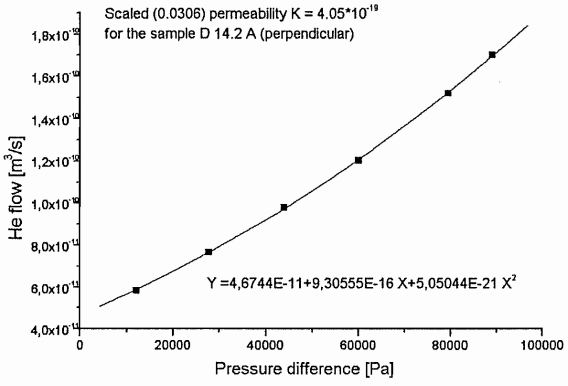

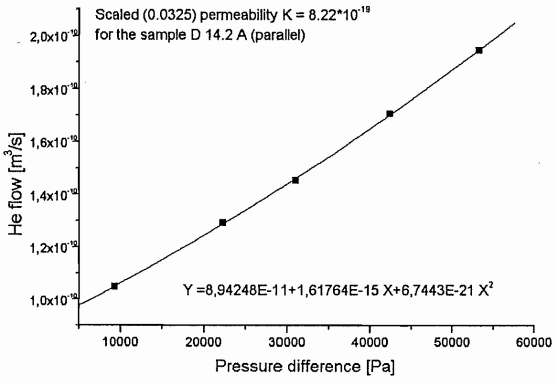

Appendix F

Permeability measurements on the cubic samples

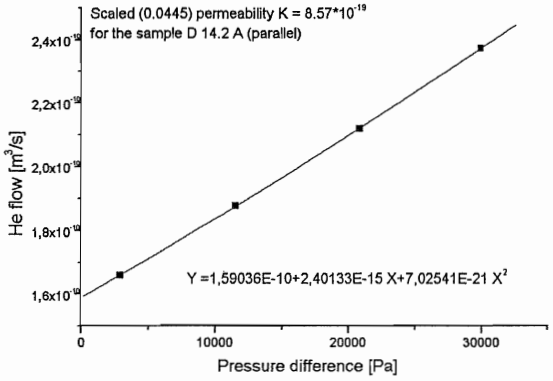

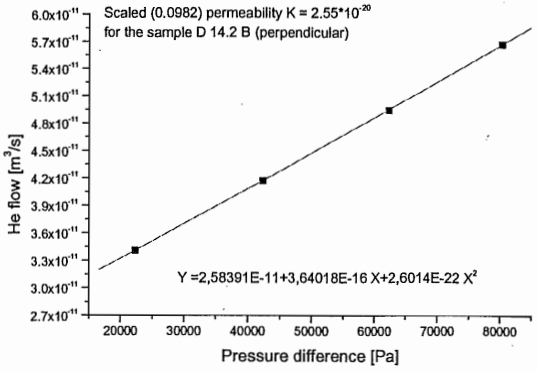

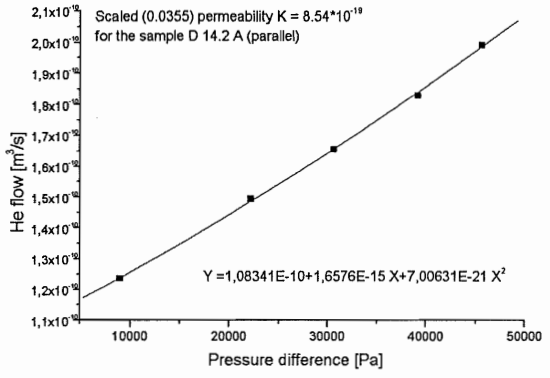

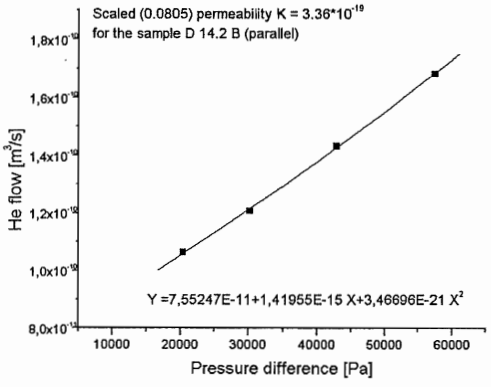

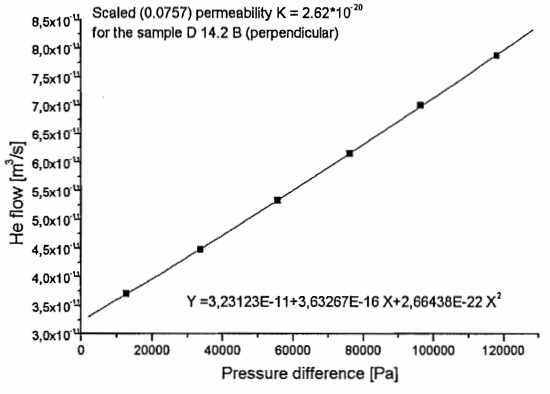

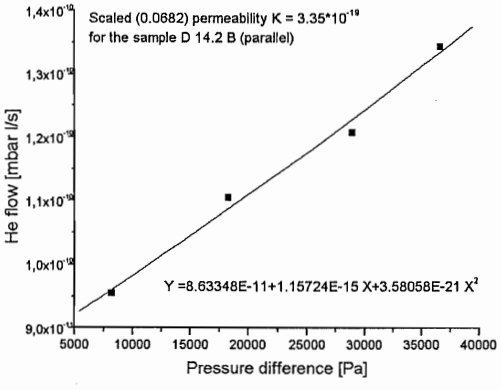

Appendix F

Permeability measurements on the cubic samples

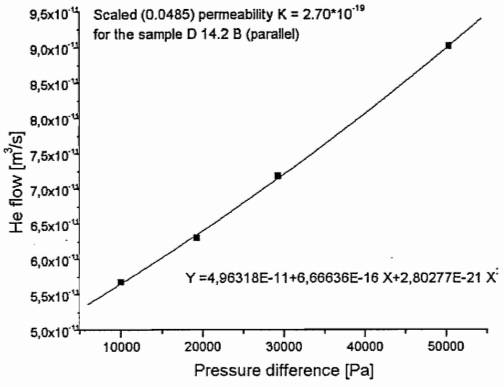

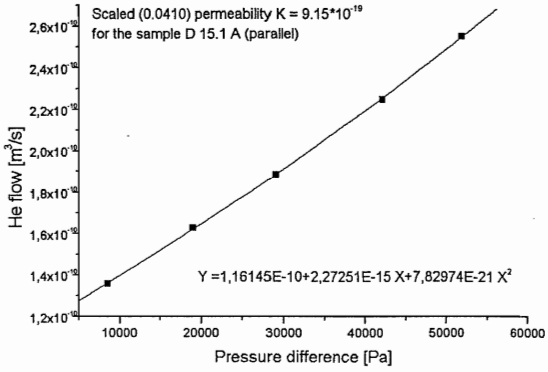

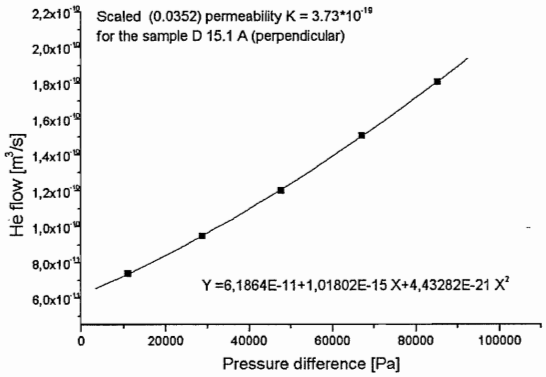

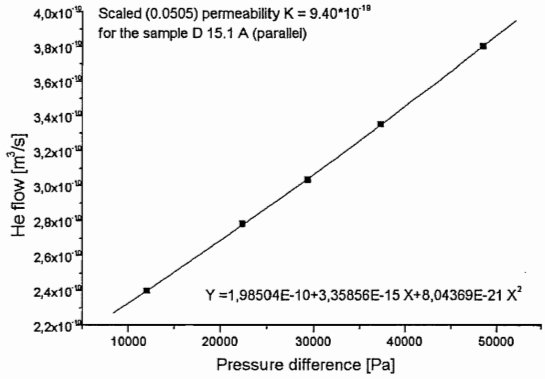

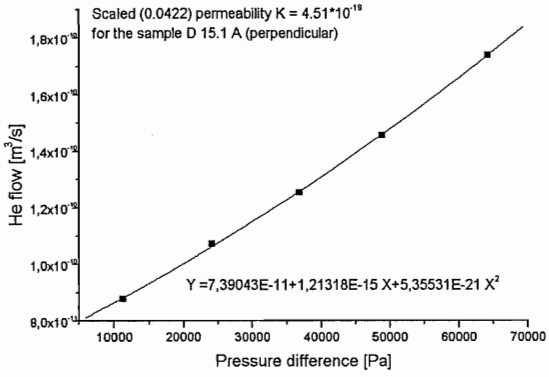

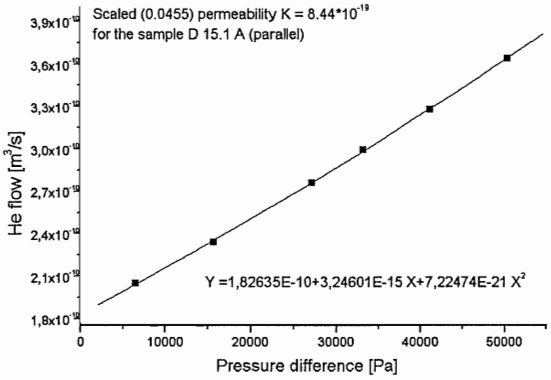

Appendix F

Permeability measurements on the cubic samples

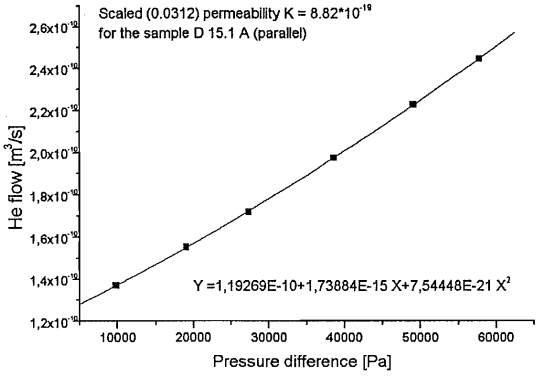

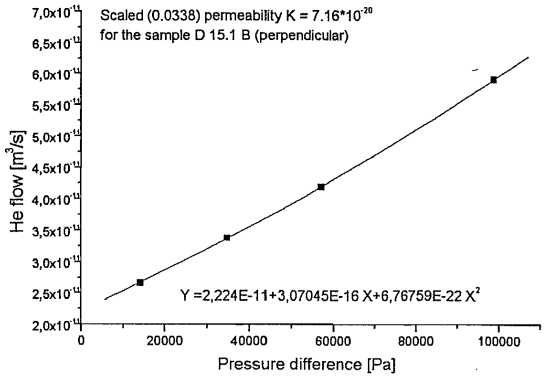

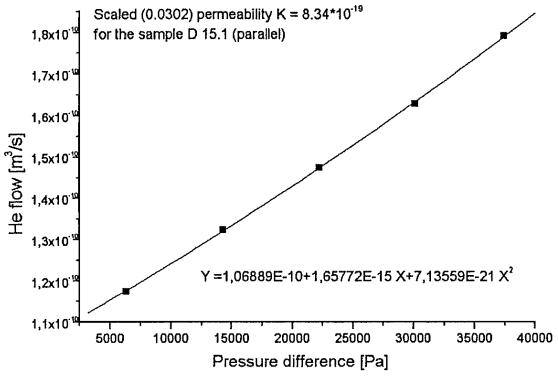

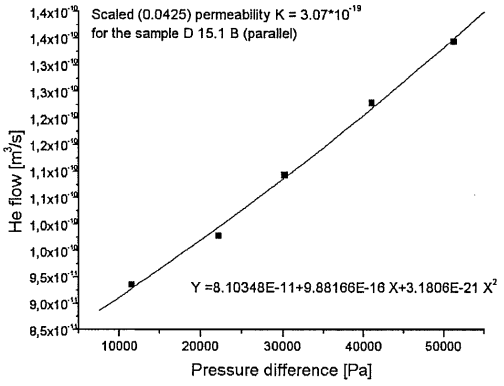

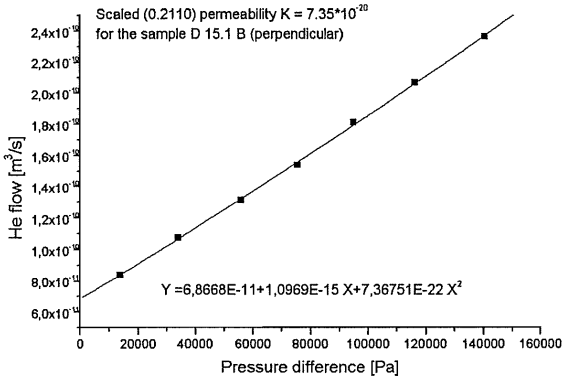

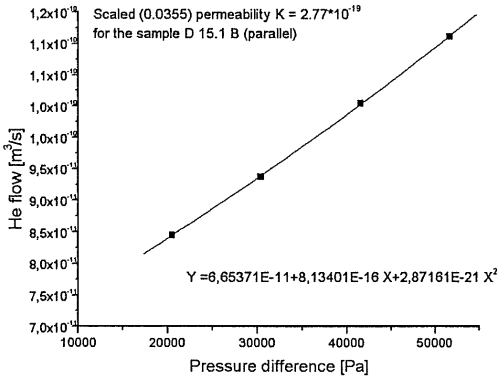

Appendix F

Permeability measurements on the cubic samples